ENHANCEMENT OF PHYSICAL AND MECHANICAL PROPERTIES OF EPOXY RESINS BY GRAPHENE/GRAPHENE OXIDE ADDITIVES

A THESIS SUBMITTED TO
THE GRADUATE SCHOOL OF NATURAL AND APPLIED SCIENCES
OF
MIDDLE EAST TECHNICAL UNIVERSITY

BY

DENİZ BUDAK

IN PARTIAL FULFILLMENT OF THE REQUIREMENTS
FOR
THE DEGREE OF MASTER OF SCIENCE
IN
POLYMER SCIENCE AND TECHNOLOGY

JANUARY 2023

Approval of the thesis:

ENHANCEMENT OF PHYSICAL AND MECHANICAL PROPERTIES OF EPOXY RESINS BY GRAPHENE/GRAPHENE OXIDE ADDITIVES

submitted by **DENİZ BUDAK** in partial fulfillment of the requirements for the degree of **Master of Science** i**n Polymer Science and Technology, Middle East Technical University** by,

Prof. Dr. Halil Kalıpçılar
Dean, Graduate School of **Natural and Applied Sciences** _____

Prof. Dr. Necati Özkan
Head of the Department, **Polymer Science and Technology** _____

Assist. Prof. Dr. Erol Yıldırım
Supervisor, **Polymer Science and Technology** _____

Examining Committee Members:

Prof. Dr. Necati Özkan
Polymer Science and Technology, METU _____

Assist. Prof. Dr. Erol Yıldırım
Chemistry, METU _____

Assoc. Prof. Dr. Hande Toffoli
Physics, METU _____

Assist. Prof. Dr. Antoine Marion
Chemistry, METU _____

Prof. Dr. Dilber Esra Yıldız
Physics, Hitit University _____

Date: 23.01.2023

I hereby declare that all information in this document has been obtained and presented in accordance with academic rules and ethical conduct. I also declare that, as required by these rules and conduct, I have fully cited and referenced all material and results that are not original to this work.

Name Last name : Deniz Budak

Signature :

ABSTRACT

ENHANCEMENT OF PHYSICAL AND MECHANICAL PROPERTIES OF EPOXY RESINS BY GRAPHENE/GRAPHENE OXIDE ADDITIVES

Budak, Deniz
Master of Science, Polymer Science and Technology
Supervisor : Assist. Prof. Dr. Erol Yıldırım

January 2023, 108 pages

Control of interfacial interactions is essential for the preparation of polymer matrix composites with enhanced physical, mechanical, thermal and electrical properties. The performance of the graphene and graphene oxide (GO) additives can be improved by achieving strong adhesion and uniform dispersion of GO in the epoxy matrix. In this study, modeling and simulation of DGEBA (Bisphenol A diglycidyl ether)/DETA (Diethylenetriamine) based epoxy nanocomposites containing graphene and graphene oxide (GO) additives were performed. Density functional theory and classical mechanics methods were used to investigate interaction energies and Young's Modulus values in the nanocomposite system. The objective of this study is to demonstrate the role of the amount, ratio and type of functional groups on the interaction energy and Young's modulus values. Improvement in the interaction energies was studied by controlling the epoxy:hardener ratio, type and the number of oxygen-containing functional groups on the GO, mass percentage of filler in epoxy, size of GO and dispersion in the cell. It was founded that functional groups with up to 10% oxygen coverage significantly increase interaction energy, and after there is only a slight enhancement of up to 18% oxygen. However, when

DETA:DGEBA ratio in epoxy resin molecules was changed, a different trend was observed for a single layer GO. For the low oxygen ratio on GO, increasing amine groups of DETA decreases the interaction energy. Carboxylic acid and hydroxyl groups on GO are important groups for increasing the hydrogen bonds and affinity with the epoxy matrix. Epoxy and hydroxyl groups are main groups that enhance the dispersion of the GO. Hydroxyl groups in the epoxy chain perform better than the amine groups in the epoxy chain to form hydrogen bonds with GO surface.

Keywords: Epoxy, Graphene, Graphene Oxide, Nanocomposites, Molecular Dynamics Simulations.

ÖZ

EPOKSİ REÇİNELERİN FİZİKSEL VE MEKANİK ÖZELLİKLERİNİN GRAFEN/GRAFEN OKSİT KATKILARI İLE GELİŞTİRİLMESİ

Budak, Deniz
Yüksek Lisans, Polimer Bilim ve Teknolojisi
Tez Yöneticisi: Dr. Öğr. Üy. Erol Yıldırım

Ocak 2023, 108 sayfa

Polimer matris kompozitlerin geliştirilmiş fiziksel, mekanik, termal, elektriksel özelliklerde üretilmesi için ara yüzey etkileşimlerinin kontrol edilmesi gereklidir. Grafen/grafen oksit (GO) katkı maddelerinin performansı, epoksinin yüzeye güçlü yapışması ve GO'nun homojen dağılımı sağlanarak geliştirilebilir. Bu çalışmada grafen ve GO katkı maddeleri içeren nanokompozitlerin modellenmesi ve simülasyonu için DGEBA (Bisfenol A diglisidil eter)/DETA (Dietilentriamin) tabanlı epoksi sistemi kullanılmıştır. Etkileşim enerjilerini ve Young Modülü değerlerini araştırmak için yoğunluk fonksiyoneli teorisi ve moleküler dinamik simülasyonları kullanılmıştır. Bu çalışmanın amacı, fonksiyonel grupların miktarının, oranının ve türünün etkileşim enerjisi ve Young Modülü üzerindeki etkisini göstermektir. Etkileşim enerjilerindeki gelişme, epoksi:sertleştirici oranı, GO üzerindeki oksijen fonksiyonel gruplarının türü ve sayısı, epoksideki dolgu maddesinin kütlece yüzdesi, GO boyutu ve hücre içindeki dağılımı kontrol edilerek incelenmiştir. Fonksiyonel grupların etkileşim enerjisini %10 oksijen oranına kadar önemli ölçüde artırdığı, ardından %18 oksijen oranına kadar çok hafif bir artış olduğu gösterilmiştir. Ancak epoksi reçine molekülündeki DETA:DGEBA oranı değiştiğinde farklı bir eğilim gözlenmiştir. GO üzerindeki düşük oksijen oranı için,

artan amin grupları etkileşim enerjisini azalmaktadır. GO üzerindeki karboksilik asit ve hidroksil grupları, epoksi matrisi ile hidrojen bağlarını ve etkileşimini artırmak için önemlidir. Epoksi ve hidroksil grupları ise GO'in homojen dağılımını arttırmak için önemlidir. Epoksi zincirindeki hidroksil gruplarının, GO yüzeyi ile hidrojen bağları oluşturmak için epoksi zincirindeki amin gruplarından daha iyi performans gösterdiği belirlenmiştir.

Anahtar Kelimeler: Epoksi, Grafen, Grafen Oksit, Nanokompozitler, Moleküler Dinamik Simülasyonları.

To my beloved family…

ACKNOWLEDGMENTS

I would like to express my deepest gratitude to my supervisor Assist. Prof. Dr. Erol Yıldırım for his valuable suggestions, guidance and support.

This work was funded by European High-Performance Computing Joint Undertaking (JU) under grant agreement No 951745, FF4EuroHPC project with the project name EPOGRAHPC. We acknowledge the support from the 2232 International Fellowship for Outstanding Researchers Program of TUBITAK (118C251). The numerical calculations in this study were partially performed at TUBITAK ULAKBIM, High Performance and Grid Computing Center (TRUBA resources).

I would also thank Assoc. Prof. Dr. Hande Toffoli for her contributions during computational studies. Experimental data provided by Tuğçe Gür, Hüseyin Alagöz from Nanografi Company and Harun Özkanaktı from Alti Dynamics are greatly acknowledged. I also thank Sevil Sarıkurt Malcıoğlu and Feyza Eryol for their assistance in using TRUBA resources.

I am thankful to my lab mates Erhan Özdemir, Tuğba Hacıefendioğlu Aydın, Esra Kan, Oğuzcan Taneroğlu, and Berin Sak for all their support and encouragement.

My deepest appreciation belongs to my family, my mother Filiz Budak and my father Yılmaz Budak for believing in me in every step of my life. I am also grateful to Selin Şahin, Ezgi Gözde, Deniz Işık, Nisa Erişen, Gizem Minnetoğlu, Onur Yıldız and Özer Erdoğan for their endless support and being always by my side.

TABLE OF CONTENTS

LIST OF TABLES

TABLES

LIST OF FIGURES

FIGURES

LIST OF ABBREVIATIONS

ABBREVIATIONS

B3LYP: Becke three-parameter Lee-Yang-Parr

BSSE: Basis set superposition error

CPU: Central Processing Unit

COMPASS: Condensed-phase Optimized Molecular Potentials for Atomistic Simulation Studies

DETA: Diethylenetriamine

DFT: Density Functional Theory

DGEBA: Bisphenol A diglycidyl ether

E: Energy

F: Force

GGA: Generalized Gradient Approximation

Gr: Graphene

GO: Graphene oxide

GPa: Gigapascal

H: Enthalpy

HF: Hartree-Fock

KS: Kohn-Sham

LDA: Local Density Approximation

L-J: Lennard-Jones

MW: Molecular weight

MD: Molecular Dynamics

MC: Monte Carlo

MM: Molecular Mechanics

N: Number of atoms

NMR: Nuclear Magnetic Resonance

NPH: Constant Pressure and Enthalpy

NPT: Constant Pressure and Temperature

NVE: Constant Volume and Enthalpy

NVT: Constant Volume and Temperature

P: Pressure

PCFF: Polymer Consistent Force Field

PMC: Polymer matrix composites

PPPM: Particle-Particle-Particle-Mesh

rGO: Reduced graphene oxide

SciPCFF: Scienomics Polymer Consistent Force Field

T: Temperature

V: Volume

vdW: van der Waals

XC: Exchance-Correlation

LIST OF SYMBOLS

SYMBOLS

Å: Angstrom

a: Acceleration

π: Pi

σ: Stress

ε: Strain

C: Stiffness

$\hat{H}$: Hamiltonian Operator

Ψ: Wave function

∇: Gradient

θ: Bond angle

ϕ: Dihedral angle

χ: Improper dihedral angle

μ: Chemical potential

g: Gram

°C: Degree Celsius

k: Stiffness

K: Kelvin

kJ: Kilojoule

m: Meter

nm: Nanometer

μm: Micrometer

ρ: Density

δ: Partial charge

q: Electric charge

r: Distance

MPa: Megapascal

S: Siemens

t: Time

TPa: Terapascal

v: Velocity

W: Watt

Z: Atomic number

CHAPTER 1

INTRODUCTION

Novel polymer matrix composites are being produced by introducing nanofillers as a reinforcement material into the polymer matrix. Nanofillers have a high surface to volume ratio and high aspect ratio, therefore the resulting nanocomposite exhibits enhanced characteristics even with the addition of small amounts of filler. Materials can become lighter and stronger with improved thermal, mechanical and electrical performance. Graphene (Gr) is a promising nanofiller for polymer nanocomposites due to its extraordinary properties; such that it is one of the strongest and the thinnest material with high electrical and thermal conductivity.[1] In this study, mechanical properties and interfacial molecular interactions of epoxy-graphene/graphene oxide nanocomposites are investigated through mainly classical and partly first principle computational chemistry methods. This chapter provides background information to understand the physical and structural properties of these materials to build accurate molecular models.

1.1 Polymer Matrix Composites (PMC)

Polymer matrix composites are multiphase systems consisting of physically and chemically different matrix and reinforcement materials. Matrix is the continuous polymeric phase that surrounds the reinforcement materials. Reinforcement materials are dispersed in a polymer matrix and act as load-bearing components. Matrix, reinforcement, and interfacial characteristics directly affect the performance of the composite materials. For improved mechanical performance, the matrix phase should have good adhesion properties and the ability to distribute the applied load uniformly. Composites not only retain the basic properties of the matrix and reinforcement materials but also gain high mechanical and functional properties with

the combination of these components. PMCs have attracted the attention of many industries including aerospace, automotive, electronics, energy storage, biomedical, sports, and others, due to their superior mechanical, thermal, electrical, and optical properties. The performance of the composite materials is enhanced by adding suitable fillers into the polymer matrix. Metal/metal oxide particles, carbon black, carbon nanotubes, clay nanoparticles, graphene, and graphene oxide are the mostly used nanofillers in polymers. [2]

Gr and graphene oxide (GO) stands out among these fillers because their superior mechanical characteristics. The primary challenge for improving the mechanical performance of graphene reinforced polymer nanocomposites is to achieve homogeneous dispersion of well-packed graphene sheets while maintaining strong adhesion with the polymer matrix. Oxidation and chemical functionalization methods can be used to disperse the graphene layers to improve the interfacial interaction as well as to prevent their self-aggregation. [3]

GO is used as a filler in various polymer matrices such as epoxy, Poly(methyl methacrylate) (PMMA), Polystyrene (PS), Polyurethane (PU), Poly(vinyl alcohol) PVA, Polycaprolactone (PCL) to improve the mechanical, thermal and electrical properties of the material. Graphene is a suitable filler material for improving mechanical properties due to its high strength and Young's Modulus characteristics. However, GO shows better performance as a filler since the strength of the interface interaction is the key property for the mechanical property enhancement of PMCs. Functional groups on GO improve the compatibility with the polymer matrix by forming new hydrogen bonds and dipole-dipole interactions. [4] Liao et al. (2014) reported that functionalized graphene sheets can improve Young’s Modulus of PMMA by 25% even with small additive amounts as low as 1 wt% added into the polymer matrix. [5]

The electrical conductivity of GO is less than pristine graphene since the addition of functional groups damages the conjugated structure of graphene. Therefore, the reduction of excess oxygen-containing functional groups will be a better choice for

improving electrical properties. [4] Stankovich et al. (2006) investigated the improvement of electrical conductivity by adding reduced graphene oxide (rGO) into the PS. The addition of the filler up to a volume percent at 1% increases the electrical conductivity from 10^{-5} S m^{-1} to 0.1 S m^{-1}, which makes the nanocomposite material suitable for many electrical applications. [6]

Moreover, the thermal stability and thermal conductivity of polymers can be improved with the addition of GO fillers. Ramanathan et al. (2008) reported that the glass transition temperature increases by 30°C for PMMA, 46°C for poly(acrylonitrile) (PAN) and 20°C for poly(acrylic acid) (PAA) with the addition of 1 wt% GO. Also, the thermal degradation temperature increased by 57°C for PMMA. [7] According to the study by Wang et al. (2009), the thermal conductivity of pure epoxy is 0.20 W/mK, and the addition of 5 wt% GO filler increases thermal conductivity to 0.85 W/mK that shows GO is a promising material for heat dissipation. [8]

Graphene oxide has a high affinity for epoxy due to oxygen-containing polar functional groups on its surface. Therefore, epoxy can be a good selection as a polymer matrix to produce GO-polymer nanocomposites with enhanced physical, thermal and mechanical properties.

1.2 Epoxy Polymers

Polymer matrices in PMCs can be thermoplastic or thermosetting polymers. Thermoplastics melt and flow like viscous liquids when heat is applied, and solidify when the system cooled. They can be reshaped while retaining their chemical properties. Unlike thermoplastics, thermosets are crosslinked structures. Because of these strong chemical bonds, thermosets cannot be melted and reprocessed by heating.

Epoxies are one of the most commonly used thermoset resins in PMCs due to their excellent properties such as high strength, durability, resistance to solvents and chemicals, and high performance at elevated temperatures. Epoxy molecules have an epoxide or oxirane group in their structure which is a three membered ring consisting of one oxygen atom and two carbon atoms given in Figure 1.1. [9]

Figure 1.1. Molecular structure of epoxide or oxirane group.

Epoxies are produced by crosslinking reactions between low molecular weight liquid epoxy monomers and curing agent (hardener) molecules. As the crosslinking process continues, strong covalent bonds form between the epoxy monomer and the hardener molecules, leading to the formation of the mixture transformed from a liquid to a solid state. This is an irreversible reaction, and epoxies cannot be melted or processed again once they have been cured. [9] Epoxies have high stiffness and strength properties due to their 3D network structure. However, with increasing crosslinking density, epoxies become more brittle and less resistant to crack initiation and growth.[10]

Epoxies have wide application areas as composite matrices, paints, adhesives, coating materials, electronic applications and construction materials. Glass transition temperatures from 60°C to 250°C can be achieved for epoxy resins with the combination of different components. Tensile strength is more than 80 MPa, one of the highest values achieved in thermosets. [11]

1.2.1 Epoxy Monomer

Epoxy resins are classified into two main groups, glycidyl ether resins and nonglycidyl ether resins. Glycidyl ether resins are the most used epoxy resins based on the bisphenol and novolac type resins. Nonglycidyl ether resins are cyclic and acyclic aliphatic resins. Among these types, bisphenol A diglycidyl ether (DGEBA) is the most common commercially used epoxy, accounting for more than 70% of total epoxy resins. DGEBA is liquid at room temperature that has two highly strained reactive epoxide groups in its structure. [11] DGEBA is produced by the reaction between bisphenol A with epichlorohydrin. High chemical and heat resistance properties are gained by the aromatic rings in the structure. Hydroxyl groups formed by ring opening provide adhesion properties to the epoxy resin. Figure 1.2 represents the chemical structure of DGEBA. [12]

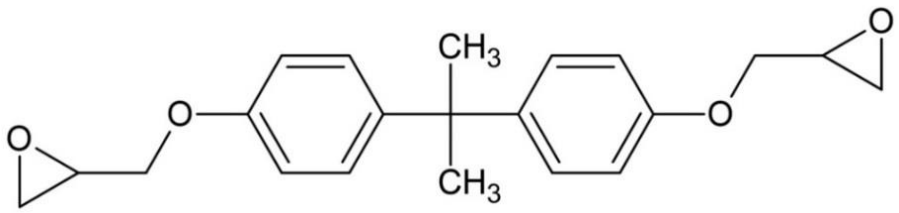

Figure 1.2. Molecular structure of bisphenol A diglycidyl ether (DGEBA).

1.2.2 Curing Agent (Hardener)

Curing agents are classified into three categories as amine, acid and anhydride hardeners. Amine type curing agents are widely used for epoxy resins. Diethylenetriamine (DETA) is an amine type curing agent in the liquid phase which has a very low viscosity at room temperature. DETA has three amine groups in its structure which can be activated during the curing reaction. Primary amine groups

react with two epoxy groups and secondary amine group reacts with one epoxy group. The structure of DETA is given in Figure 1.3. When DETA is used as a hardener for DGEBA based epoxy, curing can be completed at 23°C within several days or at 100°C in 1-2 hours. It is advantageous for reducing processing costs, as the reaction does not require elevated temperatures. [9]

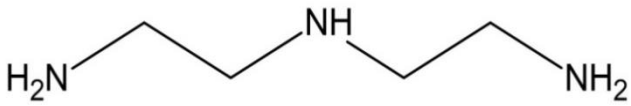

Figure 1.3. Molecular structure of diethylenetriamine (DETA).

1.2.3 Curing (Crosslinking) Reaction

Curing is a reaction where strong covalent bonds are formed between the epoxy monomer and the hardener. These covalent bonds are known as crosslinks, and their formation makes the material harder and more rigid. Curing reactions with epoxide rings occur by nucleophilic addition for DETA and DGEBA systems. Epoxide groups in the DGEBA interact with the active hydrogen (H) atoms of the amine (NH) groups in the DETA molecules. This reaction breaks the C-O bond in the epoxide by ring opening reaction. Consequently, cross-links are formed between the DETA and the DGEBA molecules. The reaction mechanism was represented in Figure 1.4. The activation reaction for epoxy and amine functional groups was given in Figure 1.5. The ratio of the total number of crosslinked sites to the maximum allowable reactions is known as the crosslinking density. The number of crosslinks in the mixture directly affects the density, viscosity, physical properties, and adhesion characteristics of the epoxy polymer. [9]

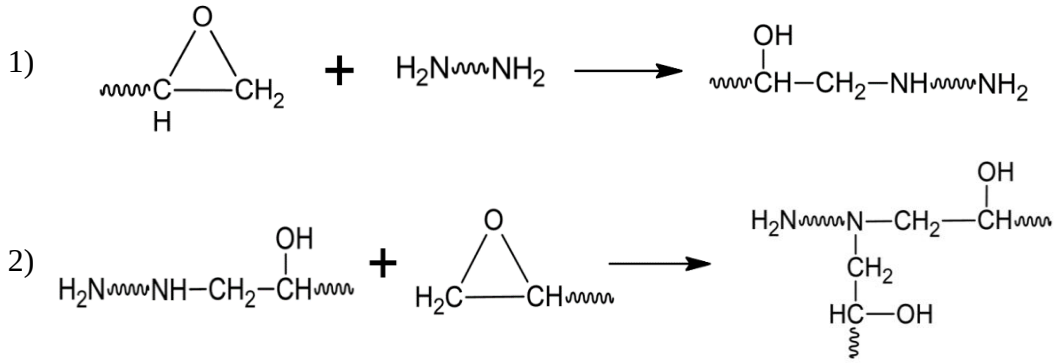

Figure 1.4. Crosslinking reaction between epoxide and amine groups. [9]

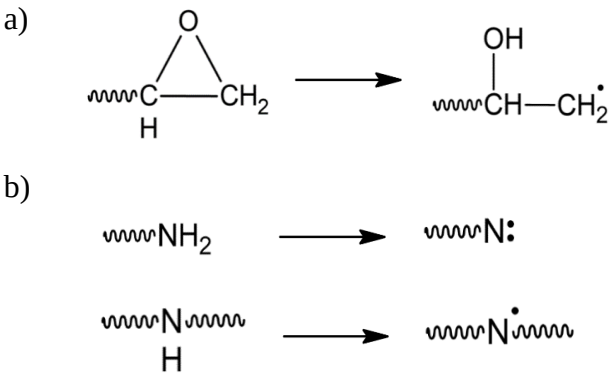

Figure 1.5. Activation of a) epoxy and b) amine groups. [13]

The type and stoichiometric amount of hardener in the polymer matrix should be carefully selected to achieve improved mechanical properties. According to the study by Possart et al. [14], crosslinking density and material stiffness decrease when an excess amount of hardener is used. Excess hardener results in an increased number of free chain ends, so DGEBA molecules become insufficient to saturate all amines in the mixture leading to reduced crosslinking density. Results show that after

DGEBA:DETA content reaches 100:30 w/w ratio, stiffness and elastic modulus are significantly reduced by the addition of more hardener molecules. Similar effect is observed when hardeners with long chains are used. An increase in the molecular length of the hardener decreases the average crosslinking density per unit volume due to an increase in the number of internal degrees of freedom and results in a low elastic modulus. [14]

1.3 Graphene

Graphite is a three-dimensional (3D) allotrope of carbon made up of multiple layers of graphene stacked on top of each other with vdW interactions. It is mostly used inside lead pencils. Andrei Geim and Kostya Novoselov were awarded the 2010 Nobel Prize in physics for their work "groundbreaking experiments regarding the two-dimensional material graphene". With this study, they become the first researchers to isolate a single graphene sheet and demonstrate its extraordinary properties. Before this study, it was believed that 2D crystals were thermodynamically unstable and could not exist. They obtained graphene sheets from graphite by mechanical exfoliation method by using a scotch type method. Following the development of this simple and inexpensive method for obtaining a single sheet of graphene, many researchers started to show interest in this material, and the graphene research area began to grow fast. [15]

Graphene is a 2D material consisting of sp^2 bonded carbon atoms arranged in a hexagonal lattice. Edges of graphene have a zigzag or armchair arrangement. C-C bonds in graphene sheets are strong covalent bonds with a length of 1.42 Å. [16]. Graphene is an advantageous material because it has a large specific surface area (2360 $m^2 g^{-1}$), the highest Young's modulus (~ 1 TPa) and strength (~130 GPa), high electrical (108 S m^{-1}) and thermal conductivity (~5000 W m^{-1} K^{-1}). [1]

Figure 1.6 represents the unit cell structure of graphene and a cell containing graphene with dimensions of 10x10 Å.

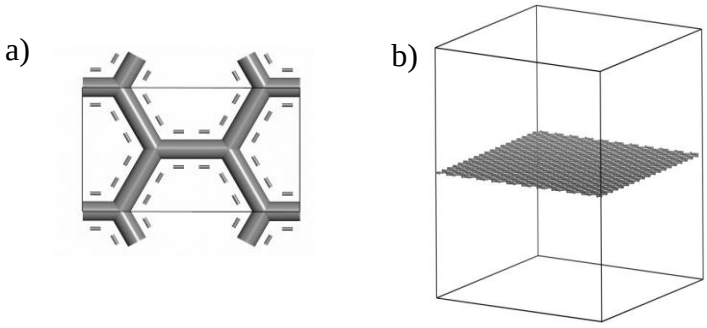

Figure 1.6. Representation of a) Unit cell structure of graphene b) 10x10 Å cell with graphene.

Graphene can be produced by several methods such as mechanical exfoliation, chemical vapor deposition, epitaxial growth and redox methods. They are mainly used in semiconductors, energy applications such as solar cells, battery electrodes and super capacitors, flexible displays, composite preparation for the aerospace and automotive industries, chemical sensors, anti-corrosive inks and pastes, and other applications. [16] Configuration of graphene sheets (layer number, defect, and lateral size), distribution in the polymer matrix, and interfacial interaction between graphene and polymer strongly affect the performance of polymer/graphene nanocomposite material. Graphene sheets tend to agglomerate due to the strong van der Waals (vdW) force (5.9 kJ mol^{-1} per carbon) between them, which reduces the effectiveness of graphene as a reinforcement material. The mechanical properties of nanocomposites are strongly affected by the distribution of graphene in the polymer matrix. To distribute graphene homogeneously in the polymer matrix, functionalization of graphene is required to reduce vdW forces, and improve compatibility and interfacial interactions between graphene and the polymer matrix. The interface acts as a link between the reinforcement material and the matrix, which transfers the stress from the matrix to the reinforcement material. Weak interfacial

interactions lead to a loss of strength in the nanocomposite material. Hydrogen bonds, dipole-dipole interactions, π-π interactions and covalent bonds are the type of interfacial interactions. Control of the C/O ratio and type of functional groups in graphene oxide structures can control the interfacial interactions and their performance as a filler. [1]

1.4 Graphene Oxide

Graphene oxide has a plane of carbon atoms similar to graphene with the addition of oxygen-containing functional groups to its pristine structure. Large-scale production of high-quality graphene is costly and time-consuming. Graphene oxide can be produced from graphite with cost effective chemical methods. Hummers' method is the most used process to produce graphene oxide nanosheets from graphite. With this method, graphite is mixed with concentrated sulfuric acid, potassium permanganate, and sodium nitrate for the oxidation process. Adding oxygen-containing functional groups onto the graphene surface facilitates the separation of nanosheets and also makes them more hydrophilic. After the exfoliation process, excess functional groups can be removed by thermal or chemical reduction methods, and reduced graphene oxide (rGO) is produced. rGO has a more stable structure and properties similar to graphene, but with better polymer compatibility and dispersibility. [17]

Experimental characterizations and molecular dynamics simulations have been used to predict the GO chemical structure, however the exact composition of GO is still unclear since it is non-stoichiometric and nearly amorphous. Moreover, the chemical structure of GO may change depending on production methods and environmental conditions. Different models are developed by researchers to represent the chemical structure of GO and the Lerf-Klinowski [18] model is a widely accepted one in the literature. To build this model, the graphene oxide structure was investigated with the NMR method and oxygen-containing functional groups were detected. Results

showed that phenyl rings contain epoxy (C-O-C), hydroxyl (-OH), and carboxylic acid (-COOH) groups which are distributed randomly.

Besides, epoxy and hydroxyl groups are mostly located on the basal plane whereas carboxylic acid is located at the edges. Gao et al.[19] updated this model by adding carbonyl groups. They also found that oxygen-containing functional groups hydroxyl and epoxy are intermittently located on the basal plane whereas carbonyl (C=O) groups are mostly present at the edges of GO in addition to the carboxylic acid groups. Erickson et al.[20] suggested that the dominant functionalities of hydroxyls and epoxies, which are more stable groups on the surface, is to restore the graphitic character of the GO. Other functional groups like carbonyls would induce bond breakage during formation and this results in the hole creation and expansion. Thus, they are most likely to be formed at the edges of the GO structure. Graphene oxide structure was given in Figure 1.7.

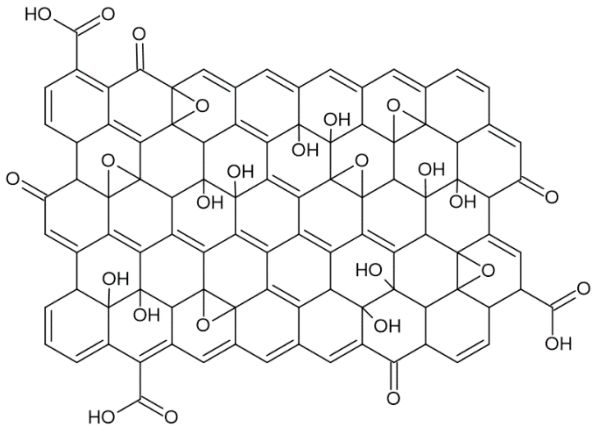

Figure 1.7. Molecular structure for a graphene oxide model. [19]

CHAPTER 2

THEORETICAL AND COMPUTATIONAL CHEMISTRY METHODS

Theoretical and computational chemistry studies aim to investigate molecular geometry, physical and mechanical properties, molecular interactions, chemical reactivity, equilibrium and transition states, and other chemical properties of the molecules at the electronic, molecular and mesoscale levels. A system model is essentially built based on applicable theories and equations that are solved by a computer using specific algorithms with computer simulations or calculations. In this way, the static and dynamic behavior of a system under given initial conditions can be studied. Highly complex models can be created using computer simulations to observe real-life processes that bridge the gap between theory and experiments. Material behavior and molecular interactions that cannot be studied with experimental methods can be thoroughly investigated in detail. Theoretical and computational chemistry methods are useful for guiding the design of experiments; they provide both economic and time advantages which have the potential to substitute and support laboratory measurements partly in the future. [21]

The development of equations, parameters, or simulation techniques that characterize behavior at different lengths and time scales is referred to as multiscale modeling. Multiscale modeling methods are separated into three categories as molecular scale methods which include first principle calculations and molecular dynamics simulations, mesoscale simulations and macroscale methods at the continuum. Molecular scale calculations are based on the atoms and molecules while mesoscale calculations are based on coarse grained units, particles, and monomers. Macroscale calculations are focused on the continuous domains at the device and engineering level. Each method has a different application area and utilizes different equations to calculate processes occurring at diverse lengths and time scales.

As an example, quantum mechanics methods use Schrödinger equations which are effective for calculating electronic structure and energy. Molecular dynamics methods are based on classical Newtonian equations and statistical mechanics that are used to calculate thermodynamic properties, mechanical properties and molecular interactions. [22]

The hierarchy between commonly used models is given in Figure 2.1, representing relevant time and length scales. Small scale calculations give more detailed and accurate information about the system properties. Some of the molecular interactions and effects are neglected while working with larger scales and homogeneous systems. However, first principle calculations at small scales are more complex, more costly, and take a longer time to complete due to the inclusion of electrons in the calculations. [23]

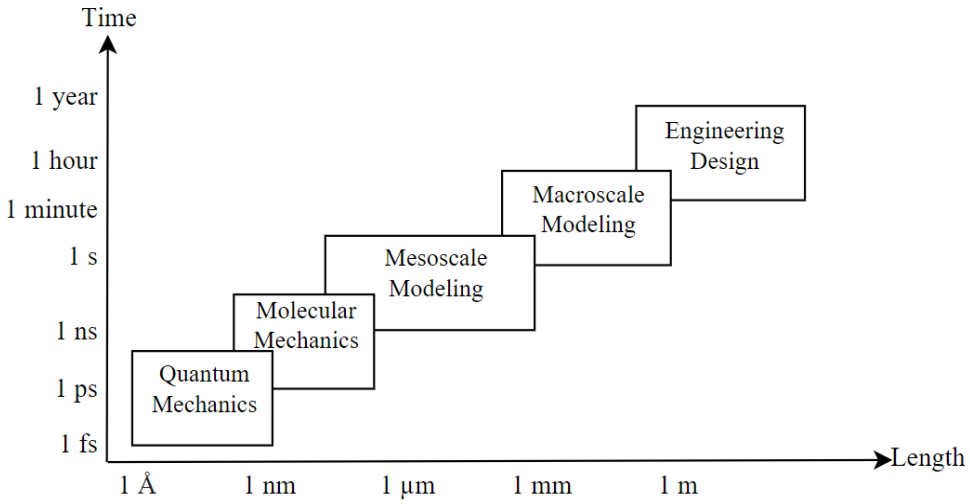

Figure 2.1. Time and length scales of multiscale modeling methods. [24]

Molecular simulation methods are classified into two categories as quantum chemistry methods and molecular mechanics methods. The difference between these methods is that the fundamental interacting particles in the system are considered

electrons for quantum chemistry methods, and atoms for classical mechanical methods. [25]

2.1 First Principle Calculations

Quantum mechanics theories are based on electron delocalization where wave functions are used to characterize electron distribution. Born's rule states that the probability of distribution of an electron is proportional to the square of the magnitude of an electromagnetic wave. Energy levels and wave functions are obtained by solving the Schrödinger equation. The Schrödinger equation cannot be solved precisely if there is more than one electron, therefore for the systems with large numbers of atoms, various assumptions and approximations are needed to determine the wave function. Quantum mechanics calculations are computationally intensive and give very accurate results for representing intermolecular and intramolecular interactions, however, they are not suitable for investigating structures containing a large number of atoms such as proteins or polymers. [21]

The time-independent Schrödinger equation is mostly used in computational chemistry calculations for practical use. Time-independent Schrödinger equation is expressed in Equation 2.1 as:

$$\hat{H}\Psi = E\Psi \tag{2.1}$$

Where H is the Hamiltonian operator that represents the total kinetic and potential energy of the system. For a Coulombic system, it is calculated by Equation 2.2.

$$\hat{H} = -\sum_{i} \frac{1}{2}\nabla_i^2 - \sum_{iA} \frac{Z_A}{|r_i - r_A|} + \sum_{i>j} \frac{1}{r_{ij}} \tag{2.2}$$

Z_A represents the charge of the nuclei (atomic number) of atom A, r_{ij} is the distance between electrons i and j and r_{iA} is the distance between electron i and nucleus A. $-1/2\ \nabla^2$ is the kinetic energy term. Ψ is the wave function which is a function of the positions of the nuclei and the electrons and E is the numerical value of the energy of the state described by the wave function. [26]

Electrons in a molecule are significantly lighter than the nuclei when compared in mass. Born-Oppenheimer [27] approximation states that the coordinates of the nuclei in a molecule are fixed while electrons are moving. With this approximation, the Schrödinger equation can be simplified by developing two different equations as electronic and nuclear Schrödinger equations. The total energy is calculated by the sum of electronic energy which depends on the electron positions and the constant nuclear repulsion term. [28]

Quantum chemistry methods are ab-initio, semi-empirical, and density functional theory (DFT) calculations. These calculations are based on the solutions of Schrödinger equations. The ab-initio method solves the Schrödinger equation to calculate energy and wave function. Wave function determines the electronic structure, which provides information about molecule properties such as polarity. For semi-empirical methods, parameterization is based on fitting solutions into experiments that lead to faster calculations compared to the ab-initio methods. DFT calculations use functions of the electron density rather than the wave functions to calculate energy. [29]

2.1.1 Ab-initio Calculations

Ab-initio has a meaning of “from the start” in Latin. The ab initio method uses quantum mechanics calculations to solve the electronic Schrödinger equation. This first principle method is suitable for investigating novel molecules to calculate properties such as molecular geometries, energies, electron affinities, ionization potentials and vibrational frequencies. This method produces very accurate results although it is not computationally efficient and is only applicable to systems with less than 1000 atoms. In ab-initio calculations, the Hartree-Fock method is used for approximating the molecular wave function and expressing the molecular energy. The wave function is expressed by the occupied spin orbitals as a Slater determinant expressed in Equation 2.3.

$$\Psi = \frac{1}{\sqrt{N!}} \begin{vmatrix} \varphi_1(\overrightarrow{x_1}) & \varphi_2(\overrightarrow{x_1}) & \cdots & \varphi_N(\overrightarrow{x_1}) \\ \varphi_1(\overrightarrow{x_2}) & \varphi_2(\overrightarrow{x_2}) & \cdots & \varphi_N(\overrightarrow{x_2}) \\ \vdots & \vdots & \vdots & \vdots \\ \varphi_1(\overrightarrow{x_N}) & \varphi_2(\overrightarrow{x_N}) & \cdots & \varphi_N(\overrightarrow{x_N}) \end{vmatrix} \quad (2.3)$$

$\varphi_i(\overrightarrow{x_i})$ are spin orbitals consisting of spatial orbital $\phi_i(\vec{r})$ and two spin functions spin up (α_s) and spin down (β_s).

$$\varphi(\vec{x}) = \phi(\vec{r})\sigma(s), \quad \sigma = \alpha, \beta \quad (2.4)$$

The Hartree-Fock method has a disadvantage in the proper treatment of electron correlation. Electrons minimize their interaction energy by correlating their motions in reality; however, the Hartree-Fock method uses the average positions of other electrons to represent the movement of an electron in the electric field. Post-HF methods such as MP2-4, CCSD and CI have been developed to reduce electron-electron interaction energies which improves the reliability of the results.[29]

2.1.2 Density Functional Theory (DFT) Calculations

Density functional theory (DFT) is another calculation method based on quantum mechanics calculations that enable the investigation of molecules at the electronic level. In contrast to ab-inito and semi-empirical calculations, this method derives electron distribution directly from the electron density rather than calculating the wave function. Using electron density for energy calculations is simpler since wave function is dependent on 4N variables, which means for N electrons three spatial and one spin variable. Electron density is a function of the position including only three coordinates which is represented by ρ(x,y,z). Moreover, it is possible to visualize electron density by X-ray diffraction or electron diffraction methods.

DFT calculations are based on two theorems established by Hohenberg-Kohn. [30] The first theorem states that the ground state electron density function, $\rho_0(x,y,z)$, describes the molecular properties at the ground electronic state. The second theorem indicates that a trial electron density function provides an equal or higher energy than

the actual ground state energy. Current molecular DFT calculations are based on Kohn-Sham equations [31] which are used to calculate energy from electron density functions.

Kohn-Sham approach defines a system involving non-interacting electrons that has the same ground state electron density distribution with the real system ($\rho_r=\rho_0$) to formulate energy. Energy is minimized with Kohn-Sham (KS) orbitals and equations concerning electron density. [29]

The ground state electronic energy is given in Equation 2.5 as: [26]

$$E[\rho] = T_s[\rho] + V_{Ne}[\rho] + J[\rho] + E_{xc}[\rho] \tag{2.5}$$

Equation 2.6 is used for calculating electron density.

$$\rho(\vec{r}) = \sum_{i}^{N} |\phi_i(\vec{r})|^2 \tag{2.6}$$

T represents the electron kinetic energies and for the set of orbitals ϕ_i and it is calculated by the following equation:

$$T_s[\rho] = \sum_{i} \langle \phi_i \left| -\frac{1}{2}\nabla^2 \right| \phi_i \rangle \tag{2.7}$$

The nucleus-electron potential energy V_{Ne} is given in Equation 2.8.

$$V_{Ne}[\rho] = \int \rho(r) v(r) \tag{2.8}$$

Where $v(r)$ is the external potential due to the nuclei which is expressed as:

$$v(r) = -\sum_{A} \frac{Z_A}{|r - R_A|} \tag{2.9}$$

$J[\rho]$ is the electron-electron repulsion energy and it is given in Equation 2.10.

$$J[\rho] = \frac{1}{2} \iint \frac{\rho(r)\rho(r')}{|r - r'|} dr\, dr' \tag{2.10}$$

$E_{xc}[\rho]$ is the exchange-correlation factor and there is no explicit form available for this term. It can be expressed by Equation 2.11.

$$E_{xc}[\rho] = \ (T[\rho] - T_s[\rho]) + (V_{ee}[\rho] - J[\rho]) \tag{2.11}$$

Electron density is derived from wave function for non-interacting electron systems. Slater determinant is used to represent anti-symmetric wave functions.

With wave function and electron density expressions, Kohn-Sham [31] equation is expressed by Equation 2.12 as:

$$\left(-\frac{1}{2}\nabla^2 + \int \frac{\rho(\overrightarrow{r_2})}{r_{12}} d\overrightarrow{r_2} + V_{XC}(\overrightarrow{r_1}) - \sum_{M}^{A} \frac{Z_A}{r_{1A}}\right)\varphi_i = \varepsilon_i \varphi_i \tag{2.12}$$

ε_i is the orbital energy eigenvalue, Z_A is the atomic number and V_{XC} is the potential due to exchange-correlation energy. It is the sum of the electron-electron repulsion energy deviation and the kinetic energy deviation from the reference system. [28]

Local density approximation (LDA) is the simplest exchange-correlation functional which only considers the density at the location where the functional is evaluated and assumes that the density represents the density of a homogenous electron gas. Generalized gradient approximation (GGA) is developed as an advancement over LDA. This approximation uses both the electron density at the given point and the gradient of the density for the calculations, to reflect the inhomogeneous characteristic of molecular densities. Moreover, hybrid functionals are developed which include GGA and HF exchange to calculate the properties more accurately. Hybrid DFT that uses B3LYP (Becke three-parameter Lee-Yang-Parr) functional is one of the most commonly used exchange-correlation functional. [32]

As a disadvantage, exchange-correlation functional $E_{xc}[\rho]$ is not exactly known and various approximations are used for the calculation of this term. Therefore, it is not possible to improve results systematically. Other ab-initio methods enable lower energies and keep improving the results by using larger basis sets and extending the correlation approach. However, DFT is the most widely used method among all first principle methods, since it is a computationally efficient and simpler method as

compared with other wave function methods. DFT gives more accurate results for the calculation of geometry and relative energies by using electron density and applying built-in correlations especially. [29]

2.2 Molecular Mechanics (MM) Methods

In molecular mechanics calculations, molecules are represented as a collection of balls (atoms) that are connected by springs (bonds). Electrons are not included in this model, so electronic properties cannot be studied. The energy of a molecule is represented by a force field: a mathematical expression including bond stretching, angle bending, dihedral angles, and non-bonded interaction parameters. MM calculations are suitable for very large molecules. It can be utilized for molecular mechanics minimizations, dynamics, quenching and simulated-annealing type of calculations.[29] MM methods use classical mechanics for calculations where force field equations and force field parameter sets define the total potential energy of the system. Differentiating this potential energy concerning the position of atoms gives the force acting on each atom ($F_i = -dE/dx_i$), and the position and velocity of the atoms can be predicted during the molecular dynamics (MD) simulation steps. [25] Each atom contributes to the total potential energy of a system via bonded and non-bonded interactions. Bonded interactions are bond length stretching, bond angle bending, proper dihedral angles (torsion) and improper dihedral angles. Non-bonded interactions are intermolecular and intramolecular vdW and Coulomb interactions.[33]

Force fields are classified as Class I and Class II force fields. Class I force fields are developed to simulate biomolecular systems like proteins, carbohydrates, phospholipids, DNA, and RNA. Examples of Class I force fields are DREIDING, OPLS-AA, CHARMM, GROMOS, and AMBER. [25]

For class I force fields, potential energy (E) are calculated by Equation 2.13.

$$E = \sum_{bonds} k_b(b - b_0)^2 + \sum_{angles} k_\theta(\theta - \theta_0)^2 + \sum_{dihedrals} k_\phi[1 + \cos(n\phi - \delta)] + \sum_{improp} k_\chi(\chi - \chi_0)^2 + \sum_{L-J} 4\varepsilon_{ij}\left[\left(\frac{\sigma_{ij}}{r_{ij}}\right)^{12} - \left(\frac{\sigma_{ij}}{r_{ij}}\right)^{6}\right] + \sum_{Coulomb} \frac{q_i q_j}{4\pi\varepsilon_0 r_{ij}} \quad (2.13)$$

Where b is bond length, θ is the bond angle, ϕ is the dihedral angle and χ is the improper dihedral angle. b_0, θ_0, δ, χ_0 are the reference points. k's represent the stiffness of each bond type. 5th term represents Lennard-Jones (L-J) 12-6 pairwise interactions. ε_{ij} is L-J well depth and σ_{ij} is the collision diameter for the i and j atom pairs. 6th term represents electrostatic interactions defined by Coulomb's law. q_i and q_j are partial charges, ε_0 is the permittivity of free space. [25]

Figure 2.2 represents the bond lengths, angles and the other interactions used in the force field calculations.

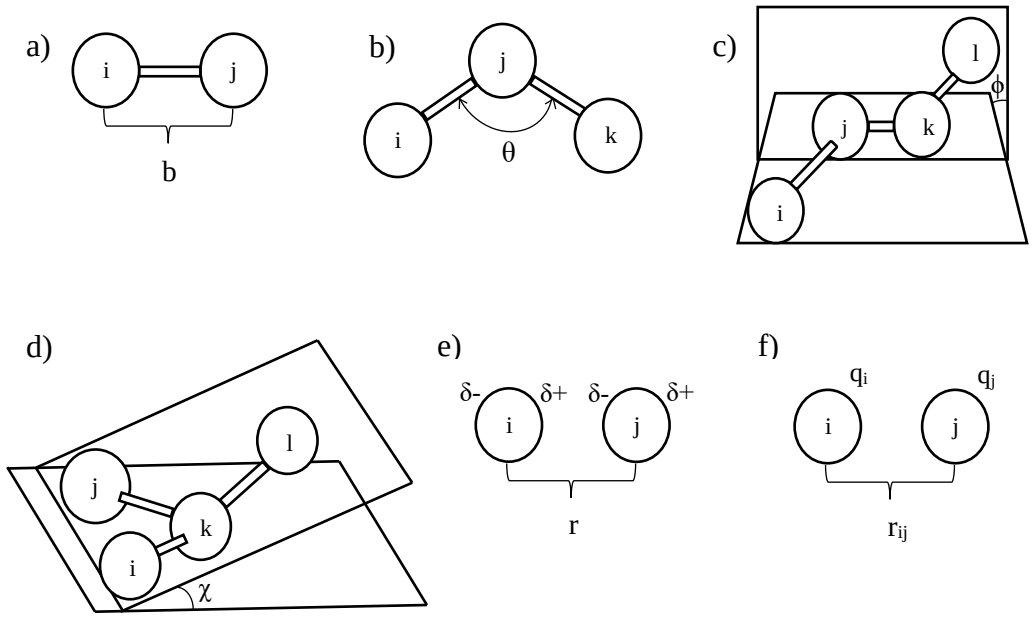

Figure 2.2. Representations of a) bond length b) bond angle c) proper dihedral d) improper dihedral e) van der Waals interactions f) coulomb interactions.

Class II force fields are second generation force fields that have cross-coupling terms between bonded interactions and offer a more accurate representation of potential energy, structures, and vibrational frequencies. They are developed based on the ab-initio calculations parameterized based on a large number of experimental data. Class II force fields are more complex and require a high amount of computational cost. They are the most used force fields for investigating polymers, metals, and ceramic-solid phase materials. Examples of Class II force fields are COMPASS, CVFF, PCFF, and MM# series. [25]

Potential energy functional form is the same for Class II, COMPASS and PCFF force fields and given in Equation 2.14 as [34]:

$$
\begin{aligned}
E = & \sum_{bonds} [K_2(b-b_0)^2 + K_3(b-b_0)^3 + K_4(b-b_0)^4] \\
& + \sum_{angles} [H_2(\theta-\theta_0)^2 + H_3(\theta-\theta_0)^3 + H_4(\theta-\theta_0)^4] \\
& + \sum_{dihedrals} [V_1[1-\cos(\phi)] + V_2[1-\cos(2\phi)] + V_3[1-\cos(3\phi)] \\
& + \sum_{\chi} K_\chi(\chi-\chi_0)^2 + \sum_{b,b'} F_{b,b'}(b-b_0)(b'-b_0') \\
& + \sum_{\theta,\theta'} F_{\theta,\theta'}(\theta-\theta_0)(\theta'-\theta_0') + \sum_{b,\theta} F_{b,\theta}(b-b_0)(\theta-\theta_0) \\
& + \sum_{b,\phi} (b-b_0)[V_1 cos\phi + V_2 cos2\phi + V_3 cos3\phi] \\
& + \sum_{b',\phi} (b'-b_0')[V_1 cos\phi + V_2 cos2\phi + V_3 cos3\phi] \\
& + \sum_{\theta,\phi} (\theta-\theta_0)[V_1 cos\phi + V_2 cos2\phi + V_3 cos3\phi] \\
& + \sum_{\theta,\theta',\phi} K_{\theta,\theta',\phi}(\theta-\theta_0)(\theta'-\theta_0') cos\phi + \sum_{L-J} \left[\frac{A_{ij}}{r_{ij}^9} - \frac{B_{ij}}{r_{ij}^6}\right] \\
& + \sum_{Coulomb} \frac{q_i q_j}{\varepsilon_0 r_{ij}}
\end{aligned}
$$

There are stretch-stretch (b,b'), stretch-bend (b,θ), stretch-torsion (b,ϕ), bend-torsion (θ,ϕ), bend-bend (θ,θ'), bend-bend-torsion (θ,θ',ϕ) terms in this equation. Class II COMPASS and PCFF force fields use 9-6 L-J potential as a difference from Class I force fields. However, they have the same Coulombic term for electrostatic interaction. For each atom and bond type, different values of the force field parameters are identified depending on the selected force field.

The first step in the classical Monte Carlo and molecular dynamics methods is to set up the coordinate positions and the bonded state of the atoms to build the system with the desired density and boundaries. Periodic boundary conditions are defined to construct the unit cell, and continuous systems are represented by replicating this unit cell in all directions. If a particle moves across the boundary surface and exits from one side of a unit cell, the same particle enters from the opposite boundary of the unit cell, and the total number of atoms within the system remains constant. The cut-off distance is set between 8-20 Å and cell size is set according to this distance to avoid repetitive calculation of non-bonded intermolecular interactions between the atoms in the main cell and surrounding cells. [25] Electrostatic non-bonded interactions can be calculated with Ewald or particle-particle-particle-mesh (PPPM) summation methods. The Ewald summation method is computationally effective for systems containing 10^3-10^4 atoms. However, for larger systems that contain 10^5 or more atoms, the PPPM summation method gives results faster in parallel calculations. [35]

The next step is to determine the statistical ensemble to perform the molecular simulation. The number of atoms (N), volume (V), temperature (T), pressure (P), energy (E), enthalpy (H) and chemical potential (μ) parameters can be set as constant to perform simulations similar to the real experimental conditions. Simulation packages offer different statistical ensembles as constant volume-constant energy (microcanonical, NVE), constant volume-constant temperature (canonical, NVT), constant temperature-constant pressure (isothermal-isobaric, NPT), constant pressure-constant enthalpy (isoenthalpic-isobaric, NPH) and constant chemical potential-constant temperature (grand canonical, μVT). [21]

The temperature of the system can be controlled by equilibration procedures called thermostat methods such as Andersen, Berendsen and Nosé-Hoover. Andersen thermostat method scales the translational and angular velocities of each particle to calculate the temperature and adjusts it to the desired value with an equilibration procedure. Berendsen thermostat method controls the system temperature by coupling it to a heat bath at a fixed temperature during the simulation. Velocities are

measured for each time step, and the temperature is kept constant by integrating a scaling factor. Berendsen thermostat method is an efficient way to equilibrate the system to the target temperature; however, it cannot generate trajectories with the correct canonical ensemble because this method eliminates changes in the kinetic energy in the system because of the fixed temperature. Nosé-Hoover is the most used thermostat algorithm since it represents kinetic parameters better and creates real canonical ensembles by reducing the effect of an external system. An additional dynamic variable in the equations regulates the temperature of the specified system, and the temperature is controlled with fluctuations around the target temperature.[36]

Since most experiments are carried out at constant atmospheric pressure, barostats are used to simulate constant pressure systems. There are several barostat algorithms such as Andersen, Berendsen, and Parrinello-Rahman. Andersen barostat uses an additional degree of freedom terms like the idea of the Nose-Hoover thermostat. In this method, there is an external pressure term that acts as a fictitious piston and another term that represents the internal pressure of the particles. If there is an imbalance between external and internal pressure, the volume of the system changes to achieve the target pressure. Berendsen barostat works on the same principle as the Berendsen thermostat, employing a weak coupling method that allows pressure fluctuations to approach the target pressure more realistically. The Parrinello-Rahman method is an extended version of the Andersen algorithm, which enables modeling the shape changes and is suitable for anisotropic systems. [21]

2.3 Classical Monte Carlo (MC) Calculations

Monte Carlo methods provide information about the system's conformational phase space, which is the potential energy surface as a function of atom positions. To calculate atom movements, the sampling method is used to generate possible random movements of atoms and compute an average result based on acceptance and rejection criteria. MC calculations use time-independent algorithms; hence the kinetics of molecular motion is not included in the simulations. This makes MC

calculations very fast. However, the results only provide information on the values of the thermodynamic properties of the system. MC calculations are not appropriate for investigating the dynamics of the system or the transport properties. Dynamic properties of the system can be investigated with molecular dynamics methods. [25]

2.4 Molecular Dynamics (MD) Simulations

The molecular dynamics simulation methods estimate the positions and velocities of atoms and molecules in a system over time by performing the calculations based on Newton's equation of motion in a selected statistical ensemble. Simulation results give information about how the system behaves with the selected pressure, temperature, volume, or the number of molecules. Thermodynamic, conformational, structural, rheological, and dynamic properties can be obtained for the system. The Velocity-Verlet algorithm was used in this study to determine the position of the particle by integrating Newton's equation of motion. For this method, the first step is to determine the atomic positions and velocities at the beginning of the simulations. Velocities of the atoms are assigned according to the Maxwell-Boltzmann relation that gives the velocity distribution of the particles as a function of their mass and temperature. Force field equations are used to determine the forces acting on each atom. Next, the positions and velocities are calculated at the next time step with the potential energy functions based on intramolecular and intermolecular attractions. The total velocity of the system should be zero. This algorithm is repeated for every time step and final trajectories are obtained for the system. [33] Equations 2.15, 2.16 and 2.17 are used to calculate velocity and atomic coordinates with the Velocity-Verlet method. [37]

$$v_{n+1/2} = v_n + a_n \frac{\Delta t}{2} \tag{2.15}$$

$$v_{n+1} = v_{n+1/2} + a_{n+1} \frac{\Delta t}{2} = v_n + \frac{a_n + a_{n+1}}{2} \Delta t = v(t_n + \Delta t) + O(\Delta t^3) \tag{2.16}$$

$$v_{n+1} = v_{n+1/2} + a_{n+1} \frac{\Delta t}{2} = v_n + \frac{a_n + a_{n+1}}{2} \Delta t = v(t_n + \Delta t) + O(\Delta t^3) \tag{2.17}$$

Where r is position, v is velocity, a is acceleration. t and Δt represent the time and the change in time. Figure 2.3 summarizes the MD algorithm.

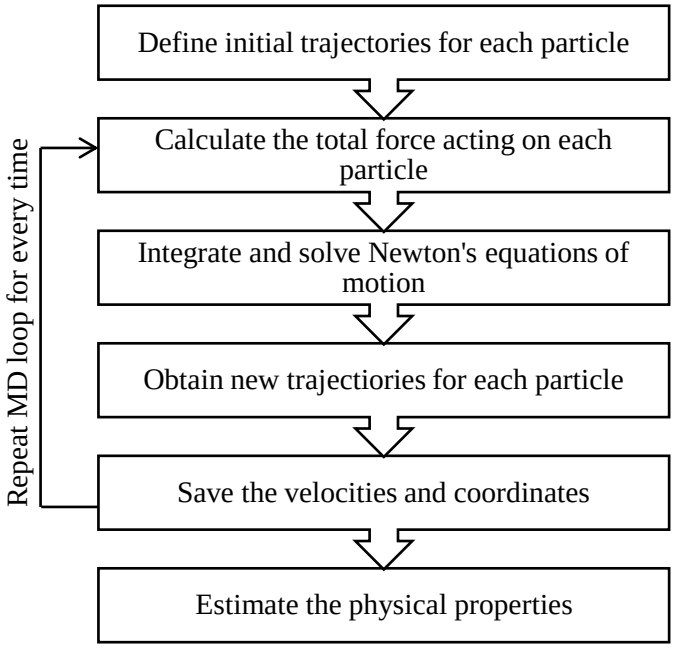

Figure 2.3. Molecular dynamics simulation algorithm.

CHAPTER 3

LITERATURE REVIEW

The properties of epoxy-graphene/GO nanocomposites are dependent on the chemical composition of the components and their intermolecular interactions. Epoxy structure, crosslinking density, type and the number of functional groups on the GO, and mass percentage of reinforcement material are the main parameters that affect the characteristics of the final nanocomposite material. In addition to the experimental studies in the literature, molecular modeling of epoxy polymers and their nanocomposites has attracted great interest. Therefore investigation of the structures and interactions at the molecular level gain importance. This chapter summarizes experimental and theoretical studies on the material properties of epoxy polymers and their nanocomposites.

3.1 Previous Studies on the Modeling of Epoxy Polymers

The two most common thermoset epoxy modeling methods in the literature are the in-situ crosslinking method and the representative molecule method. The in-situ crosslinking method allows the modeling of the random network and the fully periodic structure of the epoxy unit. In this method, reaction sites of epoxy and hardener are determined and crosslinking cut-off radius is defined mostly between 4-6 Å. Distances between crosslinking sites are continuously monitored during the MD simulations and when the distance between two atoms falls within the cut-off range, new crosslinks are formed. The representative molecule method is more straightforward than the in-situ crosslinking method and used by various researchers in the literature. In this method, the same pre-crosslinked molecules are loaded into the cell for modeling amorphous crosslinked structures. This representative molecule reflects the bulk crosslinking density and the overall crosslinked network topology.

Even though it is difficult to simulate a real crosslinked network with this method since no intermolecular crosslinks are assumed to exist between representative molecules, the results are similar to those of the in-situ crosslinking method and laboratory experiments. This method is also advantageous in the aspect of computational efficiency; it does not require complex iterative steps as in the in-situ method. [13] Besides, while investigating composite structures in terms of GO functional groups and mass percentage, keeping the epoxy models fixed will be useful to compare interactions, physical and mechanical properties.

Yu et al. [38] investigated the mechanical properties of Diglycidyl ether of bisphenol F (EPON862®) and Triethylenetetramine (TETA) epoxy-hardener system with the in-situ crosslinking method and representative molecule method. Epoxy monomer:hardener ratio was selected as 3:1. They performed an MD simulation to equilibrate the structure at 300 K and 1 atm using 900 ps of NPT simulation. They concluded that the method using representative molecules gives very close results to analytical and experimental findings. Kim et al. [13] used four different crosslinked structures as representative molecules using EPON862® and TETA with increasing crosslinking densities from 17% to 62.5%. They also used the in-situ crosslinking method to compare the results. Crosslinked structures were cooled from 500 K to 300 K with a cooling rate of 50 K/50 ps at NVT ensemble, then they performed 1 ns NPT simulation at 1 atm and 300 K to obtain the final equilibrated structure. They claimed that increasing the crosslinking density is better in terms of improving the mechanical properties and the results are in good agreement with the dynamic crosslinking method.

Choi et al. [39] and Shin et al. [40] increased the size of the representative molecules by using nine chains of EPON862® and three chains of TETA in their study. Shin et al. [40] investigated only the thermal properties and they stated that a molecule of this length is sufficient to allow entanglements and physical crosslinks to form between representative structures. These non-covalent interactions between pre-crosslinked representative molecules affect the density and physical properties of the epoxy system and describe accurately the characteristics of real epoxy. Choi et al.

[39] studied the mechanical properties by conducting a 500 ps simulation at the NVT ensemble, at 300 K followed by a 900 ps NPT ensemble at 300 K and 1 atm. They found that by changing the number of atoms in the cell or the thermal history of simulation, Young's modulus value of the epoxy system becomes higher as compared with their previous studies. For this study, a cooling-down process was performed before calculating elastic modulus which changed the optimum positions of atoms. Also, the initial representative molecule can influence the motion and final positions of atoms during MD simulations and atoms may not reach their lowest energy.

In terms of determining the force field for the system, PCFF and COMPASS are the most used force fields to simulate epoxy structures in the literature. Arab & Shokuhfar [41] investigated the effect of force field on the mechanical and physical properties of the DETA-DGEBA crosslinked structure. They used representative crosslinked molecules with DETA:DGEBA of 1:4 ratio to build cells. 500 ps molecular dynamics simulation at the NPT ensemble was performed at 298 K and 1 atm to reach the experimental density. They studied COMPASS, PCFF, Universal Force Field (UFF), and Dreiding force fields. It is concluded that for the DETA-DGEBA system COMPASS and PCFF force fields can be used for MD calculations since the results are in good agreement with experimental data. Moreover, COMPASS force field is suitable for this system since it represents long-range interactions and non-bonded interactions as vdW and hydrogen bonding interactions accurately.

3.2 Previous Studies on the Effect of Crosslinking Density on Mechanical Properties of Epoxy Resin

The ratio of the total number of crosslinked sites to the maximum allowable reaction site is known as crosslinking density. An increase in the crosslinking density improves the mechanical strength of the epoxy resin as the number of covalent bonds increases. [13] Table 3.1 represents Young's modulus and density values of DETA:DGEBA systems with different crosslinking densities in the literature. Results showed that the increasing crosslinking density significantly improves Young's modulus values of the polymer.

Table 3.1. Young's modulus and density values for DETA:DGEBA epoxy resins.

Type of Study	Crosslinking Density %	Density (g/cm^3)	Young's Modulus (GPa)	Ref.
MD	20-80 %	-	0.3-3.1	[42]
Experimental	-	1.16	3.4	[43]
MD	50 %	1.12	2.8	[44]
MD	0-81 %	1.08-1.15	2.8-3.8	[45]
MD	80 %	1.08	3.16	[41]

Increased crosslinking density may seem to be a desirable property at first glance, however, the interaction energy between the polymer and graphene oxide must be considered to obtain highly dispersed fillers. According to the studies of Putz et al. [46], Hadden et al. [47] and Kim et al. [13] as crosslinking density increases, interaction energy decreases at the interphase. When crosslinks were formed, the non-bond energies were significantly altered, and that resulted in a decrease in the interaction energy of the epoxy-GO system. Thus, an optimum crosslinking ratio might be needed to achieve better dispersion of fillers and mechanical properties.

3.3 Previous Studies on the Effect of Filler Properties, Dispersion and Mass Percentage on the Mechanical Properties of Epoxy Nanocomposites

Another factor influencing the mechanical properties of composite materials is the filler content of epoxy. As mentioned in previous sections, the primary objective is to obtain highly dispersed fillers in the epoxy matrix to improve mechanical performance. However, as the filler content increases, agglomeration becomes a problem for the efficiency of the reinforcement material. In the literature, there are various theoretical and experimental studies investigating the change in mechanical performance as filler content increases. Table 3.2 summarizes Young modulus values of different epoxy-hardener systems and filler contents in the literature.

Table 3.2. Young's modulus values for different epoxy-hardener systems containing Gr and GO fillers.

Type of Study	Type of Epoxy-Hardener	Filler %	Young's Modulus (GPa)	Ref.
Experimental	DGEBA-MHHPA	0-0.2% GO	2.9-3.1	[48]
Experimental	DGEBA-TETA	0-5% Graphene 0-5% G-EP*	2.5-4.6 2.5-5.6	[49]
Experimental	DGEBA-TETA	0-0.5% GO 0-0.5% rGO	2.6-3.43 2.6-3.35	[50]
MD	DGEBA-TETA	0% %18 Graphene %18 GO	3.16 5.63 6.36	[51]
MD	DGEBA-DEDTA	1-5% GO	2.96-5.72	[52]

*G-EP: Epoxide-functionalized graphene

The degree of dispersion of GO sheets has a significant effect on the final mechanical properties of the nanocomposite. Tang et al. [48] conducted an experimental study to investigate the effect of rGO dispersion on the mechanical properties of epoxy/graphene composites. They added rGO fillers in the epoxy matrix up to 0.2 wt % and mixed one sample with a ball mill to achieve better dispersion. The results showed that highly dispersed rGO fillers presented better elastic modulus and tensile strength compared to poorly dispersed fillers. Moreover, materials become more resistant to fracture with higher additive dispersion.

Zhao et al. [49] compared the performance of pristine graphene and epoxide-functionalized graphene oxide (G-EP) in terms of improving the mechanical properties of epoxy. They added up to 5% filler in the epoxy matrix and tested the tensile strength, Young's Modulus, and elongation at break values. They concluded that functionalized graphene has higher reinforcement efficiency as compared with pristine graphene. 124% improvement was reported in Young's modulus of epoxy with the addition of G-EP fillers. EP functionalized graphene sheets have better dispersion and adhesion properties in the epoxy matrix.

Aradhana et al. [50] experimentally investigated GO and rGO for the improvement of epoxy mechanical properties. rGO has fewer oxygen-containing functional groups than GO as a difference. According to the results, GO additives improved mechanical properties more than rGO additives. They added 0.5% and 1% filler into the epoxy matrix, and when the filler content reaches 1%, agglomerations start to form which reduced filler efficiency. This is the major barrier to using large amounts of reinforcement material. 29% improvement in Young's modulus was achieved when 0.5% GO was used.

Rahman and Haque [53] used MD simulations to investigate the effect of agglomeration and dispersion in an epoxy-graphene system. They constructed periodic cells containing three sheets of graphene, where one agglomerated and one dispersed within representative epoxy molecules. Each cell had less than 3% graphene by weight. Open-source molecular dynamics code LAMMPS [54] was

used for MD calculations. The epoxy-graphene system was equilibrated by MD simulations using NVT and NPT ensembles. Then the cell was deformed in xx-yy-zz directions. Stress-strain responses were plotted and it was concluded that dispersed graphene sheets have a higher aspect ratio and agglomeration decreases Young's Modulus values of the epoxy-graphene system.

Mechanical properties of epoxy-graphene nanocomposites were investigated by Shiu and Tsai [51] with MD simulations. They built cells containing epoxy and graphene or graphene oxide fillers with a weight fraction of 18%. GO fillers contained only epoxy and hydroxyl functional groups. MD simulations effectively demonstrated the positive effect of the dispersion of graphene sheets and functional groups. MD simulations at NVT and NPT ensembles were sequentially performed for calculations. Young's modulus of the nanocomposite increased with interactions between oxygen-containing groups and epoxy. Dispersed GO sheets possess the maximum reinforcement performance with higher interaction energy.

In the study of Yarahmadi et al. [52] the effect of the size of the graphene and the atomic ratio in epoxy on mechanical properties were investigated. They found that graphene sheet with 25 Å length have better mechanical performance compared with smaller graphene structures. When the atomic ratio was increased from 1% to 5% mechanical properties were enhanced. However, increasing the atomic ratio by 10% causes the mechanical properties to deteriorate which indicates there should be an optimum amount of filler content for higher performance.

CHAPTER 4

COMPUTATIONAL METHODOLOGY

Interaction energies between the components and the mechanical properties of the epoxy/GO nanocomposites are dependent on the composition and stoichiometry of epoxy monomer and curing agent, the crosslink density of epoxy, the number and type of functional groups on GO and the mass percentage of the filler in epoxy. These key parameters have to be optimized to increase the performance of the filler and nanocomposite. First principle calculations and molecular mechanics methods were used in this study to demonstrate the contribution of these parameters on interaction energies and Young's Modulus values. Computational studies can provide insight into the understanding of the chemical basis of reinforcement by the addition of GO filler. By using computational methods, it is possible to identify which functional groups improve interactions, adhesion and dispersibility significantly. In addition, it can be determined which of the functional groups on the epoxy structure gives the strongest interaction with the functional groups of GO fillers at the interface. Mixing energies were calculated to investigate the miscibility behavior of selected pairwise interactions between the components of Gr/GO-epoxy nanocomposites. Interaction energies were calculated by starting with more accurate DFT calculations using smaller representative models, and then MD simulations were performed for larger systems. MD simulations were performed to study the effect of type, size and mass percentage of Gr/GO filler on the Young's Modulus values. At last, radial distribution function analysis was performed for further analysis for the investigation of the main interactions of the functional groups in the equilibrated system to elucidate which interactions are mainly responsible for the reinforcement and mehanical property enhancements.

4.1 First Principle Calculations

DFT calculations were performed to study the accurate interaction energies between the functional groups on GO and the selected groups of the epoxy chain. Initial structures were prepared for small graphene and GO sheets which had only hydroxyl or epoxy functional groups on their surface as well as carboxylic acid or two carbonyl groups at the edges were represented in Figure 4.1. Functional groups of epoxy structures were selected as dimethyldiphenyl (DMDP), diamine, dialcohol, phenyletheralcohol, epoxy end group and aminealcohol were given in Figure 4.2. The most probable interactions were predicted and possible molecule configurations were constructed as initial structures using these molecules in Gaussian09. [55] More than one initial structures were prepared and geometry optimization calculations were performed for all these pairwise interactions, where one epoxy functional group has different possible configurations with graphene or GO. M06-2X functional which was developed by the Truhlar group in Minnesota [56] was selected for DFT calculations. It is one of the best performing global hybrid functional for nonbonding interactions. To include the correct asymptotic behavior of London dispersion in the long intermolecular distance regime, Grimme's D3 dispersion correction term [57] was added with the EmpiricalDispersion=GD3 command in Gaussian09. [55] Moreover, wB97XD functional which was developed by Chai and Head-Gordon was also used for the comparison of results. [58] 6-31+G(d) basis set which was developed by Pople [59] was selected for intermolecular interaction calculations. Basis set superposition error (BSSE) is an important correction parameter to consider for the calculation of intermolecular interactions. This error occurs due to the mixing of basis set functions of spatially close atoms and fragments that can result in artificial lower energy. [60] The counterpoise correction method was used to eliminate BSSE error where ghost orbitals with no protons or electrons were used to determine the mixed basis set functions.

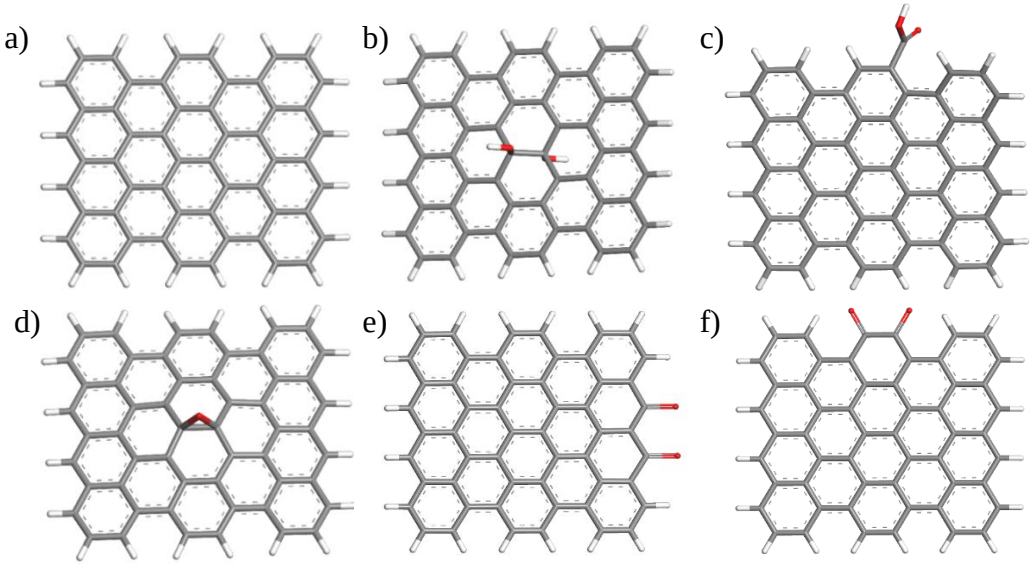

Figure 4.1. Graphene structures used for DFT calculations a) graphene (Gr) b) GO with hydroxyl group (Gr-OH) c) GO with carboxylic acid group (Gr-COOH) d) GO with epoxy group (Gr-epo) e) GO with carbonyl groups-zigzag (Gr-diketone1) f) GO with carbonyl groups-armchair (Gr-diketone2).

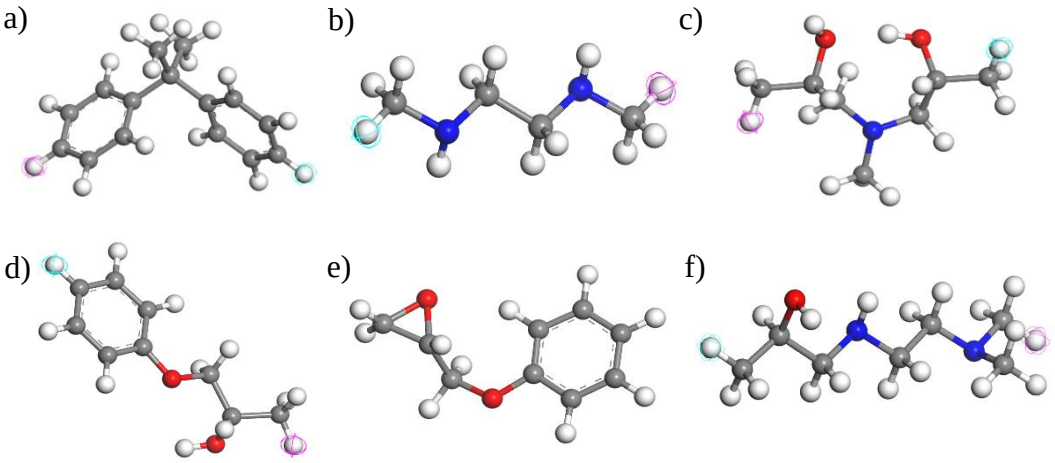

Figure 4.2. Possible functional groups in epoxy chains a) Epo-DMDP b) Epo-diamine c) Epo-dialcohol d) Epo-phenetheralcohol e) Epo-epoend f) Epo-aminealcohol.

Selected atom groups are depicted for one of the DFT based interaction energy calculation in Figure 4.3 as two groups to identify the interacting molecule pairs.

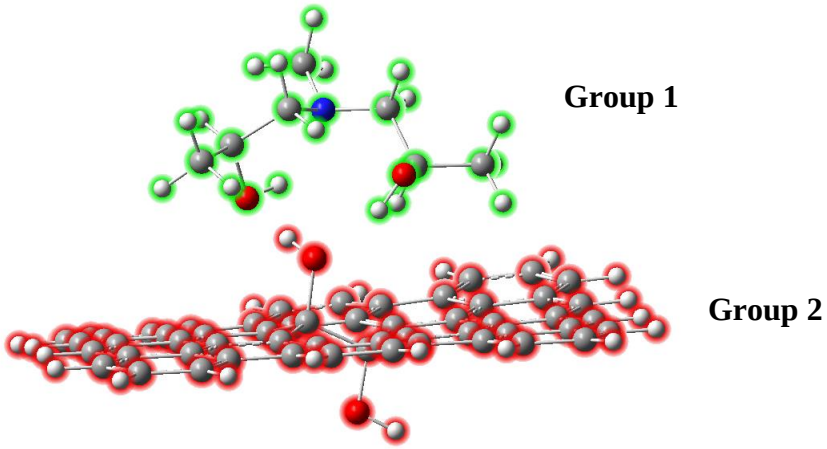

Figure 4.3. Selection of interacting functional groups for DFT calculations.

4.2 Classical Monte Carlo and Molecular Dynamics Methods

Classical Monte Carlo and Molecular Dynamics simulation methods were used to investigate the interaction energies and Young's Modulus values of different epoxy-graphene/graphene oxide nanocomposite systems. Large systems containing thousands of atoms can be studied by using classical mechanics methods and simulations which are theoretical in-silico experiments to mimic real-life in-situ experiments. MD simulations can reveal how functional groups of GO can affect mechanical characteristics at the molecular level details including bonded and non-bonded interactions as well as optimization of the parameters for improved filler dispersibility in the polymer matrix. Moreover, these interactions can be examined independently per functional group type and number, and the composition of representative epoxy chains. To demonstrate these effects, epoxy chains containing varying epoxy:hardener ratios and GO structures containing different numbers and types of functional groups were modeled in this study.

4.2.1 Calculation of Mixing and Pairwise Binding Energies Based on the Molecular Mechanics Calculations

Flory-Huggins [61] model is a well-known theory that represents the miscibility behavior of the binary systems. Free energy of mixing per mole (ΔG_{mix}) was calculated from Equation 4.5.

$$\frac{\Delta G_{mix}}{RT} = \frac{\phi_i}{n_i} ln\phi_i + \frac{\phi_j}{n_j} ln\phi_j + \chi\phi_i\phi_j \quad (4.5)$$

Where R is the gas constant, T is the absolute temperature, χ is the interaction parameter. For the components i and j, n_i and n_j represents the degree of polymerization, and volume fractions were given with ϕ_i and ϕ_j.

Interaction parameter (χ) was calculated from Equation 4.6.

$$\chi = \frac{E_{mix}}{k_B T} \quad (4.6)$$

Where E_{mix} is the mixing energy and k_B is the Boltzmann constant.

In this study, the miscibility behavior of the Gr/GO functional groups and epoxy molecules was calculated by the combination of Flory-Huggins model and molecular mechanics techniques. Coordination numbers and the binding energies for each molecular pair were determined by performing Monte Carlo type minimizations of a large number of cluster interactions. As a difference with Flory-Huggins theory, the interaction parameter was explicitly calculated depending on temperature by using Boltzmann factor, exp (-E/RT). Moreover, molecular simulations were used to determine coordination numbers for each molecular pair and the molecules were not placed on a regular lattice. [62] To accurately represent the behavior of a real chain, the head and tail atoms of a polymer backbone are chosen to not interact. Geometry optimizations were performed by using semiempirical PM6 calculations. Merz-Kollman based ESP algorithm [63] for B3LYP basis set at DNP level was used to calculate atomic charges of geometry optimized structures. Tkatchenko-Scheffler

(TS) [64] parameters were applied for vdW dispersion and hydrogen bonding corrections. The average binding energy at room temperature was calculated by creating 10^7 different block configurations and using the average of the weighted distribution function (P_{ij}), which was shown in Equation 4.8.

$$\langle E_{ij} \rangle_T = \frac{\int dE\ E\ P_{ij}(E) e^{-\frac{E}{RT}}}{\int dE\ P_{ij}(E) e^{-\frac{E}{RT}}} \tag{4.7}$$

Mixing energy, which is the difference in free energy due to the interaction between the mixed and pure state was given in equation 4.8. It was calculated by forming 10^5 clusters.

$$E_{mix} = \frac{1}{2}(Z_{ij}\langle E_{ij}\rangle_T + Z_{ji}\langle E_{ji}\rangle_T - Z_{ii}\langle E_{ii}\rangle_T - Z_{jj}\langle E_{jj}\rangle_T) \tag{4.8}$$

where E_{ij} is the binding energy and Z is the coordination number.

Additional possible GO structures to the ones given in Figure 4.1, were also investigated to calculate mixing energies and pairwise binding energies for hydroxyl and carbonyl groups for different configurations. These structures were given in Figure 4.4.

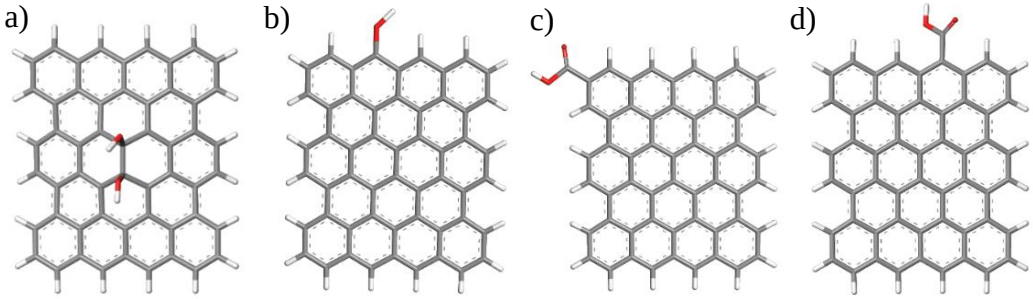

Figure 4.4. GO structures for mixing energy calculations a) GO with hydroxyl groups at same side (Gr-OH2), b) GO with one hydroxyl group at edge (Gr-OH3), c) GO with carboxylic acid group at corner-edge (Gr-COOH2) d) GO with carboxylic acid group at zigzag-edge (Gr-COOH3).

4.2.2 Effect of the Number of Oxygen-Containing Functional Groups on the Interaction Energies

In this section, change in the interaction energy was investigated for fix the composition of epoxy chains, while systematically increasing the amount of oxygen-containing functional groups on the GO surface. Epoxy models were created according to the possible reactions and ratios between repeat units as a first step for the MD simulations. The representative molecule method was used to build epoxy molecules since this method has been proven to give results very close to experiments by different researchers. It is also computationally effective to utilize the same epoxy molecules for every calculation which can generate consistent results while changing the type and number of GO functional groups. Crosslinking ratio was determined by dividing occupied reaction sites by the number of possible reaction sites of the DETA molecule. DETA molecule has five reaction sites including primary and secondary amine groups. Therefore, each DETA molecule can react with five DGEBA molecules to generate a fully crosslinked structure. This ratio was calculated by modeling the first representative epoxy molecule model manually which was shown in Figure 4.5. This structure has ten DGEBA and four DETA molecules with a 65% crosslinking ratio and it was mainly used in this study for building nanocomposites containing different GO structures.

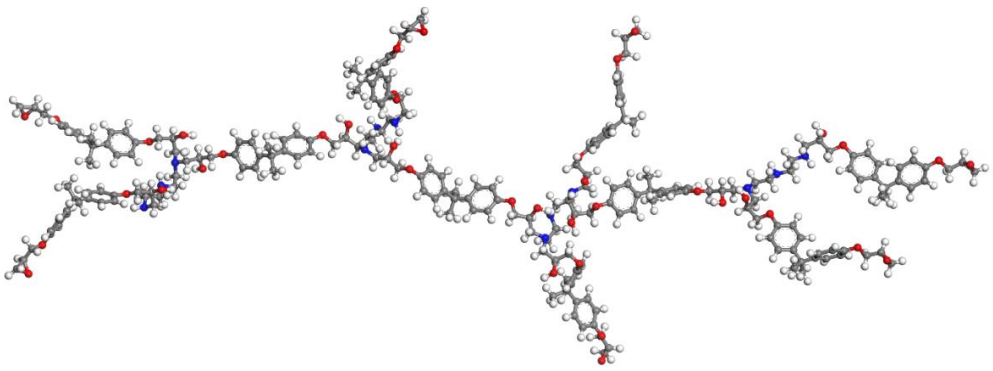

Figure 4.5. Representative epoxy molecule DGEBA:DETA = 10:4.

As a next step, an infinite-sized periodic graphene or graphene oxide sheet was placed at the center of a 46x46x120 $Å^3$ sized super cell to investigate the effect of the number of functional groups on the interaction energies and mechanical properties. It should be noted that graphene sheets can have more than 100 nm sizes that can be accepted as infinite surfaces for the MD simulations. Hydroxyl and epoxy functional groups were present only on the surface of these GO structures since the Lerf-Klinowski GO model [18] predicts that carbonyl and carboxyl groups are primarily located at the edges. Graphene oxide models contain 836 carbon atoms for each cell. Epoxy and hydroxyl groups were attached on both sides of the GO surface randomly at different oxygen ratios. GO structures with oxygen percentages of 0%, 5%, 8%, 10%, 13%, 15%, 18% and 20% were prepared and some of them were given in Figure 4.6 as a representation. GO sheets were used for interaction energy calculations since they possess a larger surface area and can represent the interactions with epoxy functional groups more clearly.

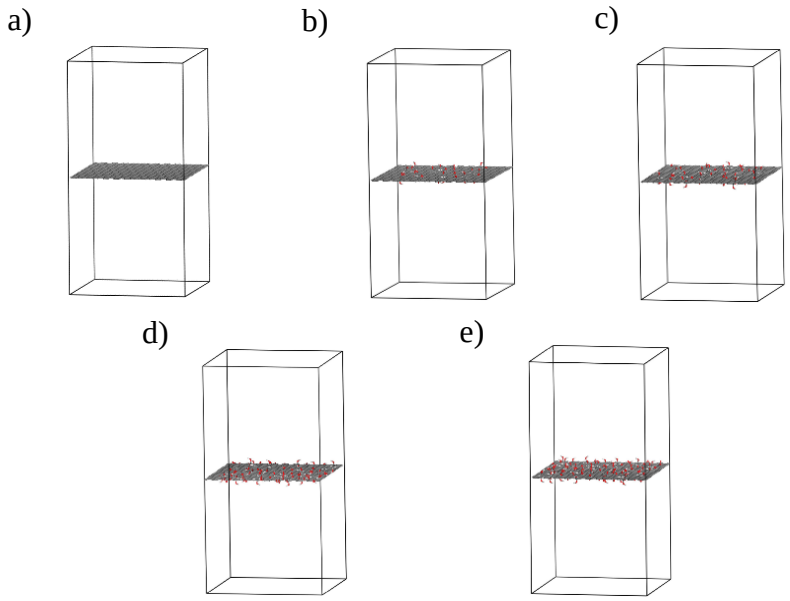

Figure 4.6. GO structures under periodic boundary conditions with a) graphene with 0% oxygen, b) GO with 5% oxygen, c) GO with 10% oxygen, d) GO with 13% oxygen, e) GO with 15% oxygen.

MAPS software package (Materials and Process Simulations, Version 4.4) developed by Scienomics which provides a direct interface for the LAMMPS software was used to build and simulate models. Initial conformations were generated within the Amorphous Builder. Amorphous cells containing disorganized polymer conformations were created with a method developed by Theodorou & Suter [65] which uses the Monte Carlo sampling method and minimizes close contact between atoms to build structures with realistic conformations. Position, orientation and torsion values for input molecules were added in a stepwise manner for each molecule and every molecule was positioned accordingly into the cell. Torsion states are considered continuous and every conformational state is defined by a torsion potential by using the parameters of the selected force field. The maximum number of attempts to load all epoxy model chains into the cell was selected as 2000 steps.

The initial density was defined as 0.6 g/cm^3, the final temperature was selected as 298 K and there was no external pressure during the packing procedure. After building at least 50 cells for every structure, geometry optimization was performed for a maximum of 10000 iterations for each cell with energy convergence criteria of 0.001 kcal/mol and force criteria of 0.5 kcal/mol/Å. Structures with the lowest potential energy configurations were determined to prevent energy fluctuation errors during the MD simulations. For the electrostatic summation method, the PPPM method was selected since it gives faster results for large systems at high CPU units compared to the Ewald summation method. The cut-off distance was selected as 12.5 Å for non-bonded vdW interactions.

After the selection of the composite cell structures with the lowest potential energies for each set, MD simulations were performed with the open-source software package LAMMPS (Large-scale Atomic/Molecular Massively Parallel Simulator).[54] The simulations were run at TUBITAK ULAKBIM, High Performance and Grid Computing Center (TRUBA resources) at levrek grid.

As a force field, SciPCFF (Scienomics Polymer Consistent Force Field) was used since it contains bonded and non-bonded parameters for all atom types and functional

groups in epoxy and graphene oxide. Moreover, this force field enables modeling of the cell structures with the density, mechanical and other physical properties having close values with the experimental data. SciPCFF is a consistent Class II force field parameterized by using quantum chemical calculations and experimental data using the improved set of molecular interaction equations as PCFF. [66] However, the 9-6 Lennard-Jones (LJ) potentials and the bond increment parameters from COMPASS [34] are also included in the SciPCFF equations as an improvement. MD simulations were performed at the NPT ensemble at 298 K temperature under 1 atm pressure. The Nose/Hoover thermostat and barostat method was used to keep the temperature and pressure constant with the fixed shape of the cell. 5000 ps simulations were performed with a 1 fs time step for all cells where density, energy and temperature were validated at the end of each simulation.

Potential energy including bonded, non-bonded and electrostatic terms was calculated for the nanocomposite system, epoxy molecules and periodic GO structures separately to determine the interaction energy. Interaction energies were calculated by subtracting the total energy of epoxy molecules (E_{Epoxy}) and GO (E_{GO}) molecules from the total energy of the system (E_{system}) as given in Equation 4.1.

$$Interaction\ Energy\ \left[\frac{kcal}{mol}\right] = E_{system}\left[\frac{kcal}{mol}\right] - (E_{Epoxy} + E_{GO})\left[\frac{kcal}{mol}\right] \qquad (4.1)$$

4.2.3 Effect of the Epoxy:Hardener Ratio on the Interaction Energies

In this part, different epoxy representative structures having different epoxy:hardener ratios were used in simulations. Epoxy molecules with different DETA:DGEBA ratios were used to build nanocomposite structures containing periodic GO sheets with an increasing number of functional groups. Five pre-crosslinked epoxy structures used in the MD simulations were given below in Figure 4.7. To build molecules of nearly equal size, the total number of DETA and DGEBA molecules is kept constant at 18. For this part, periodic GO sheets containing epoxy and hydroxyl functional groups with oxygen percentages of 5%, 12% and 18% were

used for calculations. It was aimed to observe the effect of the DETA:DGEBA ratio on interaction energies and mechanical properties for low, medium and high oxygen amounts on GO. Cells were constructed with 0.5 g/ cm^3 initial density and the same geometry optimization and MD simulation methodology were followed as given in the previous section.

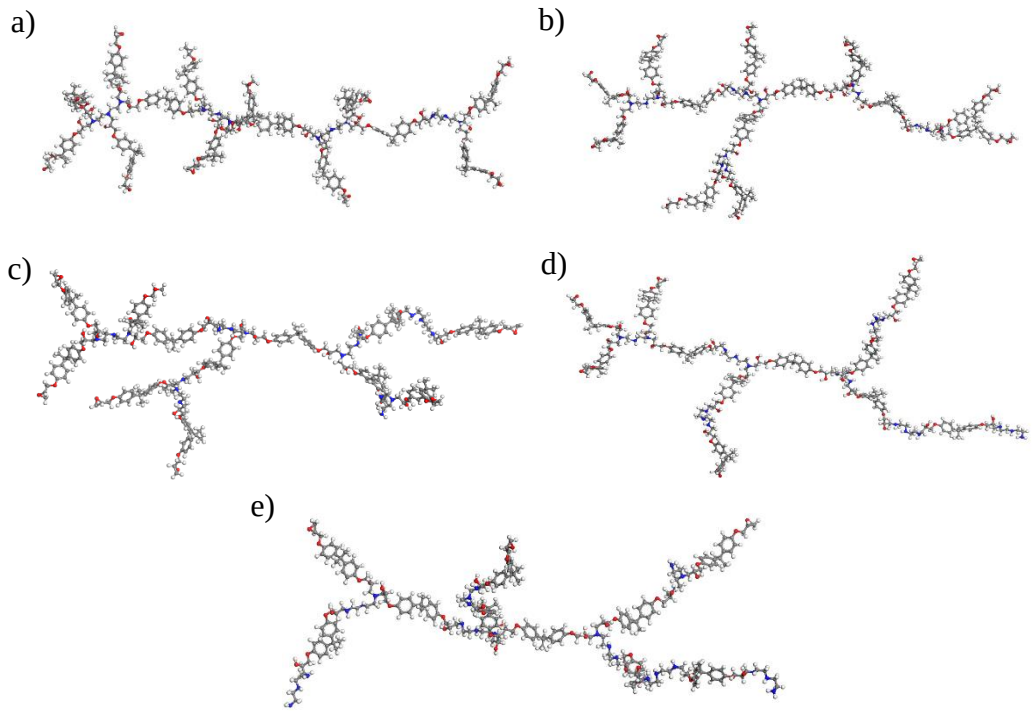

Figure 4.7. Representative epoxy molecules a) DETA:DGEBA = 4:14, 85% crosslinked b) DETA:DGEBA = 5:13, 68% crosslinked c) DETA:DGEBA = 6:12, 56% crosslinked d) DETA:DGEBA = 7:11, 49% crosslinked e) DETA:DGEBA = 8:10, 38% crosslinked.

4.2.4 Effect of GO Type on the Interaction Energies

Chemical composition of GO was controlled according to the experimental data provided by our industrial collaborator and the same type of the representative epoxy chain was used for investigation of interaction energies in this section. Since the experimental GO structure contains carbonyl and carboxylic acid functional groups at the edges, small GO representative structures were built to study the effect of these functional groups located at the edges. Graphene structures were constructed at 2.4 nm size which was determined for end-to-end C-C distance, containing 252 carbon and 44 hydrogen atoms with a molecular mass of 3071.12 g/mol. Hydroxyl, epoxy, carboxylic acid and carbonyl functional groups were randomly located on the GO structure with the oxygen atomic ratios at 6%, 13% and 18% as shown in Figure 4.8. GO structures containing 13% oxygen (AA90) and 18% oxygen (AA50) were built by using the experimental data provided by Nanografi Company. Fourier-transform infrared spectroscopy (FTIR) and X-ray photoelectron spectroscopy (XPS) method were used to determine the compositions of the samples. The percentages of all functional groups in the structures were given in Table 4.1. Cells were built with the size of 46x46x90 Å and one sheet of graphene or GO was placed in the middle of the cell as shown in Figure 4.9. Representative epoxy molecules containing ten DGEBA and four DETA molecules were packed into the cell with 0.5 g/cm^3 initial density. The same geometry optimization and MD procedure were followed as given in the previous sections.

Table 4.1. Chemical compositions of GO structures.

	GO with 6% Oxygen	**GO with 13% oxygen (AA90)**	**GO with 18% oxygen (AA50)**
O (%)	6	13	18
C (%)	94	87	82
-OH (%)	40.0	45.9	37.8
C-O-C (%)	40.0	41.8	40.1
C=O (%)	13.3	10.7	18.6
-COOH (%)	6.7	1.6	3.5

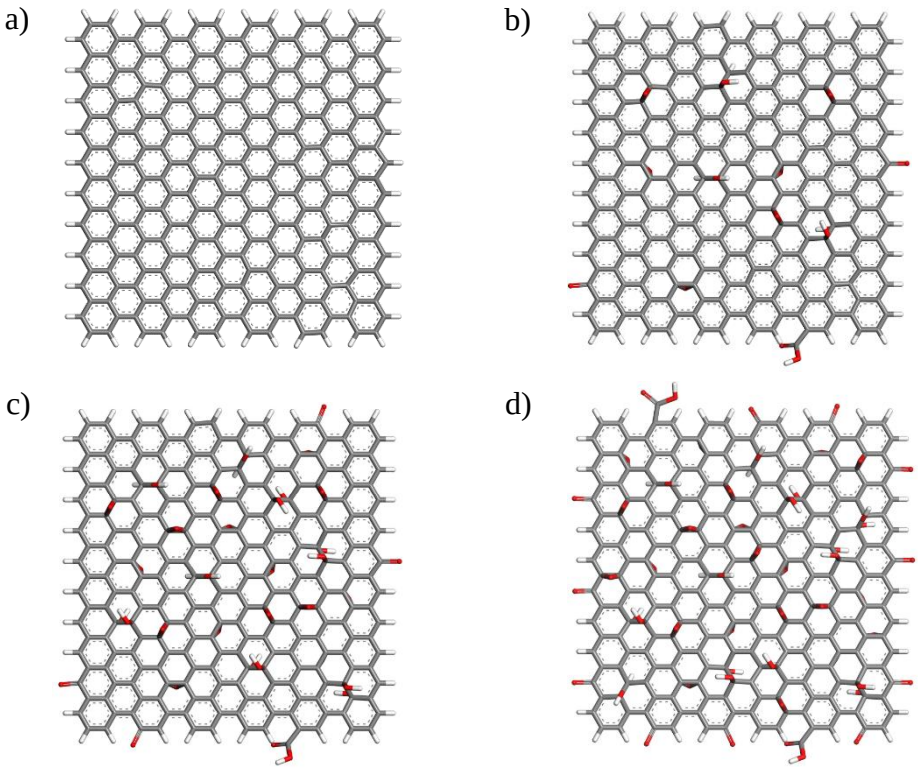

Figure 4.8. Gr and GO filler structures as a) graphene, b) GO with 6% oxygen c) GO with 13% oxygen (AA90) and d) GO with 18% oxygen (AA50).

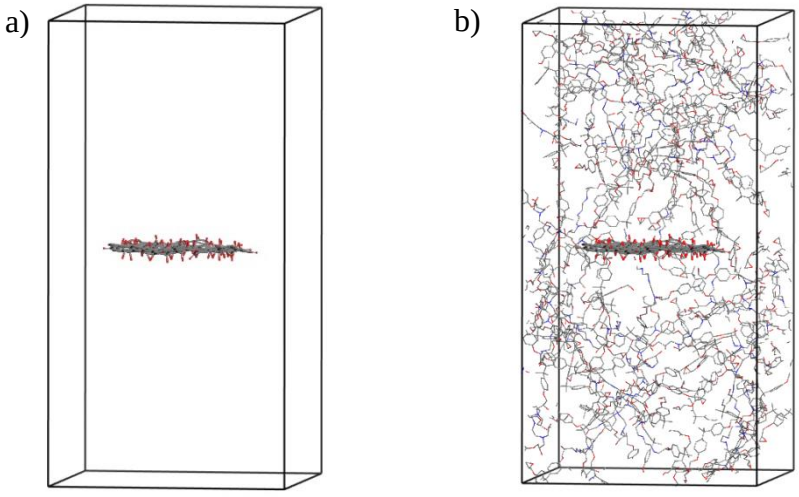

Figure 4.9. Molecular Model for a) Cell containing 1 sheet of GO (AA50) b) cell after packing with representative epoxy molecules.

4.2.5 Effect of GO Type and Mass Percentage on the Young's Modulus and the Interaction Energies

To study the effect of the type and mass percentage of the filler, larger cells with 85x85x85 Å dimensions were prepared to contain GO fillers with 2%, 4%, 6% and 8% by weight. AA50 and AA90 GO sheets containing different amounts of oxygen-containing functional groups were packed into the cells randomly and the same representative epoxy molecule containing a DETA:DGEBA ratio of 4:10 were packed into this cell with 0.5 g/cm^3 initial density. Nanocomposite structures with various filler percentages prepared by increasing the number of GO sheets were given in Figure 4.10.

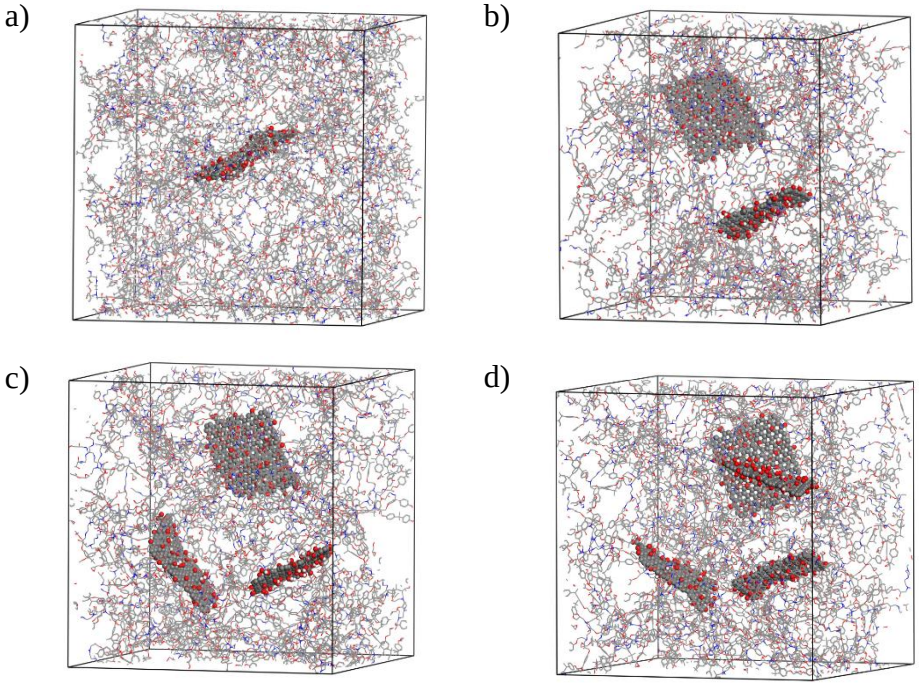

Figure 4.10. Epoxy-GO nanocomposites with a) 2 wt% filler b) 4 wt% filler c) 6 wt% filler d) 8 wt% filler.

Geometry optimizations were performed for each cell with 5000 iteration steps by optimizing the atomic coordinates without cell parameter optimization. 50 amorphous cell structures were built for each set and structures with the lowest energy configurations were selected as initial structures for performing MD calculations. 5000 ps simulation at the NPT ensemble was performed at 1 atm and 298 K similar to the previous sections.

For Young's Modulus calculations, the final trajectory was used for analysis. Young's modulus was calculated with the constant strain method. [65] Maximum strain amplitude was selected as ±0.003 with the number of strains as 4. Structures were pre-optimized while keeping the cell parameters constant to obtain the lowest energy configuration and prevent incorrect results.

Elastic Modulus or Young's Modulus is calculated by the ratio of the stress to strain and gives the material's resistance to elastic deformation. [67] The strain tensor is defined with Equation 4.2.

$$\varepsilon = \begin{pmatrix} \varepsilon_{11} & \varepsilon_{12} & \varepsilon_{13} \\ \varepsilon_{21} & \varepsilon_{22} & \varepsilon_{23} \\ \varepsilon_{31} & \varepsilon_{32} & \varepsilon_{33} \end{pmatrix} \tag{4.2}$$

Moreover, the stress tensor can be determined by selecting a constant number of atoms and temperature as the change in free energy with respect to strain. The stress tensor (σ) is calculated by:

$$\sigma = -\frac{1}{V}\sum_{i=1}^{N} \langle m_i v_i {v_i}^T + \frac{1}{2}(r_i {F_i}^T + F_i {r_i}^T) \rangle \tag{4.3}$$

Where m_i is the mass, v_i is the velocity, r_i is the position, F_i is the force of particle i, V is volume and N is the number of particles.

Generalized Hooke's law can be used to describe the stress-strain behavior of the material and it is given in Equation 4.4.

$$\sigma_i = C_{ij}\varepsilon_j \tag{4.4}$$

The stress vector is represented by σ_i in the Voigt notation of the stress tensor, while the strain vector is represented by ε_j. C_{ij} is the 6x6 stiffness matrix.

Moreover, the effect of dispersion on interaction energies was investigated by integrating stacked GO sheets in the cell. AA90 structures tend to aggregate more than AA50 since they contain fewer oxygen-containing functional groups. Thus, the AA90 structure was selected for preparing configurations with four layer pi-stacked sheets and two layer pi-stacked sheets, which were given in Figure 4.11. The weight percentage of the samples was fixed to 8 wt% and compared with the dispersed GO configurations.

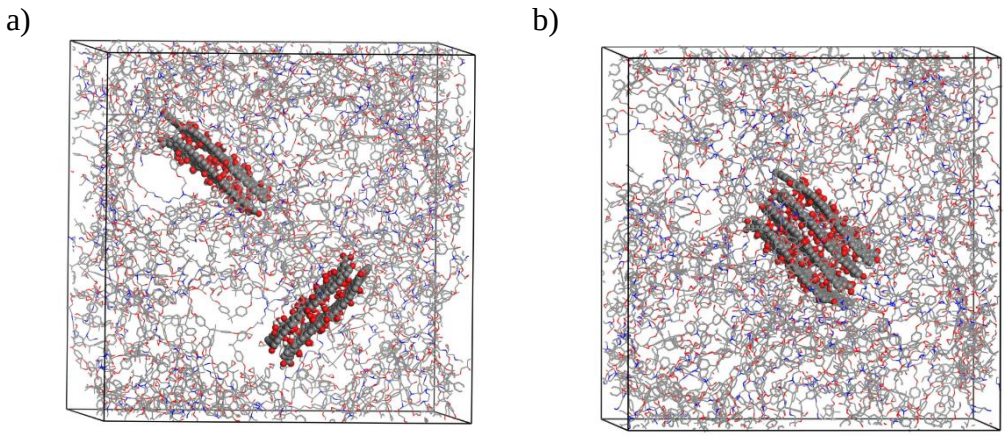

Figure 4.11. Cell models with stacked GO structures a) two layer pi-stacked b) four layer pi-stacked

4.2.6 Effect of Epoxy:Hardener Ratio on the Young's Modulus and the Interaction Energies

Different representative epoxy molecules with DETA:DGEBA ratios of 4:14, 5:13, 6:12, 7:11 and 8:10, given in Figure 4.5, were used in this part of MD simulations to investigate the effect of epoxy:hardener ratio on the Young's Modulus values. GO type was fixed for this part and GO model named AA50 was used for construction of nanocomposites. Three AA50 sheets were placed into the cell with a 6 wt% ratio, similar to Figure 4.8c. 85x85x85 Å sized cells were built with 0.5 g/cm^3 density and 5000 ps NPT dynamics was performed at 1 atm and 298 K to equilibrate the structures. Interaction energy and Young's Modulus values were calculated by following the same procedure given in the previous sections.

4.2.7 Effect of the Size of the Filler on the Young's Modulus and the Interaction Energies

Three GO structures with different-size were prepared to investigate the effect of filler size parameters on Young's Modulus and interaction energies. The type of the representative epoxy molecule was fixed with the model which has DETA:DGEBA ratio of 4:10. Figure 4.12 was demonstrating the developed GO structures, which have 252, 132 and 66 carbon atoms with the size of 2.4 x 2.4 nm, 2.4 x 1.2 and 1.1 x 1.2 nm. Relatively small sized GO structure has 14, medium sized GO structure has 28 and large sized GO has 56 oxygen-containing functional groups which were randomly attached on the surface and the edges which is 21% oxygen for every structure. 85x85x85 Å cells containing 2, 4 and 8 GO fillers were prepared by keeping the total oxygen amount of the system constant which was given in Figure 4.13. Amount of GO in the system is 7 wt%. The same MD calculation procedure was followed similarly to the previous sections and Young's Modulus and interaction energies were calculated for each nanocomposite system.

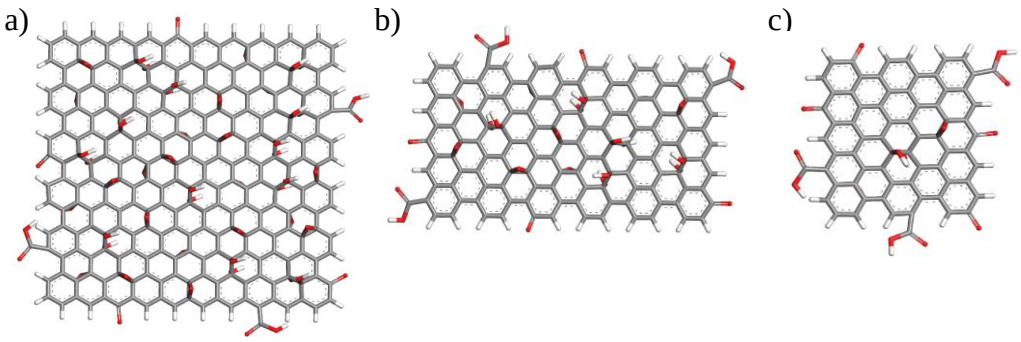

Figure 4.12. GO models with a size of a) 2.4 x 2.4 nm (GO252) b) 2.4 x 1.2 nm (GO132) c) 1.1 x 1.2 nm (GO66).

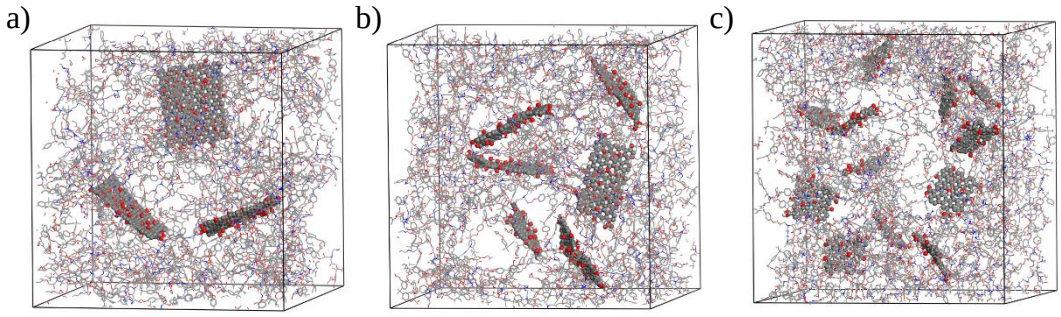

Figure 4.13. Cell models containing a) 2.4 x 2.4 nm, b) 2.4 x 1.2 nm and c) 1.1 x 1.2 nm GO fillers.

CHAPTER 5

RESULTS & DISCUSSION

5.1 Density Functional Theory (DFT) Calculations

DFT calculations were performed to investigate the interactions between Gr/GO functional groups and different groups on the epoxy chains. These calculations were performed for the structures given in Figure 4.1 and Figure 4.2. Counterpoise corrected complexation energy results were summarized in Table 5.1 for two different functionals. The strongest interaction energy was observed between Gr-COOH group at the edges and Epo-dialcohol group for both two DFT functionals used for the calculations. Optimized structures were depicted in Figure 5.1 where the atomic distances were given in the units of Angstrom (Å). Three separate hydrogen bonds were determined between oxygen groups of Gr-COOH and hydrogens of epoxy -OH groups, and between the hydrogen group of Gr-COOH and nitrogen of the epoxy amine group. One of these interactions was very strong in that there was a shared proton that can be transferred from the carboxylic acid to the amine group as given in Figure 5.1a and Figure 5.1b. Calculations showed that there are two possible geometries for the interaction between Gr-Epo and Epo-dialcohol where proton stayed on the –COOH edge of the GrO and proton is transferred to the amine group on epoxy. Second one is slightly more stable that resulted in the formation of carboxylate anion group and ammonium cation leading to the highly increased intermolecular interaction between counterparts. The second strongest interaction was observed between Gr-OH and Epo-aminealcohol as given in Figure 5.1c. There were also two hydrogen bonds between the nitrogen of the epoxy amine group and hydrogen of the Gr-OH group, as well as between the hydrogen of the epoxy -OH group and oxygen of the Gr-OH group.

Table 5.1. Interaction energies between GO functional groups and epoxy functional groups by using two different DFT functionals at 6-31g(d) basis set.

Graphene Part	Epoxy Part	E_{int} (M06-2X-D3) (kcal/mol)	E_{int} (wB97XD) (kcal/mol)
Gr	Epo-dialcohol	-12.20	-15.20
	Epo-aminealcohol	-15.27	-17.80
	Epo-diamine	-11.50	-13.35
	Epo-DMDP	-13.50	-17.31
	Epo-epoend	-13.53	-16.14
	Epo-phenetheralcohol	-16.19	-19.08
Gr-OH	Epo-dialcohol	-23.48	-25.41
	Epo-aminealcohol	-24.07	-25.97
	Epo-diamine	-21.36	-22.96
	Epo-DMDP	-12.44	-15.00
	Epo-epoend	-15.45	-16.57
	Epo-phenetheralcohol	-18.53	-20.53
Gr-COOH	Epo-dialcohol	-28.75 (-134.13)*	-29.67 (-133.82)*
	Epo-aminealcohol	-15.76	-17.03
	Epo-diamine	-20.23	-20.74
	Epo-DMDP	-13.50	-17.18
	Epo-epoend	-16.01	-16.30
	Epo-phenetheralcohol	-18.24	-19.77
Gr-epo	Epo-dialcohol	-10.96	-16.75
	Epo-aminealcohol	-13.89	-15.66
	Epo-diamine	-11.87	-12.89
	Epo-DMDP	-14.94	-17.54
	Epo-epoend	-14.10	-16.39
	Epo-phenetheralcohol	-12.50	-13.89
Gr-diketone1	Epo-dialcohol	-20.87	-23.51
	Epo-aminealcohol	-20.83	-22.30
	Epo-diamine	-12.85	-14.12
	Epo-DMDP	-18.41	-19.62
	Epo-epoend	-14.12	-16.19
	Epo-phenetheralcohol	-19.03	-24.70
Gr-diketone2	Epo-dialcohol	-16.82	-17.18
	Epo-aminealcohol	-17.98	-20.23
	Epo-diamine	-11.65	-12.52
	Epo-DMDP	-14.86	-17.05
	Epo-epoend	-13.25	-15.16
	Epo-phenetheralcohol	-19.03	-20.62

* Interaction energy after the proton transfer from Gr-COOH to the amine group.

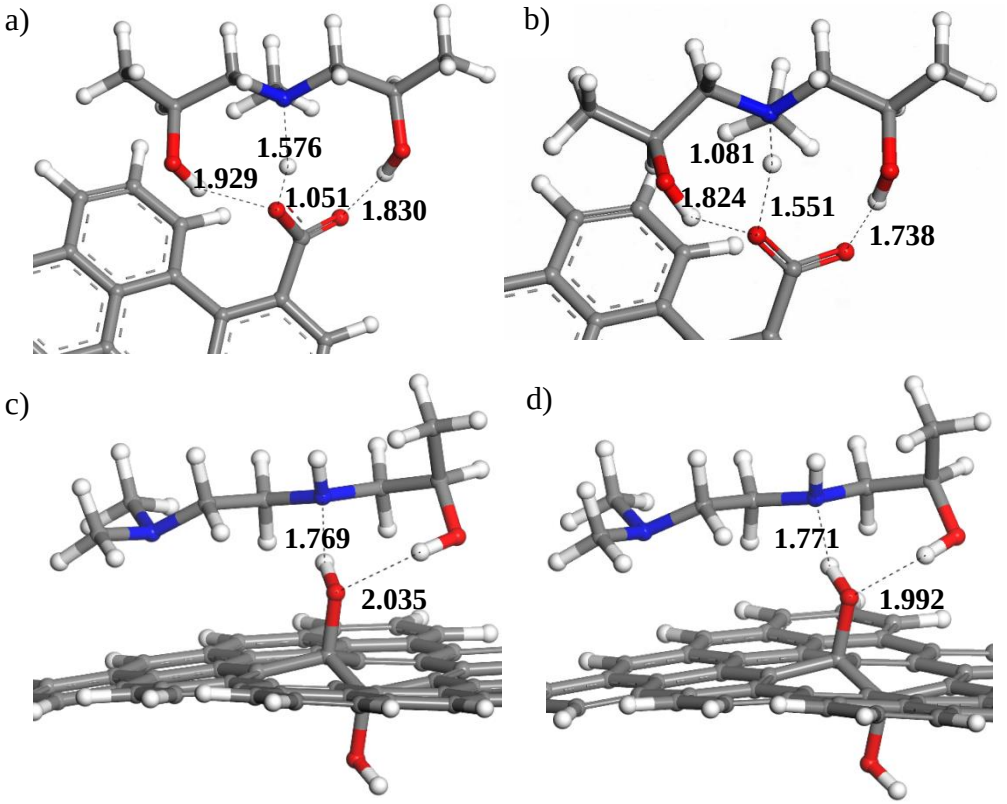

Figure 5.1. Hydrogen bonds and atomic distances between Gr-Epo and Epo-dialcohol by using M06-2X functional a) proton is close to the –COOH on GrO b) proton transferred to the amine group on epoxy. Hydrogen bonds and atomic distances between Gr-OH interaction with Epo-aminealcohol by using c) M06-2X functional d) wB97XD functional.

Hydrogen bonding and lowest atomic distances for the optimized geometries were given for each possible set of pairs from Figure 5.2 to Figure 5.7. The weakest interactions were observed mainly for the pristine unmodified graphene structure and Gr-epo structures in interaction with different epoxy functional groups. Intermolecular distances were significantly higher for these weak interactions. All the intermolecular distances are higher than 2.7 Å for graphene intermolecular interactions as given in Figure 5.2 since graphene has not any functional groups on its surface to interact with epoxy functional groups. Since there are polar groups such

as alcohol, amine and ether on the epoxy resin, non-polar functional groups on the graphene cannot enhance the intermolecular interactions. For the Gr-OH structures given in Figure 5.3, the hydrogen bond distance between atoms is as low as 1.7 Å and the intermolecular interactions were increased. For this part, Gr-OH and Epo-DMDP provide the lowest interactions as expected, since phenyl and methyl groups on the epoxy functional group do not have any oxygen or amine atoms in their structure and they could not form any hydrogen bonds. The highest interaction energies were observed when two hydrogen bonds were present between Gr-OH and nitrogen and oxygen atoms of epoxy chains. Gr-COOH has the highest interaction energies since -COOH has both hydrogen bond donor proton and hydrogen bond acceptor oxygen atoms to form hydrogen bonds. When the number of -NH and -OH groups were increased on the epoxy chain, interactions can be increased. Similarly, the highest distance and lowest energy were observed with Epo-DMDP since there were not any hydrogen bonds present as given in Figure 5.4. For Gr-Epo structures in Figure 5.5, atomic distances were higher and interaction energies were lower compared to the Gr-OH and Gr-COOH since they are less polar groups. A significant increase in the interaction energies was not observed for Gr-Epo structures compared with the interactions of pristine graphene with epoxy functional groups. For two different configurations of carbonyl groups as given in Figure 5.6, Gr-diketone1 provided higher interaction energies compared to Gr-diketone2. The location of carbonyl groups on the zigzag edge is more suitable for the formation of two hydrogen bonds compared to the two neighboring carbonyl groups on the armchair edge due to the closer distance. It should be noted that these results are only for epoxy, thus different polymers can form different intermolecular interactions with GO. It can be speculated that the GO structure should have more polar groups to form strong interactions with the polar polymers such as polyurea that have many polar units. Epoxy resin that has average polarity with both polar and nonpolar groups on it requires an average amount of polar functional groups on GO. This means that companies should include different GO structures in their products to be used as filler for different polymers.

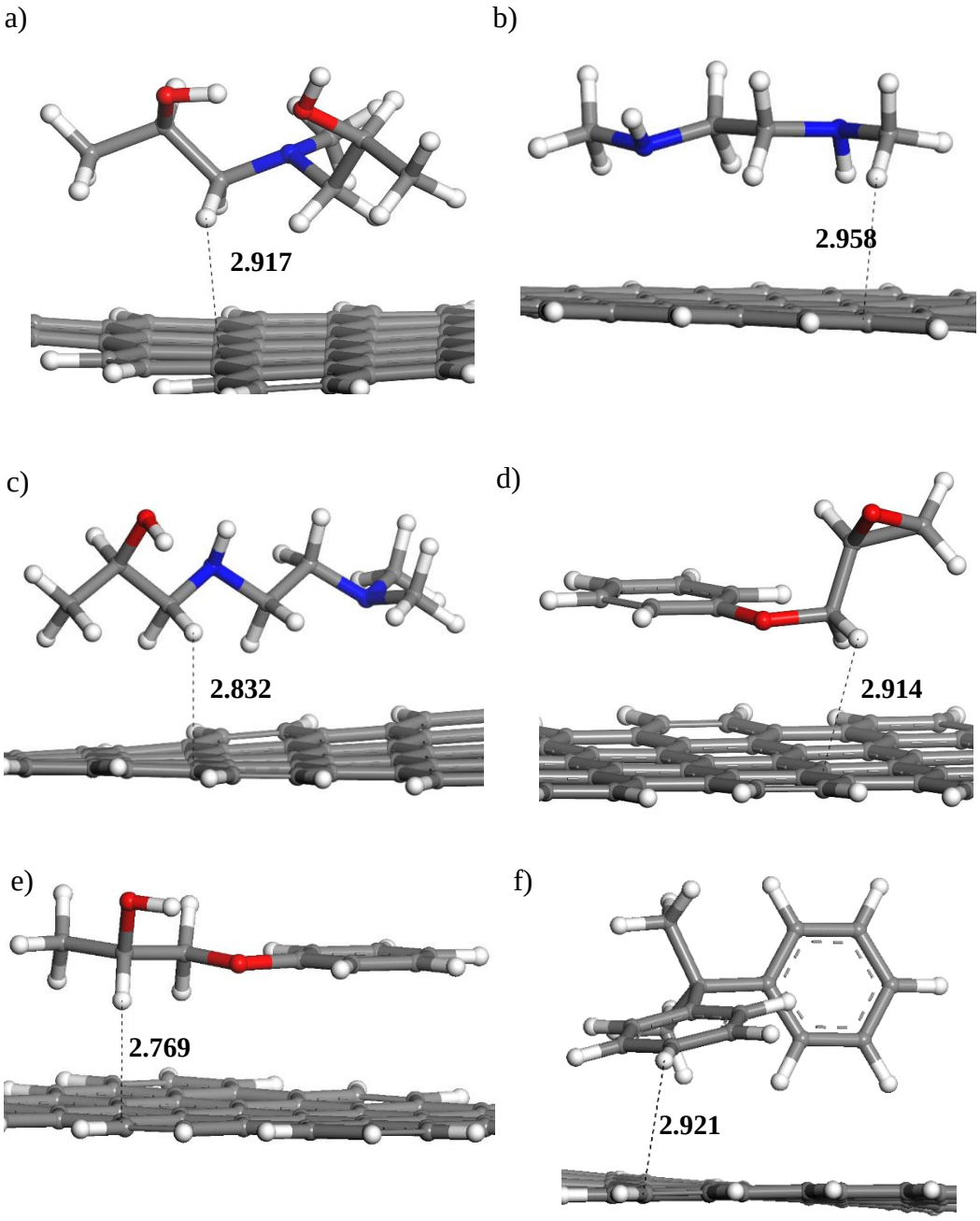

Figure 5.2. Atomic distances between Gr and a) Epo-dialcohol b) Epo-diamine c) Epo-aminealcohol d) Epo-epoend e) Epo-phenetheralcohol f) Epo-DMDP.

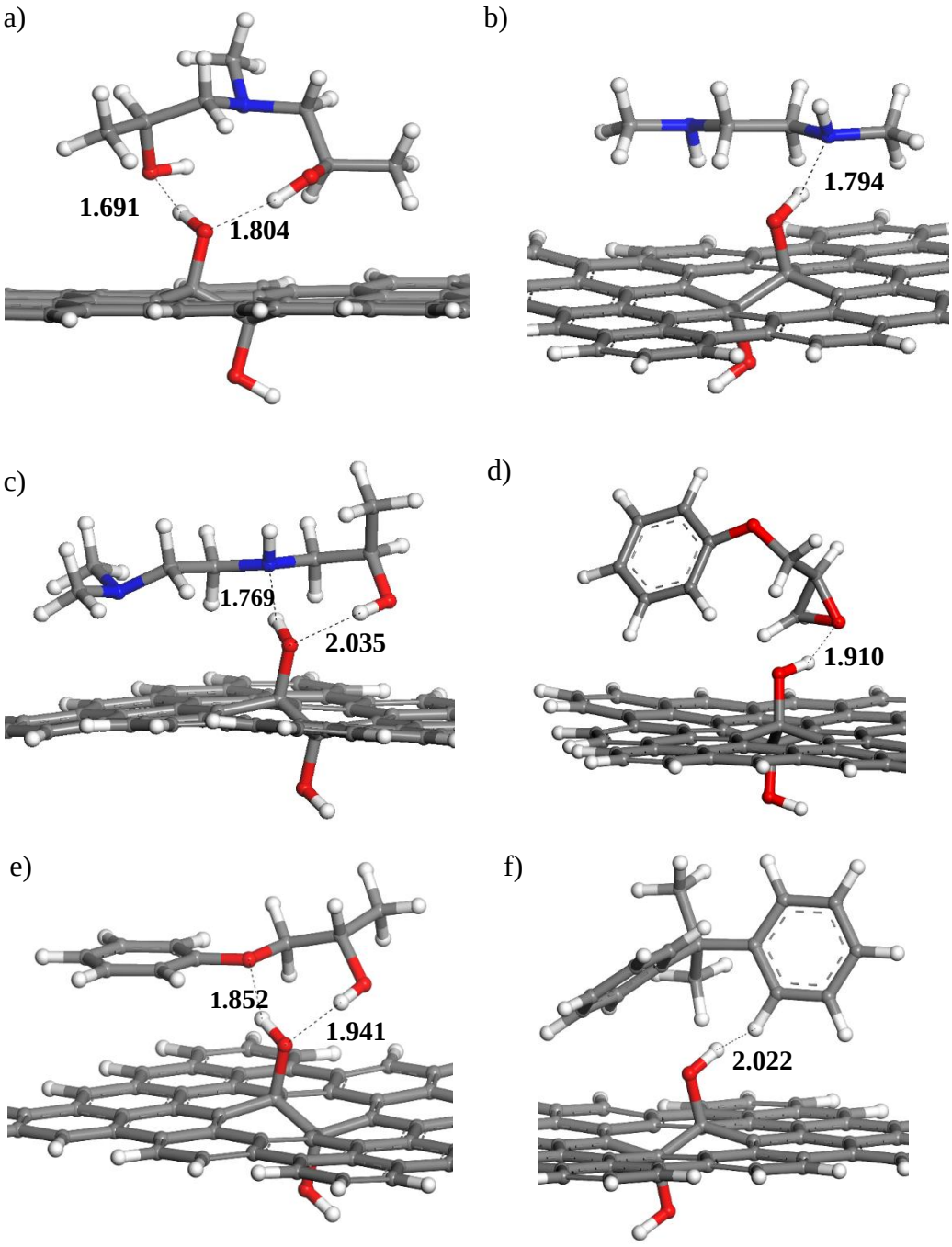

Figure 5.3. Hydrogen bonds and atomic distances between Gr-OH and a) Epo-dialcohol b) Epo-diamine c) Epo-aminealcohol d) Epo-epoend e) Epo-phenetheralcohol f) Epo-DMDP.

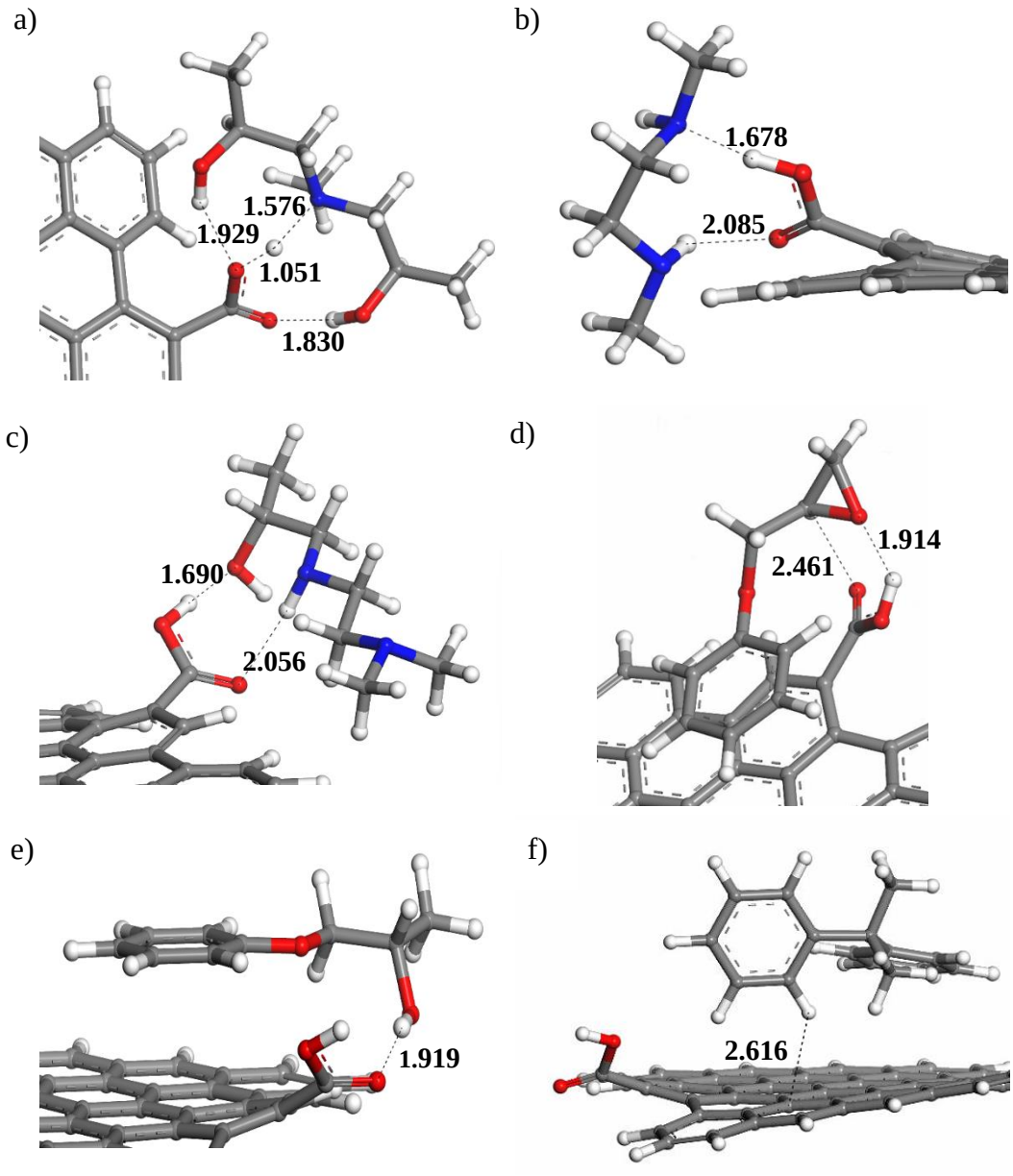

Figure 5.4. Hydrogen bonds and atomic distances between Gr-COOH and a) Epo-dialcohol b) Epo-diamine c) Epo-aminealcohol d) Epo-epoend e) Epo-phenetheralcohol f) Epo-DMDP.

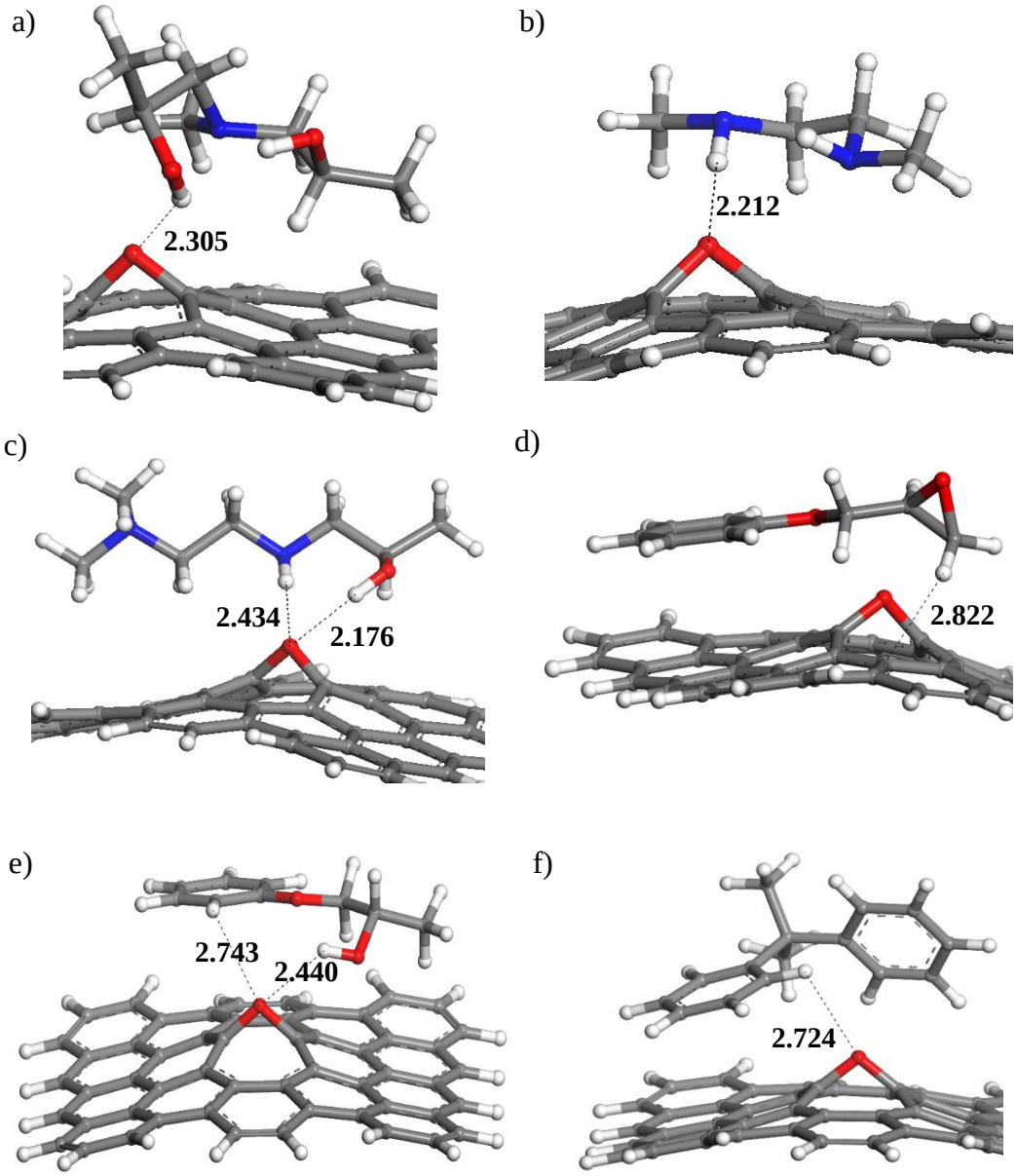

Figure 5.5. Hydrogen bonds and atomic distances between Gr-Epo and a) Epo-dialcohol b) Epo-diamine c) Epo-aminealcohol d) Epo-epoend e) Epo-phenetheralcohol f) Epo-DMDP.

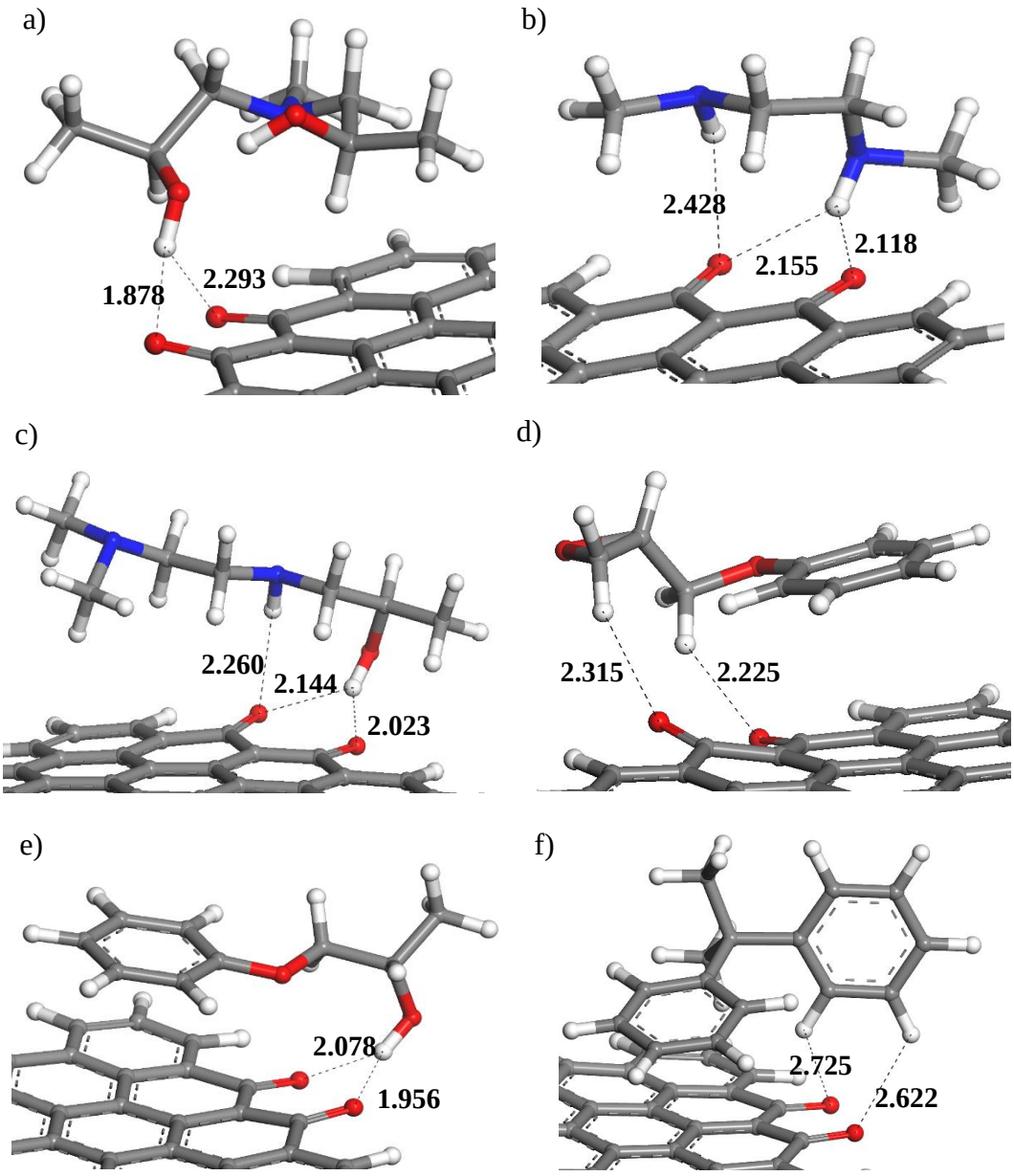

Figure 5.6. Hydrogen bonds and atomic distances between Gr-diketone1 and a) Epo-dialcohol b) Epo-diamine c) Epo-aminealcohol d) Epo-epoend e) Epo-phenetheralcohol f) Epo-DMDP.

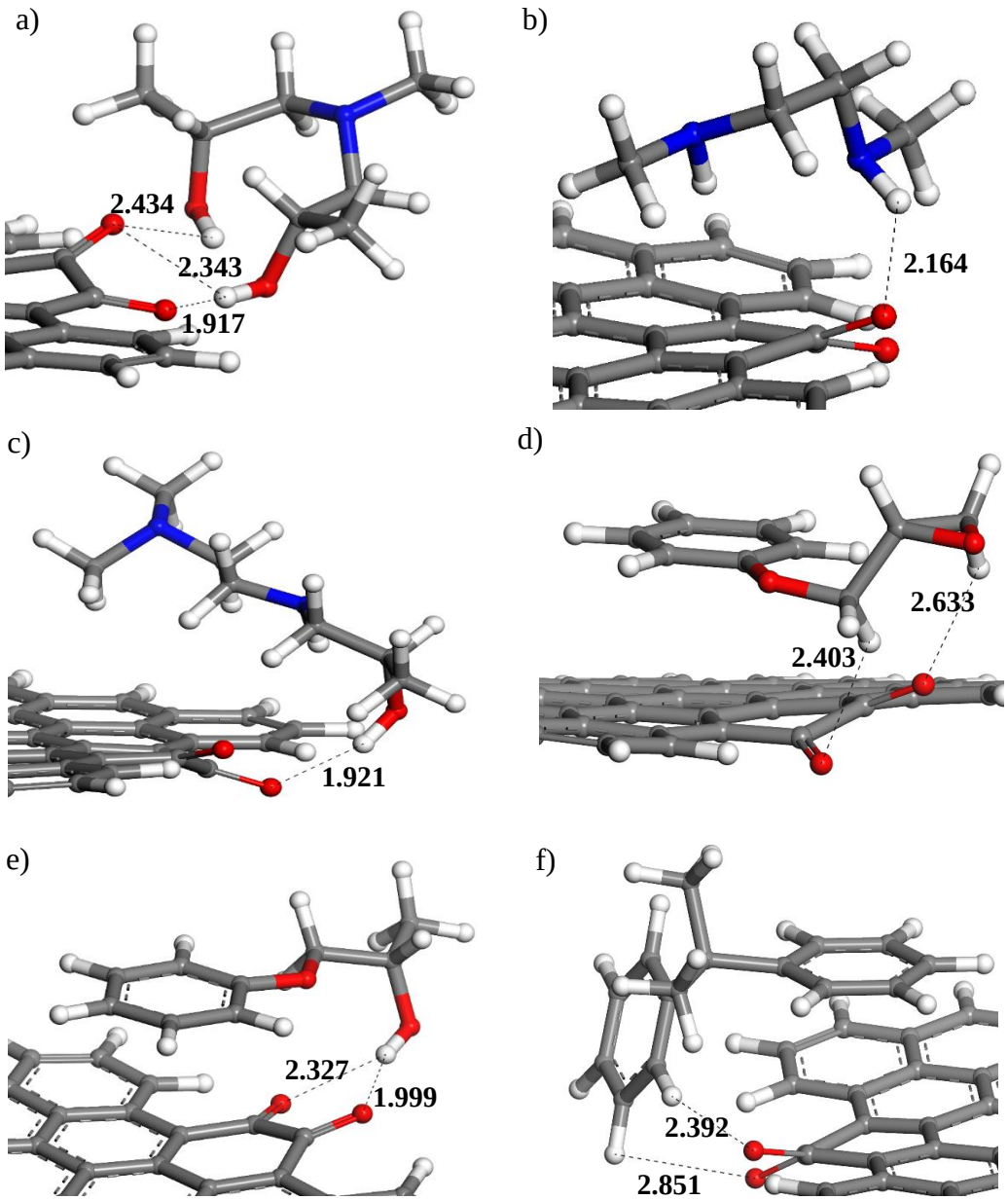

Figure 5.7. Hydrogen bonds and atomic distances between Gr-diketone2 and a) Epo-dialcohol b) Epo-diamine c) Epo-aminealcohol d) Epo-epoend e) Epo-phenetheralcohol f) Epo-DMDP.

Although there are some differences observed for the two interaction energies used in the DFT calculations for different DFT functional, the geometry optimized structures were compared for these structures such as for the one given in Figure 5.8 and only slight structural differences were observed for the atomic distances between these two functionals even when different interaction energies were calculated.

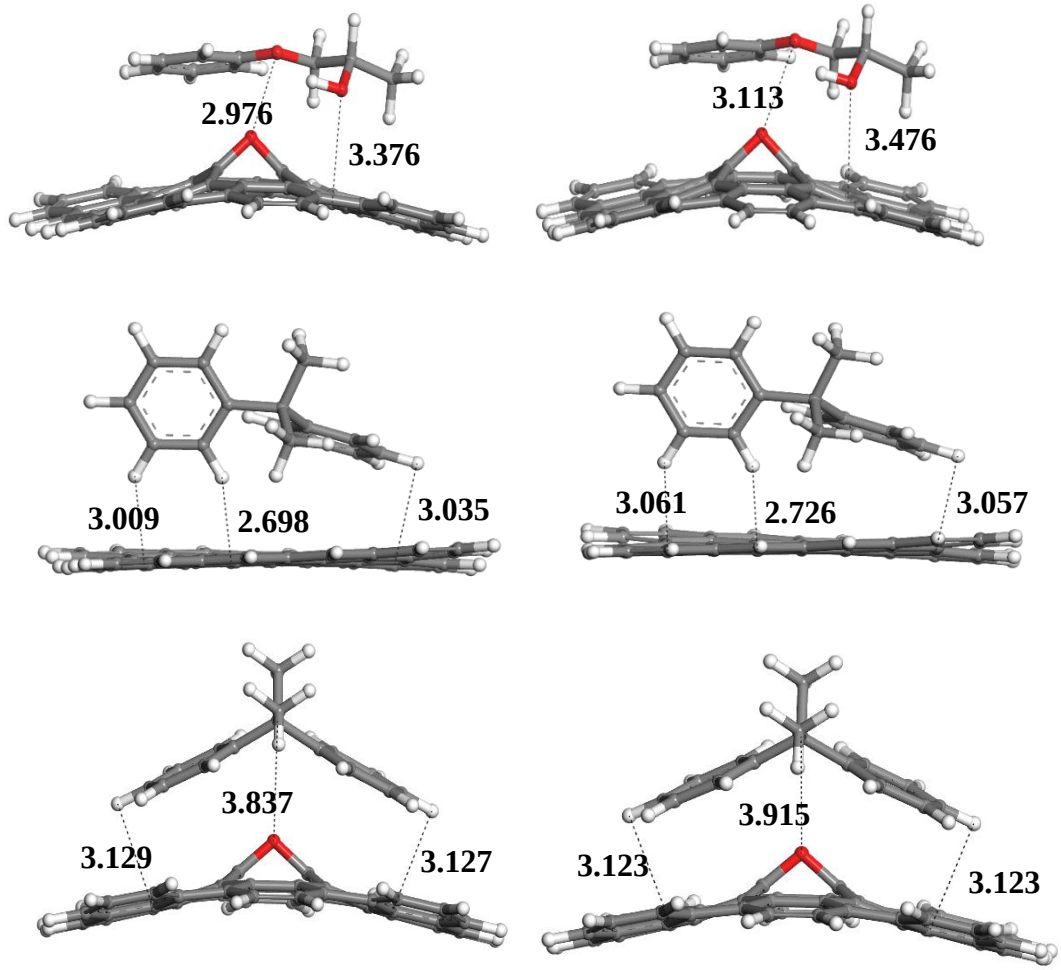

Figure 5.8. Comparison of atomic distances for different functionals wB97XD (right) and M06-2X-D3 (left).

It should be noted that for the epoxy group to be stable on the graphene model surface, graphene size should be large enough as given in Figure 5.9. For small graphene representative models, ether group formation was observed due to C-C bond dissociation, indicating that a larger conjugated system is required to model GrO.

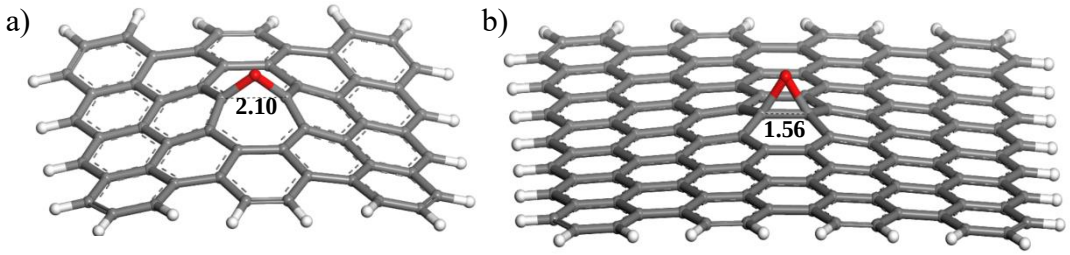

Figure 5.9. Geometry optimized structure for the epoxy group on the graphene surface for model with a) 54 carbon b) 120 carbon.

5.2 Classical Monte Carlo and Molecular Dynamics Methods

5.2.1 Mixing Energy Calculations between the Components of Epoxy-GO Nanocomposites

Although DFT calculations are more accurate to calculate pairwise interaction energies and atomic distances, they only contain one-to-one binary interactions and they do not include self-interactions of the molecules and coordination numbers. To include the effect of coordination numbers and self-interactions for these calculations, mixing energies were calculated by using pairwise self and intermolecular binding energies by generating a large number of molecular clusters via molecular mechanics methods. Although E_{i-j} binding energies are all negative which indicates attractive interaction between the epoxy chains and GO surface, E_{i-i} and E_{j-j} self-binding energies were also negative that give positive mixing energy as

a result. The main reason for the positive mixing energy is the significantly strong self-interaction of GO sheets. Gr-OH and Gr-OH2 structures had the lowest positive mixing energies with functional groups of epoxy chains due to their high polarity. The second lowest positive mixing energies were observed for Gr-epo structures that are different compared to the DFT calculations. Gr-epo structures had one of the lowest interactions with epoxy functional groups in DFT calculations due to the lack of hydrogen bonds. When E_{i-i} self-binding energies for GO structures were compared, the highest (least negative) energies were found for Gr-OH and Gr-epo self-interactions, indicating that repulsion occurred within these functional groups that provide better mixing with other components. Thus, it was concluded that Gr-OH and Gr-epo were important functional groups to prevent the agglomeration of filler. Even though epoxy functional groups on GO are not suitable to improve adhesion to epoxy chains, these groups are required on the graphene structure for enhanced dispersion of the sheets. It is advantageous to use -OH functional groups to improve the dispersion of the filler as well as adhesion to the epoxy matrix. Gr-OH functional groups with two -OH groups on both sides of the graphene sheets had lower mixing energy than Gr-OH2 which has two -OH functional groups on the same side of the graphene sheet. When the -OH group was located at the edge of the graphene, the mixing energy was increased. Therefore, -OH groups performed better in improving dispersion when they were positioned on the surface of the graphene sheet and both sides if possible. Moreover, Gr-COOH structures provide the third lowest mixing energies. These groups were also capable of forming strong hydrogen bonds as observed by the DFT calculations and RDF analysis will be given in the MD simulations. Thus, increasing the amount of these groups also favors improved filler performance. Pristine graphene structures had lower mixing energies with relatively nonpolar parts of the epoxy chains such as Epo-epoend and Epo-phenyletheralcohol since there were similar phenyl and benzene rings on those structures. Gr-COOH provided the lowest positive mixing energy when -COOH functional groups were located on the armchair edge of the graphene. Mixing energy decreased when -COOH was located at the corner of the graphene oxide, and it

decreased more when it was located on the zigzag edge of the graphene oxide structure. Besides, carbonyl groups had the highest mixing energies and E_{i-i} self-binding energies of graphene sheets. Carbonyl functional groups can be used to improve the affinity with epoxy chains but their contribution to filler dispersion was very limited. Figure 5.10 was representing some of the low energy configurations for pristine graphene sheets and graphene sheets containing oxygen functional groups. The distance between the two graphene sheets was the closest due to their tendency to mix. The distance between Gr-OH and Gr-epo was higher than the other functional groups since they have lower mixing energies. As a result, it was determined that graphene self-interaction is one of the most important parameters for the homogeneous mixing between the components.

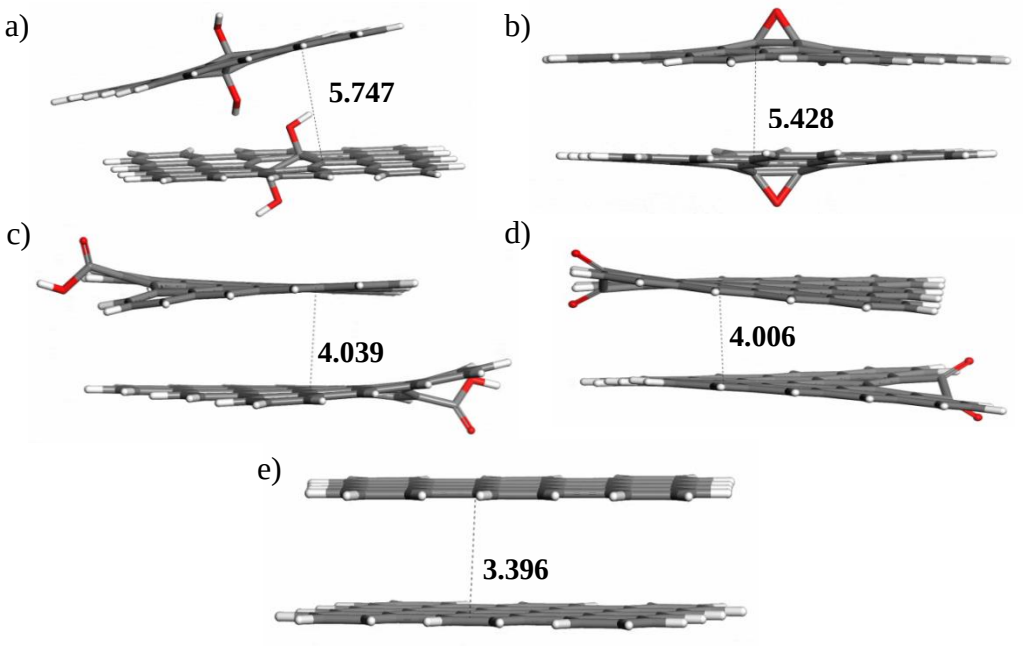

Figure 5.10. Distances between graphene functional group pairs. a) Gr-OH b) Gr-Epo c) Gr-COOH d) Gr-diketone2 e) Gr.

Table 5.2 Results for mixing energy (E_{mix}) and its components including pairwise binding energies (E_{i-i}, E_{i-j} and E_{j-j}) and coordination numbers (Z_{i-i}, Z_{i-j}, Z_{j-i} and Z_{j-i}) calculated for selected molecule configuration pairs. (by ESP based atomic charges)

i	j	E_{mix} (kcal/mol)	E_{i-i} (kcal/mol)	E_{i-j} (kcal/mol)	E_{j-j} (kcal/mol)	Z_{i-i}	Z_{i-j}	Z_{j-i}	Z_{j-j}
Gr-OH	Epo-epoend	10.9	-17.6	-7.5	-2.4	5.6	8.1	3.8	5.6
Gr-OH	Epo-phenetheralc	15.2	-17.6	-7.6	-2.8	5.6	7.1	3.6	4.6
Gr-OH	Epo-DMDP	17.4	-17.6	-7.1	-2.4	5.6	6.7	3.9	4.7
Gr-OH	Epo-aminealc	18.5	-17.6	-6.7	-2.3	5.6	7.0	3.8	4.8
Gr-OH	Epo-dialcohol	20.3	-17.6	-6.6	-3.1	5.6	7.4	3.7	4.9
Gr-OH	Epo-diamine	22.4	-17.6	-5.8	-1.7	5.6	7.3	3.2	4.3

i	j	E_{mix} (kcal/mol)	E_{i-i} (kcal/mol)	E_{i-j} (kcal/mol)	E_{j-j} (kcal/mol)	Z_{i-i}	Z_{i-j}	Z_{j-i}	Z_{j-j}
Gr-OH2	Epo-epoend	37.6	-31.7	-9.6	-2.4	5.6	8.2	3.8	5.6
Gr-OH2	Epo-phenetheralc	45.1	-31.7	-9.3	-2.8	5.6	7.1	3.6	4.6
Gr-OH2	Epo-dialcohol	50.9	-31.7	-8.2	-3.1	5.6	7.4	3.7	4.9
Gr-OH2	Epo-aminealc	51.6	-31.7	-7.9	-2.3	5.6	7.0	3.8	4.8
Gr-OH2	Epo-DMDP	51.7	-31.7	-8.0	-2.4	5.6	6.8	3.9	4.7
Gr-OH2	Epo-diamine	59.0	-31.7	-6.3	-1.7	5.6	7.4	3.2	4.3

Table 5.2 (continued)

i	j	E_{mix} (kcal/mol)	E_{i-i} (kcal/mol)	E_{i-j} (kcal/mol)	E_{j-j} (kcal/mol)	Z_{i-i}	Z_{i-j}	Z_{j-i}	Z_{j-j}
Gr-epo	Epo-epoend	47.7	-34.4	-9.3	-2.4	5.6	8.1	3.8	5.6
Gr-epo	Epo-phenetheralc	55.3	-34.4	-8.9	-2.8	5.6	7.1	3.6	4.6
Gr-epo	Epo-dialcohol	60.0	-34.4	-7.9	-3.1	5.6	7.4	3.7	4.9
Gr-epo	Epo-aminealc	61.3	-34.4	-7.5	-2.3	5.6	7.0	3.8	4.8
Gr-epo	Epo-DMDP	61.4	-34.4	-7.7	-2.4	5.6	6.7	3.9	4.7
Gr-epo	Epo-diamine	67.9	-34.4	-6.1	-1.7	5.6	7.3	3.2	4.3

i	j	E_{mix} (kcal/mol)	E_{i-i} (kcal/mol)	E_{i-j} (kcal/mol)	E_{j-j} (kcal/mol)	Z_{i-i}	Z_{i-j}	Z_{j-i}	Z_{j-j}
Gr-COOH	Epo-epoend	63.9	-39.7	-9.0	-2.4	5.6	8.2	3.8	5.6
Gr-COOH	Epo-phenetheralc	68.4	-39.7	-9.2	-2.8	5.6	7.1	3.6	4.6
Gr-COOH	Epo-dialcohol	74.9	-39.7	-7.9	-3.1	5.6	7.5	3.6	4.9
Gr-COOH	Epo-DMDP	75.4	-39.7	-7.8	-2.4	5.6	6.8	3.8	4.7
Gr-COOH	Epo-aminealc	75.5	-39.7	-7.7	-2.3	5.6	7.0	3.7	4.8
Gr-COOH	Epo-diamine	83.0	-39.7	-6.1	-1.7	5.6	7.4	3.1	4.3

i	j	E_{mix} (kcal/mol)	E_{i-i} (kcal/mol)	E_{i-j} (kcal/mol)	E_{j-j} (kcal/mol)	Z_{i-i}	Z_{i-j}	Z_{j-i}	Z_{j-j}
Gr	Epo-epoend	67.6	-40.1	-8.6	-2.4	5.6	8.1	3.8	5.6
Gr	Epo-phenetheralc	73.0	-40.1	-8.6	-2.8	5.6	7.0	3.6	4.6
Gr	Epo-dialcohol	77.5	-40.1	-7.7	-3.1	5.6	7.4	3.7	4.9
Gr	Epo-aminealc	78.0	-40.1	-7.4	-2.3	5.6	6.9	3.8	4.8
Gr	Epo-DMDP	78.6	-40.1	-7.5	-2.4	5.6	6.7	3.9	4.7
Gr	Epo-diamine	85.1	-40.1	-5.9	-1.7	5.6	7.3	3.2	4.3

Table 5.2 (continued)

i	j	E_{mix} (kcal/mol)	E_{i-i} (kcal/mol)	E_{i-j} (kcal/mol)	E_{j-j} (kcal/mol)	Z_{i-i}	Z_{i-j}	Z_{j-i}	Z_{j-j}
Gr-OH3	Epo-epoend	71.8	-41.8	-8.7	-2.4	5.6	8.1	3.8	5.6
Gr-OH3	Epo-phenetheralc	77.3	-41.8	-8.7	-2.8	5.6	7.0	3.6	4.6
Gr-OH3	Epo-dialcohol	81.8	-41.8	-7.8	-3.1	5.6	7.4	3.7	4.9
Gr-OH3	Epo-aminealc	82.2	-41.8	-7.6	-2.3	5.6	6.9	3.8	4.8
Gr-OH3	Epo-DMDP	82.8	-41.8	-7.6	-2.4	5.6	6.7	3.9	4.7
Gr-OH3	Epo-diamine	89.5	-41.8	-6.0	-1.7	5.6	7.3	3.2	4.3

i	j	E_{mix} (kcal/mol)	E_{i-i} (kcal/mol)	E_{i-j} (kcal/mol)	E_{j-j} (kcal/mol)	Z_{i-i}	Z_{i-j}	Z_{j-i}	Z_{j-j}
Gr-diketone2	Epo-epoend	74.3	-43.7	-9.2	-2.4	5.6	8.1	3.8	5.6
Gr-diketone2	Epo-phenetheralc	79.6	-43.7	-9.3	-2.8	5.6	7.1	3.6	4.6
Gr-diketone2	Epo-dialcohol	85.9	-43.7	-8.0	-3.1	5.6	7.4	3.6	4.9
Gr-diketone2	Epo-aminealc	86.6	-43.7	-7.7	-2.3	5.6	7.0	3.8	4.8
Gr-diketone2	Epo-DMDP	86.9	-43.7	-7.8	-2.4	5.6	6.7	3.8	4.7
Gr-diketone2	Epo-diamine	94.4	-43.7	-6.1	-1.7	5.6	7.3	3.1	4.3

i	j	E_{mix} (kcal/mol)	E_{i-i} (kcal/mol)	E_{i-j} (kcal/mol)	E_{j-j} (kcal/mol)	Z_{i-i}	Z_{i-j}	Z_{j-i}	Z_{j-j}
Gr-COOH2	Epo-epoend	75.4	-42.9	-8.6	-2.4	5.6	8.2	3.7	5.6
Gr-COOH2	Epo-phenetheralc	80.7	-42.9	-8.6	-2.8	5.6	7.1	3.5	4.7
Gr-COOH2	Epo-aminealc	85.9	-42.9	-7.4	-2.3	5.6	7.1	3.7	4.8
Gr-COOH2	Epo-dialcohol	86.0	-42.9	-7.6	-3.1	5.6	7.5	3.6	4.9
Gr-COOH2	Epo-DMDP	86.3	-42.9	-7.5	-2.4	5.6	6.8	3.8	4.7
Gr-COOH2	Epo-diamine	93.0	-42.9	-5.9	-1.7	5.6	7.4	3.1	4.3

Table 5.2 (continued)

i	j	E_{mix} (kcal/mol)	E_{i-i} (kcal/mol)	E_{i-j} (kcal/mol)	E_{j-j} (kcal/mol)	Z_{i-i}	Z_{i-j}	Z_{j-i}	Z_{j-j}
Gr-COOH3	Epo-epoend	76.2	-43.7	-8.8	-2.4	5.6	8.2	3.8	5.6
Gr-COOH3	Epo-phenetheralc	81.6	-43.7	-8.8	-2.8	5.6	7.1	3.6	4.6
Gr-COOH3	Epo-amineralc	86.9	-43.7	-7.6	-2.3	5.6	7.0	3.7	4.8
Gr-COOH3	Epo-dialcohol	87.0	-43.7	-7.8	-3.1	5.6	7.5	3.6	4.9
Gr-COOH3	Epo-DMDP	87.6	-43.7	-7.6	-2.4	5.6	6.8	3.8	4.7
Gr-COOH3	Epo-diamine	94.5	-43.7	-6.0	-1.7	5.6	7.4	3.1	4.3

5.2.2 Effect of the Number of Oxygen-Containing Functional Groups on the Interaction Energies

Interaction energies were calculated for five different cells containing continuous periodic GO sheets with 0%, 5%, 8%, 10%, 13%, 15%, 18% and 20% oxygen content and the same representative epoxy molecule (DETA:DGEBA=4:10). Amorphous cells were created with low initial density at 0.6 g/cm^3 where 15 representative chains were packed into the cell to reach the target density. After the construction of amorphous cells, geometry optimization was performed for 10000 steps to determine the lowest energy configurations. Lattice parameter optimizations were also performed in this step and the size of the cell was decreased from 46x46x120 Å^3 to 46x46x55 Å^3 and the density was increased between 0.9-1.0 g/ cm^3. Next, a 5000 ps MD simulation at the NPT ensemble was performed. As a representation, the change of the density during geometry optimization and MD simulation was given for the cell has GO with 18% oxygen amount in Figure 5.11.

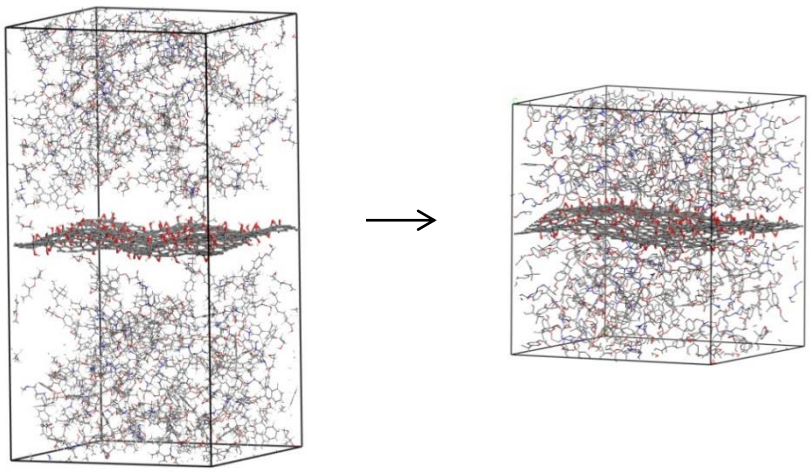

Figure 5.11. Equilibrated cell structure for a MD simulation.

The final density was between 1.0-1.1 g/ cm^3 after geometry optimization and stabilized during MD simulation for each cell as given in Figure 5.12. This density is close enough to the experimental density of epoxy resin and constant density confirmed that the system was equilibrated with this method. The temperature was stable at around 298 K and pressure was fluctuating significantly around 1 atm during the 5000 ps MD simulation time as given in Figure 5.13 and Figure 5.14 which validates the thermostat and barostat methods. The total energy and potential energy for one of the systems were also demonstrated in Figure 5.15, which were constant after 2500 ps.

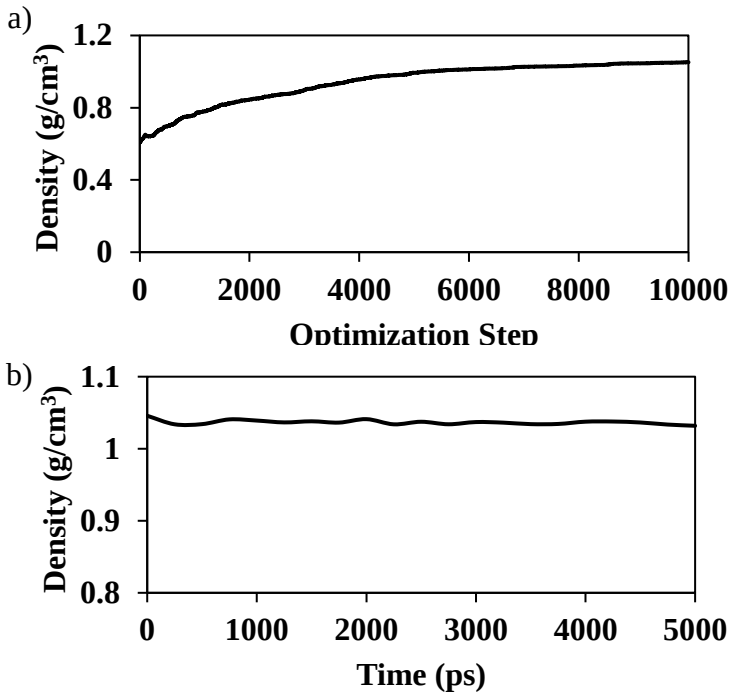

Figure 5.12. Density change for GO-Epoxy system with 18% oxygen during a) geometry optimization and b) MD simulation.

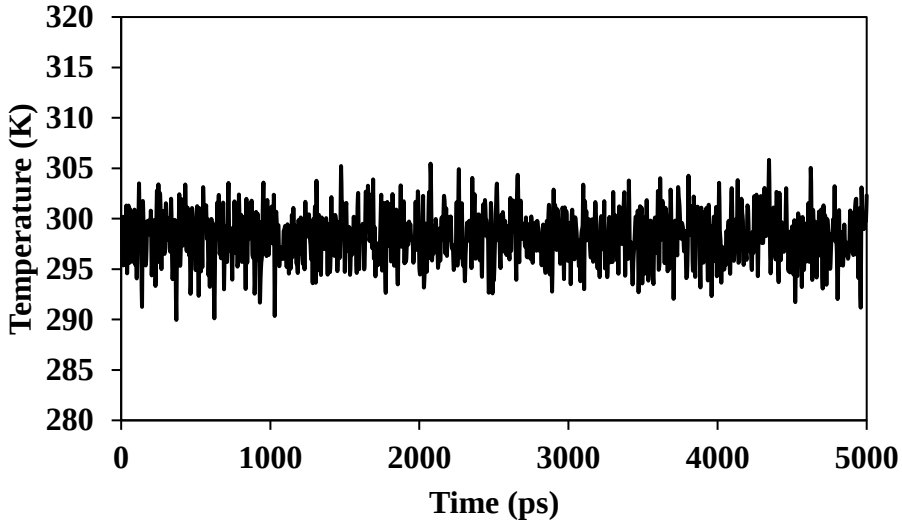

Figure 5.13. Temperature of GO-Epoxy system containing 18% oxygen during MD simulation.

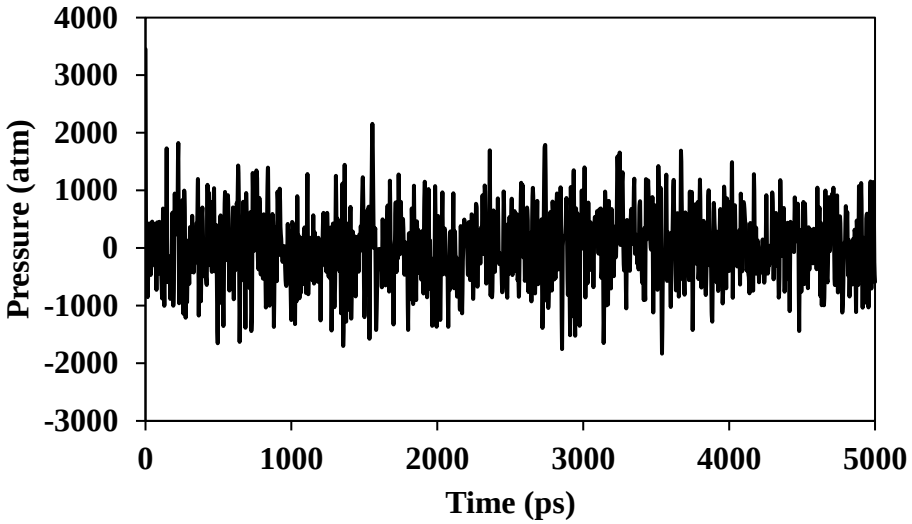

Figure 5.14. Pressure of GO-Epoxy system containing 18% oxygen during MD simulation.

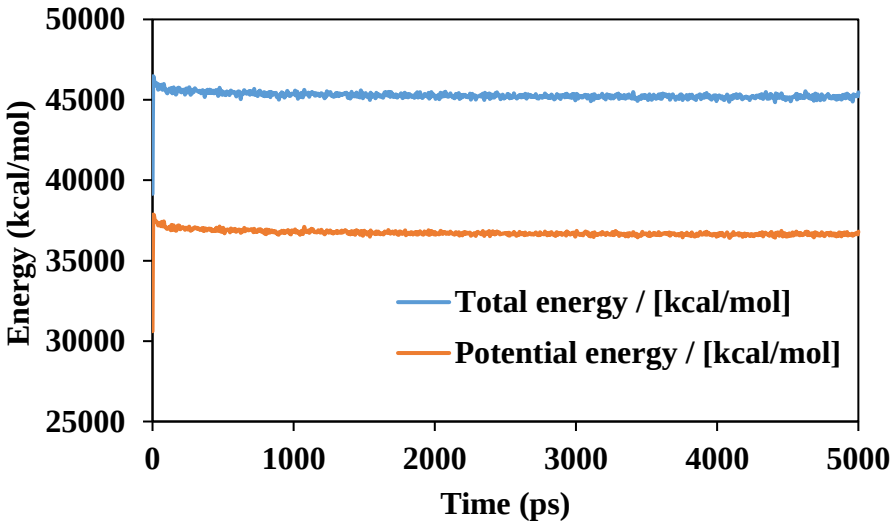

Figure 5.15. Change of energy of GO-Epoxy system containing 18% oxygen during MD simulation.

Final density of the cell and interaction energy values between the Gr/GO and epoxy functional groups were given in Table 5.3 and Figure 5.16. There was a considerable increase of interaction energy up to 10% oxygen content in GO, however, there was a slight increase of up to 18% oxygen content on GO structure due to the formation of all hydrogen bonds with the limited number of functional groups at the interfacial epoxy chains. Since there was a limited number of -NH and -OH groups on epoxy chains to interact with GO functional groups, the increase in the interaction energy was almost constant after the atomic percentage of 10% oxygen. Pure graphene has the lowest interaction energy as expected between functional groups on epoxy. It can be concluded that at least 10% oxygen-functionalized groups on GO were required for the improved interaction energy with functional groups of epoxy. This interaction energy between the filler and the polymer phase is responsible for the reinforcement and mechanical property improvement. It should be noted that self-interaction of the graphene is not included in these calculations which is a limiting factor for the interfacial interaction and mechanical property enhancement.

Table 5.3 Interaction energies for increasing oxygen ratio on GO.

GO-Oxygen %	**0%**	**5%**	**8%**	**10%**	**13%**	**15%**	**18%**	**20%**
Density (g/cm^3)	1.08	1.00	1.06	1.01	1.06	1.00	1.03	1.00
Interaction Energy (kcal/mol)	-52.0	-682.9	-1191.6	-1220.4	-1262.6	-1253.0	-1353.2	-1348.0

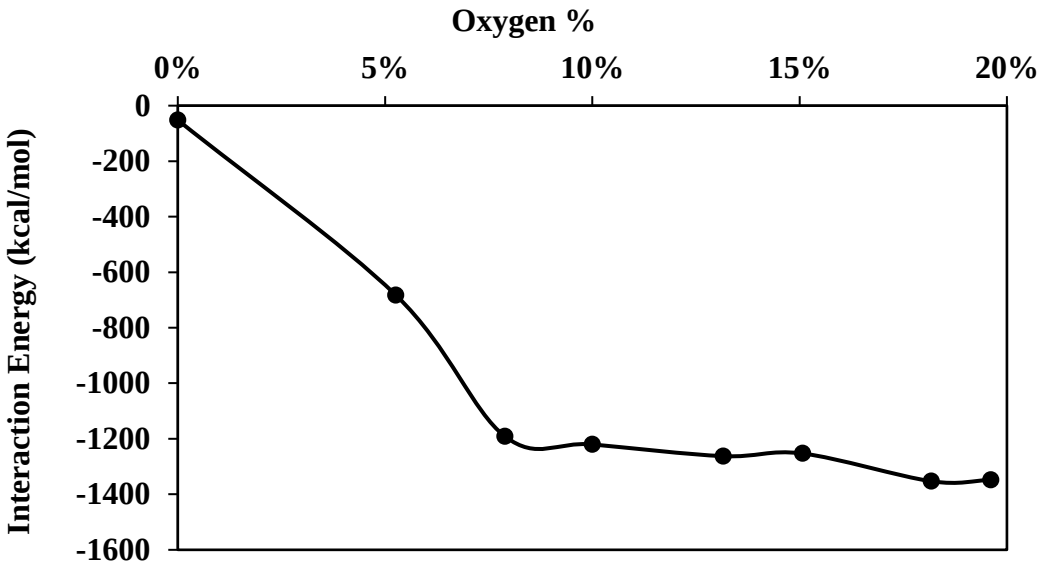

Figure 5.16. Effect of increasing oxygen amount on GO on the interaction energy.

5.2.3 Effect of Epoxy:Hardener Ratio on the Interaction Energies

For the investigation of the effect of polar epoxy amine groups on the interaction energies, five different epoxy molecules containing varying DETA:DGEBA ratios were used in addition to the oxygen content in periodic continuous GO. When a higher DETA amount was used, there would be a higher number of -NH groups present in the system and DGEBA molecules would not be sufficient to saturate all -NH groups. Thus, crosslink density decreases. In this section, interaction energies between epoxy molecules with different amine ratios and GO structures with low, medium and high oxygen content were investigated. Results were given in Table 5.4. Nanocomposite systems were equilibrated with MD simulations as a similar method to the previous section and the final density was reached between 0.9-1.1 g/cm^3. The final density was lower for higher oxygen amounts on GO characterized by the less decreased cell size due to the repulsions by the polar -OH and C-O-C functional groups on the periodic GO surface. As represented in Figure 5.17, interaction energy

decreases with increasing DETA:DGEBA ratio for the 5% oxygen amount on GO. On the contrary, interaction energy increases with increasing DETA:DGEBA ratio for 18% oxygen amount on GO. Interaction energy results for nanocomposite systems containing GO with 12% oxygen amount were between the two of them as expected. These results are important to demonstrate that for enhanced interaction energies, DETA:DGEBA ratio has to be high for high oxygen content on GO and it has to be low for low oxygen content. One should know the oxygen content in the commercial GO and DETA ratio in epoxy resin to improve interfacial interactions where DETA:DGEBA ratio and oxygen content in GO control the reinforcement together. As claimed previously, successful epoxy-GO nanocomposites can be prepared in many different ways, by controlling the content ratios and their polarities.

Table 5.4 Interaction energies for increasing oxygen ratio on GO.

Epoxy Parameters	DETA	4	5	6	7	8
	DGEBA	14	13	12	11	10
	DETA:DGEBA	0.3	0.4	0.5	0.6	0.8
	Crosslink %	85	68	56	49	38
Epoxy + GO with 5% Oxygen	Density	1.09	1.10	1.13	1.11	1.10
	Interaction Energy (kcal/mol)	-1240.0	-1157.5	-777.3	-693.7	-139.8
Epoxy + GO with 12% Oxygen	Density	1.01	1.00	1.03	1.00	1.03
	Interaction Energy (kcal/mol)	-1217.7	-1074.7	-856.7	-725.3	-534.3
Epoxy + GO with 18% Oxygen	Density	0.96	0.93	0.95	0.96	0.94
	Interaction Energy (kcal/mol)	-888.5	-1028.0	-1111.5	-1270.3	-1400.5

a)

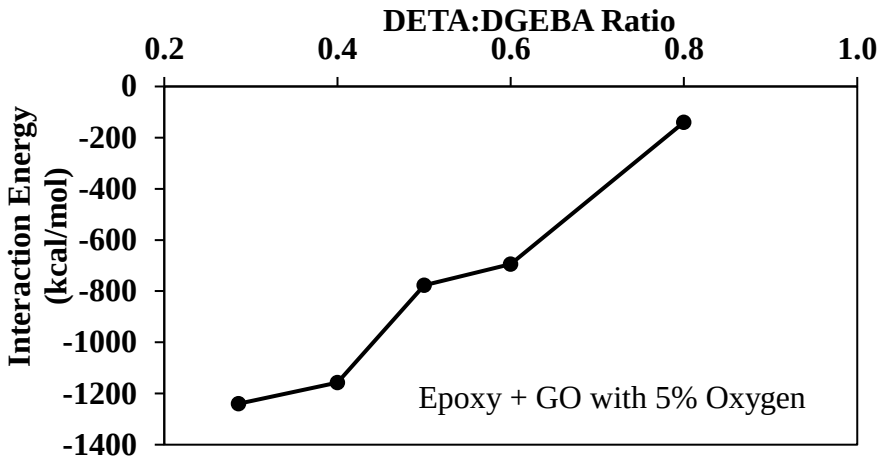

b)

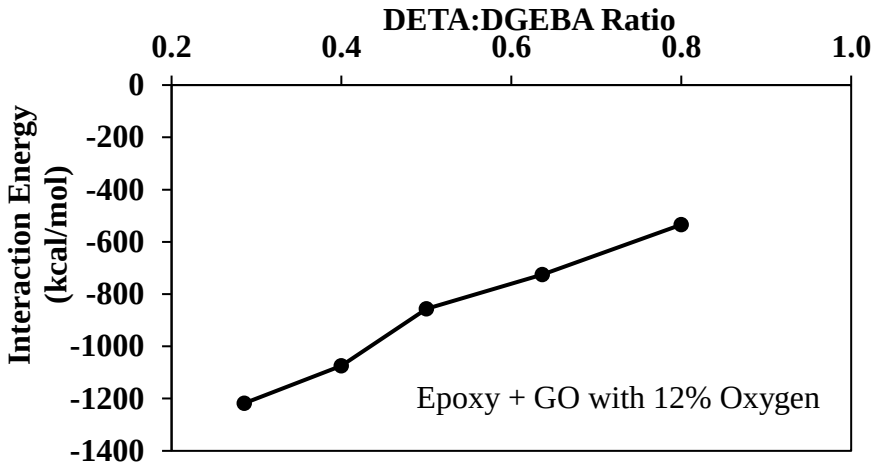

c)

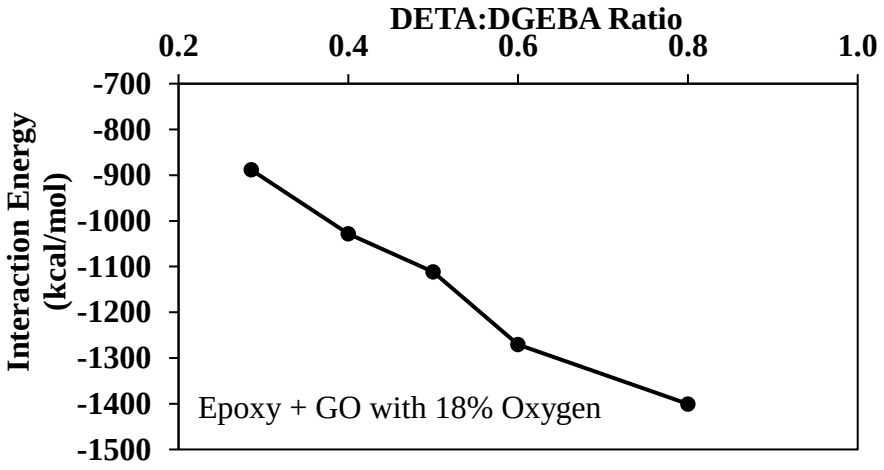

Figure 5.17. Interaction energies for varying oxygen content

5.2.4 Effect of Gr and GO Filler Types on the Interaction Energies

Interaction energies were calculated for the systems containing one sheet of Gr or GO molecule with the size of 2.4 nm which contains epoxy and hydroxyl at the surface, carboxylic acid and carbonyl functional groups at the edge. These functional groups have a high affinity to interact with different parts of epoxy molecules according to DFT and mixing energy calculations. Thus, the lowest interaction energy was observed for graphene, and when the number of oxygen-containing functional groups increased, interaction energy was also increased. Different from the calculations performed for the periodic cell structure, interaction energy tends to increase constantly as the oxygen percentage increases. The addition of edge functional groups might be responsible for the difference in the increasing trend. Density change during the 5000 ps simulation was also shown in Figure 5.18 for AA50 GO structure as a representation. It should be noted that GO in the experiments is in the 100 nm range and continuous periodic cell surface mimics the experimental conditions better for interfacial interactions compared to the small size graphene.

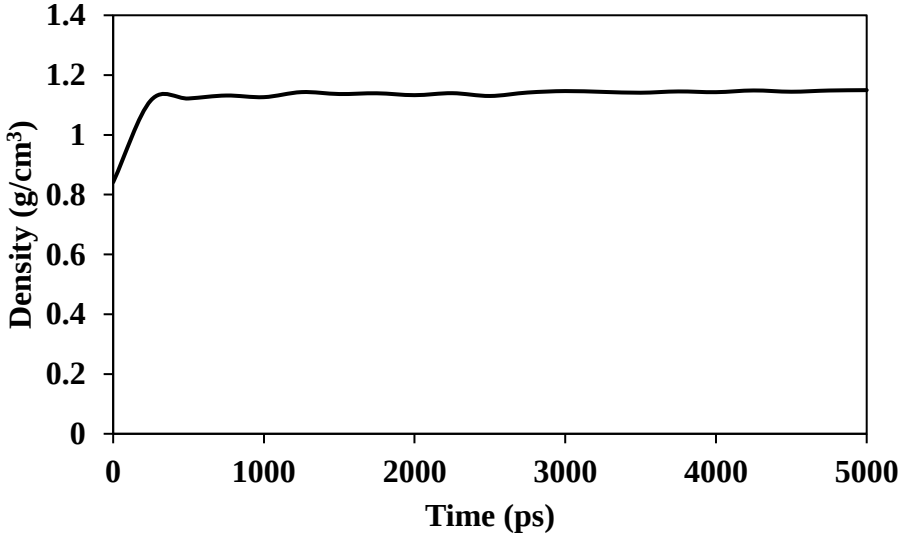

Figure 5.18. Density change during MD simulation (for AA50).

Results were summarized in Table 5.5 and Figure 5.19. As compared with pristine graphene, interaction energies were increased by 7%, 22% and 30% for the GO structures of GO-6%, AA90 and AA50 respectively.

Table 5.5. Interaction energies and final densities for different types of Gr/GO fillers

Filler Type	Graphene	GO-6%	AA90	AA50
Oxygen %	0	6	13	18
Final Density (g/cm^3)	1.15	1.14	1.16	1.15
Interaction Energy (kcal/mol)	-427.3	-456.2	-520.4	-560.4

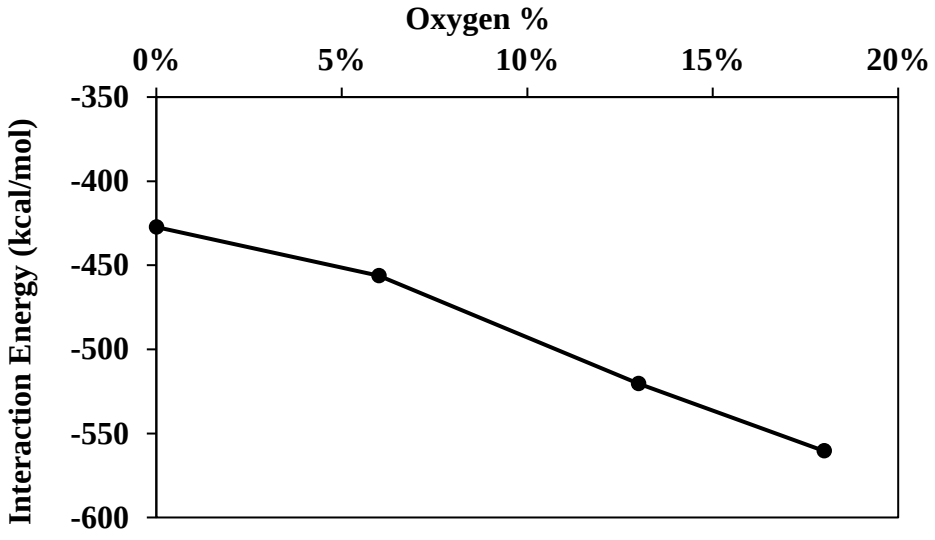

Figure 5.19. Interaction energies for different types of Gr/GO fillers

5.2.5 Effect of Different Filler Types and Epoxy:Hardener Ratio on the Interaction Energies

In this part, both filler type and epoxy:hardener ratio parameters were controlled to investigate the effect on the interaction energies. Gr and GO sheets with 2.4 nm size were placed into a cell and epoxy molecules were filled into the cell with DETA:DGEBA ratios of 4:14, 5:13, 6:12 and 7:11 until the Gr/GO reached 6 wt%. Results were given in Table 5.6. Similar to the previous results, AA50 with the highest oxygen-containing functional groups had the highest interaction energies and pure graphene had the lowest interaction energies with the epoxy chains. With an increasing DETA:DGEBA ratio, interaction energies tend to increase for the fillers containing epoxy, hydroxyl, carboxylic acid and carbonyl functional groups on their surface and edges. This increase was higher for the AA50 type than the AA90 type GO fillers. Graphene did not show such a trend since no functional groups were present on the surface to interact. It should be noted that increasing DETA amount has a negative effect on the crosslinking density since there will be more unreacted amine functional groups. Low crosslinking density decreases the mechanical properties of epoxy resin experimentally. Thus, crosslinking density optimization is required for producing nanocomposites with desired properties.

Table 5.6 Interaction energies for Gr, AA90 and AA50 fillers with increasing epoxy:hardener ratio.

DETA:DGEBA	Interaction Energies (kcal/mol)		
	Graphene	AA90	AA50
4:14	-1293.0	-1482.1	-1612.4
5:13	-1314.8	-1487.7	-1663.3
6:12	-1309.1	-1525.7	-1673.2
7:11	-1302.6	-1577.9	-1691.7
8:10	-1298.4	-1609.2	-1759.4

5.2.6 Effect of GO Mass Percentages on the Interaction Energies and Young's Modulus Values

In this section, Young's Modulus values were calculated to determine the stiffness of the nanocomposite material. Gr and GO sheets (AA50 and AA90) were placed into the cell in increasing weight ratios as 2%, 4%, 6% and 8%. These models were representing completely dispersed GO structures within the cell which is an ideal case. Nanocomposite structures were prepared for each set and geometry optimization was performed only for the molecular structure without optimizing the lattice parameters. Thus, the initial density remained as constant at 0.5 g/cm^3 after optimization before the MD simulation. Five structures with the lowest potential energies were selected from 50 samples for each set and MD simulations were performed. The volume of the cell was decreased from 85x85x85 Å^3 to 65x65x65 Å^3 after MD simulations were completed and the structure reached equilibrium. Densities were increased to 1.15 g/cm^3 for each nanocomposite system during MD simulation time as given in Figure 5.20, which is an important validation of the theoretical method reaching the experimental density accurately without any external influence.

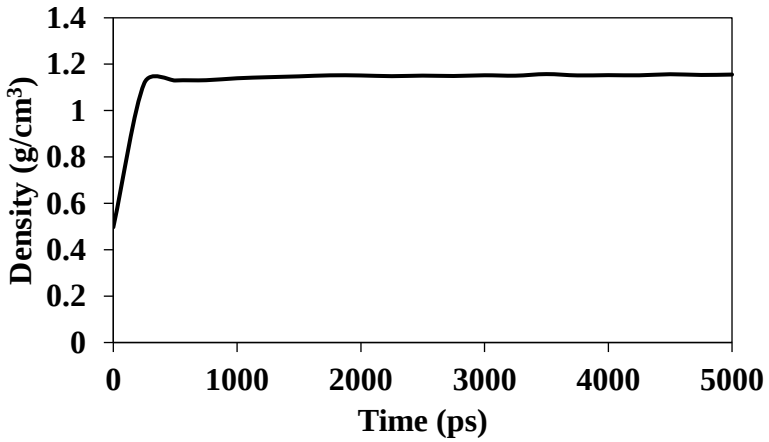

Figure 5.20. Change of density during MD simulation (for AA50 - 6 wt%).

The temperature was constant around 298 K and pressure was fluctuated around 1 atm as represented in Figure 5.21 and Figure 5.22. Potential energy and kinetic energy stayed constant after 2500 ps time as shown in Figure 5.23.

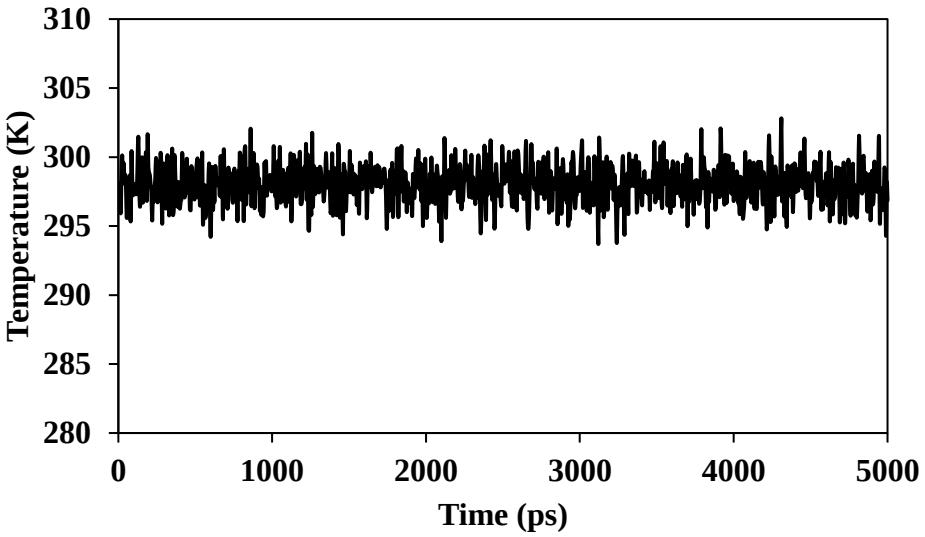

Figure 5.21. Temperature during MD simulation (for AA50 - 6 wt%).

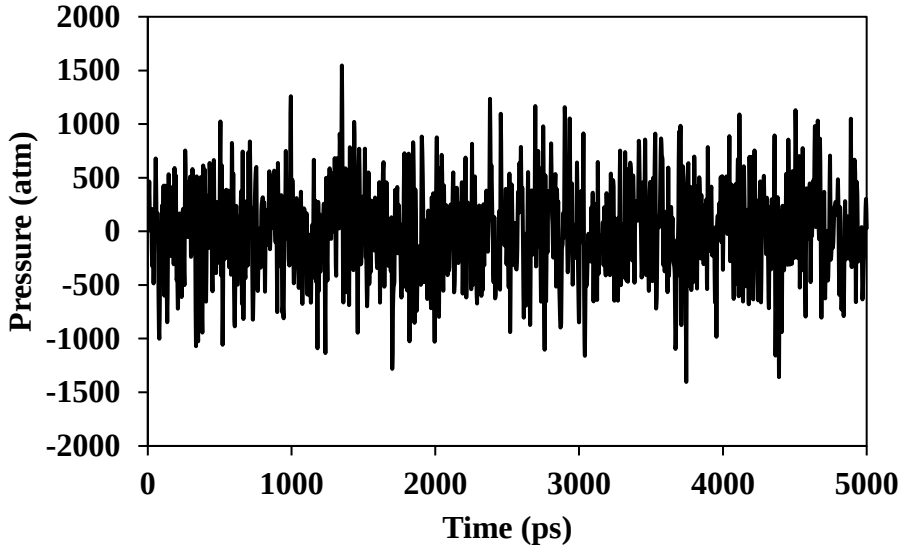

Figure 5.22. Pressure during MD simulation (for AA50 - 6 wt%).

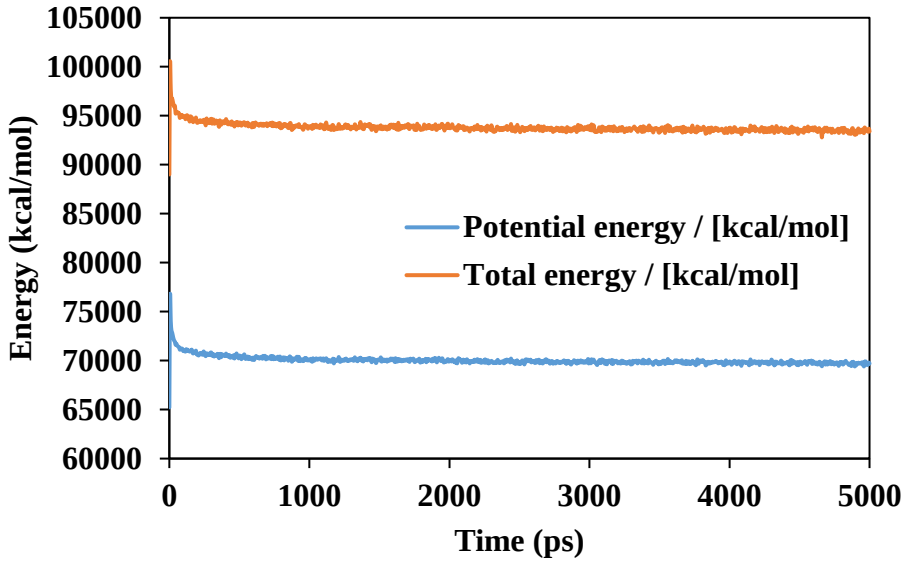

Figure 5.23. Energy during MD simulation (for AA50 - 6 wt%).

Interaction energy and Young's Modulus calculation results were summarized in Table 5.7. AA50 and AA90 fillers were performed better in terms of improving interaction energies as compared with the pristine graphene.

Table 5.7. Interaction energies and Young's Modulus values for AA50, AA90 and Gr fillers with increasing weight percentage.

	Epoxy	**Epoxy + AA50-2%**	**Epoxy + AA50-4%**	**Epoxy + AA50-6%**	**Epoxy + AA50-8%**
Interaction Energy (kcal/mol)	-	-559.1	-1122.5	-1598.8	-2171.4
Final Density (g/cm^3)	1.13	1.14	1.14	1.15	1.16
Young's Modulus (GPa)	4.20	4.31	4.54	4.81	5.07

Table 5.7 (continued)

	Epoxy	Epoxy + AA90-2%	Epoxy + AA90-4%	Epoxy + AA90-6%	Epoxy + AA90-8%
Interaction Energy (kcal/mol)	-	-487.1	-957.6	-1488.0	-2014.0
Final Density (g/cm^3)	1.13	1.13	1.14	1.15	1.15
Young's Modulus (GPa)	4.20	4.39	4.40	4.68	4.78

	Epoxy	Epoxy + Gr-2%	Epoxy + Gr-4%	Epoxy + Gr-6%	Epoxy + Gr-8%
Interaction Energy (kcal/mol)	-	-411.3	-858.5	-1305.1	-1738.7
Final Density (g/cm^3)	1.13	1.13	1.14	1.15	1.15
Young's Modulus (GPa)	4.20	4.23	4.24	4.37	4.42

The experimental density of a cell with only epoxy chains composed of DETA and DGEBA is 1.1 g/cm^3, and Young's Modulus is between 3.4-3.8 GPa according to the literature. [43], [45] In this study, Young's Modulus value for epoxy was found as 4.2 GPa after 5 ns simulations which were higher than the literature data. There could be several causes for this result. Initial representative structure which is much smaller than the real chains, cell size, simulation time and selected ensemble can be some of the factors that affect calculated Young's modulus. Increased simulation time and cell size generated stiffer structures where lower mechanical properties close to the experimental values were calculated for the preliminary studies.

Moreover, the representative epoxy molecule method might not simulate the experimental data exactly. First of all, representative molecules were not connected with covalent bonds which are different from the real system. Secondly, there were unreacted DETA or DGEBA molecules and other defects in the real system that reduces Young's modulus which was not considered in this study. Another consideration was about the equilibrated system that could be trapped in configurations with a local minimum on the potential energy surface because the simulations were nonergodic. Theodorou and Suter [65] developed a method for estimation of the mechanical properties of polymeric systems where about fifteen equilibrated configurations of the system were used for deformation experiments. Increasing the number of samples and averaging the results would be beneficial for obtaining improved Young's Modulus values. Skountzos and Mavrantzas [33] used this method in their study. They suggested that raising the temperature above the melting point of the material and then cooling it down to 300 K could overcome the local minimum potential energy problem and this result in obtaining a well-equilibrated structure. However, this annealing method did not work for the system in this study, resulting in errors during the cooling down process, particularly for the models containing GO. Thus, MD simulations were performed at the selected NPT ensemble. Besides, pressure fluctuation during the MD simulations might affect the properties of the final structure and a linear stress-strain curve could not be obtained to determine the correct Young's Modulus of the system. Averaging five configurations with the lowest energy for each set improved the results significantly. Adding more simulations can give more accurate results.

Although pristine epoxy representative cells could not produce exact experimental Young Modulus values, the improvement by the Gr/GO addition in the system was successfully determined. AA50 model performed better than AA90 for improving stiffness. The nanocomposite models with pure graphene sheets yield the lowest Young's Modulus values. Interaction energies were also in the same trend that points out the relation between reinforcement at the interface and the improved mechanical properties. The highest interaction energy was observed for nanocomposites with

AA50 fillers and the lowest interaction energy was observed for nanocomposites with graphene fillers. Hydrogen bonds that were determined as the main intermolecular interaction in the system between GO functional groups and epoxy functional groups were represented in Figure 5.24. Figure 5.24a demonstrates the hydrogen bonds between -OH functional groups on GO with amine and alcohol functional groups on the epoxy chain.

Hydrogen bonds between epoxy and alcohol groups on GO with the alcohol functional group of the epoxy chain were given in Figure 5.24b. Figure 5.24c represents the hydrogen bonds between -COOH functional group at the edge groups of GO with the amine and alcohol functional groups on the epoxy chain. Hydrogen bond between carbonyl functional group on GO with the alcohol functional group on epoxy chain was given in Figure 5.24d. These interactions which were defined in the GO-epoxy interface for the equilibrium structure of MD simulations were also confirmed by DFT calculations. Atomic distances calculated by less accurate MD simulation results were very close to DFT calculations validating the force field and method of the large scale simulations.

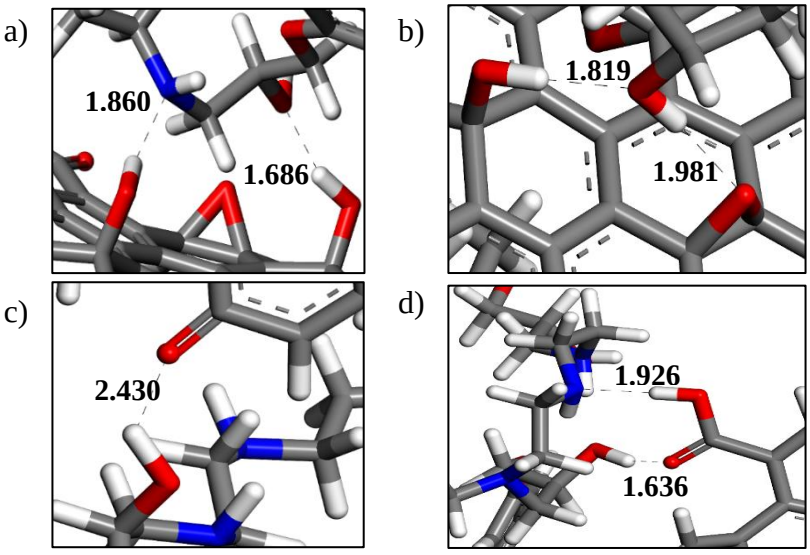

Figure 5.24. Hydrogen bonds for different GO functional groups for an equilibrated structure.

The addition of oxygen-containing functional groups on graphene structures significantly improved interaction energies and the stiffness of the material. Fillers were added into cells up to 8 wt% amount and a constant increase was observed for both interaction energies and Young's Modulus values. In the experimental studies, there was a maximum point for the wt% of the GO additive which was not observed in this study. These cells simulate nanocomposites with well-dispersed GO sheets in the epoxy matrix where Gr/GO agglomerations were ignored that they can even be observed with bare eyes in the experimental samples. The reason for the continuous increase in the results is based on the continuous increase in the interfacial interaction by increasing the surface area which was not possible in the industrial process.

To test this theory, interaction energy for the four-layer pi-stacked AA90 fillers, two double-layer AA90 fillers and homogeneously distributed four AA90 fillers with the composition of 8 wt% in the cell with epoxy chains were calculated and given in Table 5.8. It was demonstrated that dispersed GO sheets have higher interaction energy compared to the stacked GO sheets which explains the difference between reinforcement based mechanical improvement in experiments and simulations. As the amount of agglomerated graphene sheets increased, interaction energy at the interface was decreased by 32% for two-layer stacked GO sheets and by 51% for four-layer stacked GO sheets since the interacting surface area of the filler was decreased. Thus, filler dispersion is an important factor for improved physical and mechanical performance that explains the difference between the experiments and simulations. In experiments, there are always aggregations of Gr/GO layers observed for the prepared samples. It was concluded that the role of the GO preparation is not only increasing the interaction with the polymer phase but also decreasing the self-interaction by the increased interlayer distance between the GO sheets. The addition of oxygen-containing functional groups on GO surface and edges improves dispersion in the epoxy matrix and increases the interacting surface area, which enhances the performance of the GO filler in epoxy.

Table 5.8 Effect of filler dispersion on the interaction energies.

	AA90-Dispersed	**AA90 Two-Layer Stacked**	**AA90-Four-Layer Stacked**
Interaction Energy (kcal/mol)	-2014.04	-1372.01	-979.46

Interaction energies for nanocomposite systems containing mass percentage of 2%, 4%, 6%, 8%, 8% two-layer stacked and 8% four-layer stacked AA90 fillers were summarized in Figure 5.25. Interaction energy was increased with increased mass percentage of filler. However, the filler performance was dramatically decreased even for high mass percentage when aggregation was increased interaction energies.

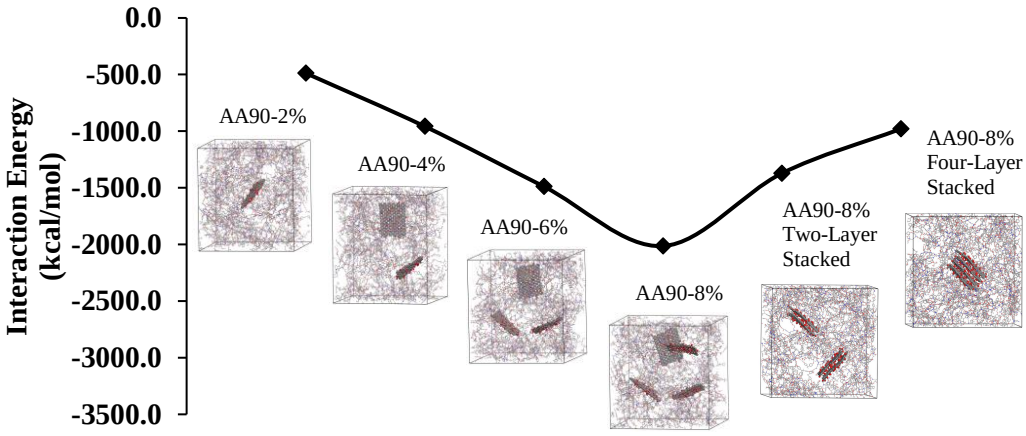

Figure 5.25. Change of the interaction energy with increasing mass percentage and aggregation of AA90 filler.

5.2.7 Effect of GO Filler Size on the Interaction Energies and Young's Modulus Values

GO structures with a size of 2.4 x 2.4 nm (GO252), 2.4 x 1.2 nm (GO132), 1.1 x 1.2 nm (GO66) were investigated in terms of Young's Modulus and interaction energy parameters. Results were given in Table 5.9. For the calculation of Young's Modulus values, the same procedure was followed given in the previous section. Structures at these three different sizes with three different configurations in the cell were prepared for each set and the average of these results was analyzed to obtain the Young's Modulus values. It was observed that the GO with a larger size provided the highest Young's Modulus and the GO with the lowest size provided the lowest Young's Modulus values. To improve stiffness, using larger GO sheets seemed to be a better option at first sight when these results were considered. However, when the interaction energies were calculated, opposite results were obtained interestingly. Decreasing filler size increased the number of edge groups that interact most with the functional groups on epoxy molecules. This resulted in increasing interactions for the relatively small-sized GO fillers. Increased interactions facilitate the dispersion of GO in the polymer matrix and better filler performance could be achieved. Whereas larger-sized bulky GO provides directional mechanical stiffness in two dimensions. Larger GO sheets yielded higher Young's Modulus values, however, agglomeration of these types of fillers and poor adhesion with the polymer matrix would result in lower enhancement in mechanical properties with increasing graphene size. The optimum filler size providing mechanical stiffness and enhanced intermolecular interaction should be selected by considering these competing effects in the experiments.

Table 5.9. Interaction energy and Young's Modulus values calculated for different GO sizes

	GO66	GO132	GO252
Interaction Energy (kcal/mol)	-2183.04	-1927.28	-1655.36
Young's Modulus (GPa)	4.12	4.33	4.98

5.2.8 Radial Distribution Function (RDF) Analysis for an Equilibrium Structure

RDF analyzes were performed to understand the molecular details in an MD simulations cell for the equilibrated structures. Nanocomposite structures containing 8 wt% AA50 type GO filler was used for RDF calculations. Normalized radial distribution functions for the different atoms and atom groups were given between Figure 5.26 and Figure 5.29.

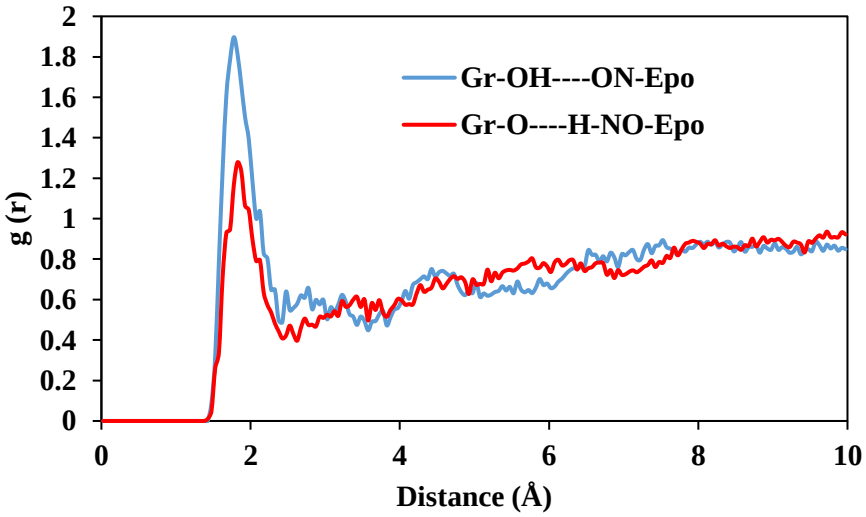

Figure 5.26. Radial distribution function for the intermolecular interaction between a) -OH and -COOH protons on GO with N and O atoms in the epoxy chains, b) oxygen atoms on GO with the hydrogen atoms in the amine and alcohol groups of epoxy chains.

In Figure 5.26, RDF for -OH and -COOH protons on GO with N and O atoms on the epoxy chains were compared with the RDF for oxygen atoms on GO with the hydrogen atoms of the amine and alcohol groups of epoxy chains. Peak was observed around 2 Å for both analyzes that correspond to the hydrogen bonds in the system. It was determined that hydrogen bonds of N and O atoms in epoxy with GO protons bonded to oxygen atoms were significantly higher compared to the hydrogen bonds of epoxy protons on amine and alcohol groups with the oxygen atoms of the GO.

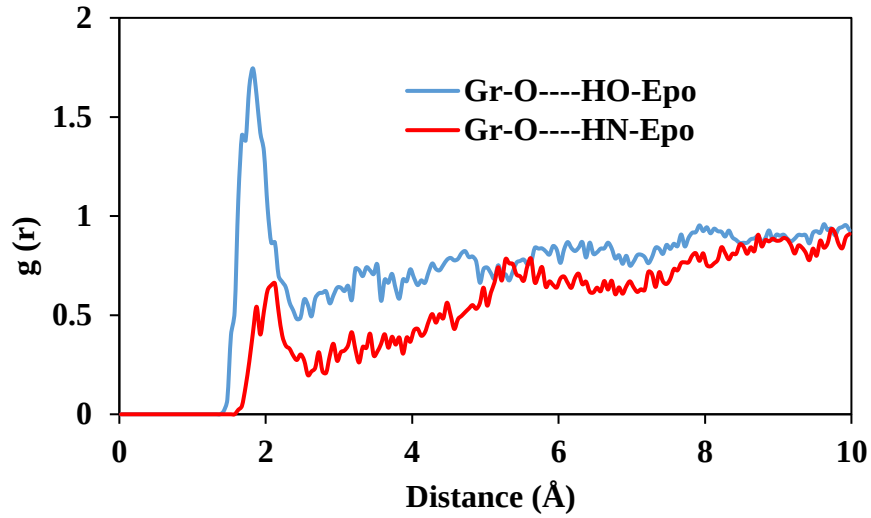

Figure 5.27. Radial distribution function for the intermolecular interaction between oxygen atoms on GO with the hydrogen atoms in the alcohol and amine groups of epoxy chains.

In Figure 5.27, RDF for GO oxygen atoms with the hydrogen atoms of the amine and alcohol groups of epoxy chains was compared. It was determined that the hydrogen bonding peak for the GO oxygen atoms with alcohol protons on epoxy chains is significantly higher than the hydrogen bonding peak for the GO oxygens with the amine protons of the epoxy chains.

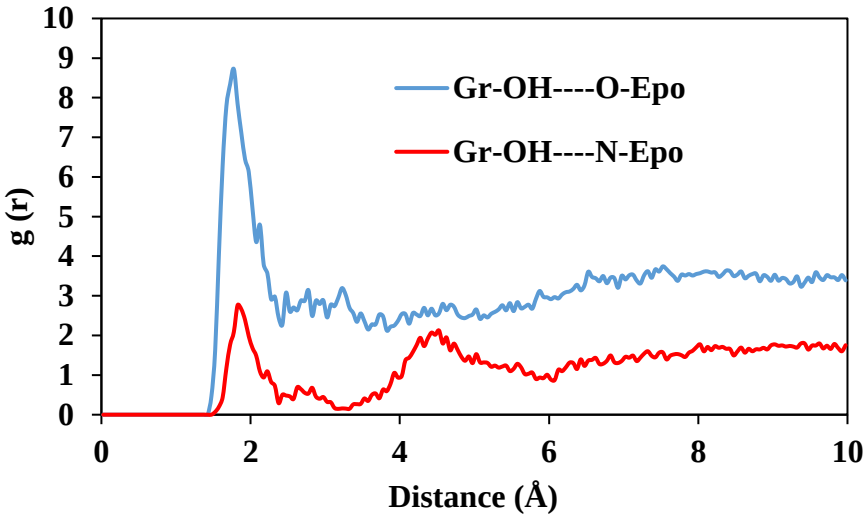

Figure 5.28. Radial distribution function for the intermolecular interaction between -OH and -COOH protons on GO with O and N atoms in the epoxy chains.

In Figure 5.28, RDF for the protons on -OH and -COOH groups of GO with the O and N atoms on the epoxy chains were compared. It was found that the hydrogen bonding peak for -OH and -COOH protons on GO with the oxygen atoms on epoxy chains is higher than the hydrogen bonding peak for -OH and -COOH protons on GO with the nitrogen atoms on epoxy chains.

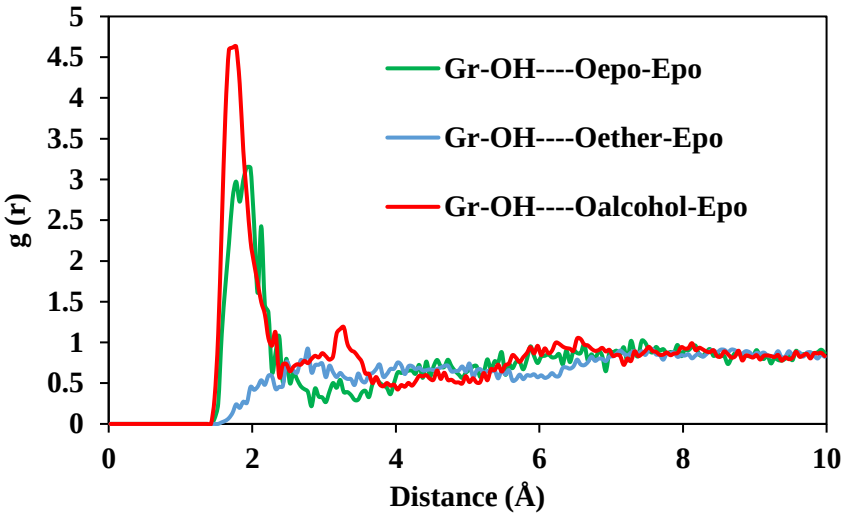

Figure 5.29. Radial distribution function for the intermolecular interaction between -OH and -COOH protons on GO with the three types oxygens atoms in the epoxy chains.

In Figure 5.29, RDF for the protons on -OH and -COOH groups of GO with the three types of O atoms on the epoxy chains were compared. It was represented that the hydrogen bonding peak for the GO proton interaction with the oxygen atoms in the alcohol groups of epoxy chains was highest, whereas the hydrogen bonding peak for the GO proton interaction with the oxygen atoms in the ether groups of epoxy chains was lowest in the RDF analysis. The hydrogen bonding peak for the GO proton interaction with the oxygen atoms in the epoxy end groups was also significantly higher than the hydrogen bonding by ether groups.

CHAPTER 6

CONCLUSIONS

In this thesis, first principle calculations and classical mechanics calculations were performed to study the interfacial interactions between graphene/graphene oxide fillers and the epoxy polymer matrix. Homogeneous dispersion and strong GO filler adhesion with the epoxy matrix are determined as the two major considerations for the production of polymer nanocomposites. Controlling the interfacial interactions can optimize these parameters, which is critical for achieving the improved mechanical and physical properties in polymer nanocomposites. Quantum mechanics and classical mechanics methods were used in this study to interpret the basis of these interactions in the nanocomposite system at the atomic level. Firstly, DFT calculations were performed to identify the interactions accurately between the functional groups of epoxy chains and the functional groups on the GO structure. Results showed that carboxylic acid and hydroxyl groups on the GO sheets are capable of forming strong hydrogen bonds with amine, epoxy and hydroxyl groups on epoxy chains. Thus, these functional groups had the strongest affinity with the epoxy matrix. Carbonyl functional groups at the edge exhibited the lowest interaction energy, followed by epoxy functional groups on GO, where they still outperformed pristine graphene in terms of interaction energy performance. Secondly, mixing energies were calculated with classical molecular mechanics methods to investigate the self-interactions and intermolecular binding energies. Therefore, attractive and repulsive interactions were determined for pairwise interactions, which are important parameters for achieving homogeneous dispersion in the epoxy matrix. It was determined that epoxy and hydroxyl functional groups provide the lowest mixing and the highest binding energies, which means that these groups are mostly responsible for preventing agglomeration of the GO fillers that is one of the main problems of GO as polymer nanocomposite filler.

After the role and performance of every functional group on GO and epoxy chains were clarified for relatively smaller scales and fewer atoms; larger scale MD simulations were performed as a next step to investigate these interactions by constructing nanocomposite systems having about 8000 and 27000 atoms. MD simulations were performed at the NPT ensemble at 298 K temperature and 1 atm pressure to mimic the experimental conditions. The achievement of an experimental density of 1.1 g/cm^3 for the equilibrated system was validated the accuracy of the MD simulation method. An increasing trend in the interaction energies was observed by increasing the oxygen content on GO, and an optimum point was determined as 10% oxygen on GO, when continuous periodic single layer GO sheets with only epoxy and hydroxyl functional groups were used for the simulations. Moreover, it was demonstrated that the epoxy:hardener ratio was another important parameter that affect the interaction energy between GO and epoxy chains. With increasing DETA amount in the epoxy chains which resulted in increasing polar amine groups in the system, interaction energy was decreased for low oxygen content (5%) from -1240 kcal/mol to -140 kcal/mol. A completely different trend was observed for high oxygen content (18%), in which the interaction energy increased from -888.5 kcal/mol to -1400.5 kcal/mol. The same trend was observed when discrete GO fillers with carboxylic acid and carbonyl edge functional groups were used in the cell. Increasing oxygen content and DETA ratio significantly improved the interaction energies with the GO fillers with high oxygen content. Hydrogen bonds were also clearly detected within the system for large-scale calculations, which were very similar type and distances to DFT results. Besides, Young's modulus values were calculated to determine the stiffness of the nanocomposite system with the filler addition amounts of 2%, 4%, 6% and 8%, and improvement was observed with increasing GO content. Both AA90 and AA50 GO fillers performed better than pristine graphene sheets in terms of improving Young's modulus; however, AA50 fillers with more oxygen content possessed the highest stiffness properties which were in good agreement with the interaction energy results. RDF analyzes were performed to investigate the stacking density of epoxy chains around GO fillers and

the distribution of the functional groups. It was determined that hydrogen bond donor protons on the GO interact better with epoxy polar functional groups compared to the hydrogen bond acceptor oxygen groups on GO with the epoxy polar functional groups. Moreover, hydroxyl functional groups on epoxy chains originated from DGEBA generated more hydrogen bonds than the amine functional groups originated from DETA groups. Homogeneous dispersion of Gr/GO sheets was determined as an important parameter to enhance these properties, and agglomeration of these fillers significantly decreased the interaction energies when two-layer and four-layer pi-stacked GO sheets were used in the simulation cell. Approximately 32% decrease was observed for the interfacial interaction calculations using two-layer stacked GO sheets, and approximately 51% decrease for the interfacial interaction was observed when four-layer stacked GO sheets were used. In addition, larger GO sheets performed better in improving Young's modulus values than smaller GO sheets. However, interaction energies were decreased when large GO sheets were used since the number of edge functional groups and the contact area were increased for the smaller GO sheets as fillers. These theoretical results can provide insight into optimizing structural parameters for the large scale production of the epoxy and GO nanocomposites with enhanced properties.

REFERENCES

[1] X. Sun *et al.*, "Recent Progress in Graphene/Polymer Nanocomposites," *Advanced Materials*, vol. 33, no. 6, p. 2001105, 2021, doi: 10.1002/adma.202001105.

[2] R.-M. Wang, S.-R. Zheng, and Y.-P. Zheng, *Polymer matrix composites and technology*. Woodhead Publishing Limited, 2011. doi: 10.1533/9780857092229.

[3] T. Krithiga and J. Aravind Kumar, "Polymer Nanocomposite Matrix," in *Handbook of Polymer and Ceramic Nanotechnology*, Springer, Cham, 2021. doi: 10.1007/978-3-030-10614-0_67-1.

[4] V. Mittal, *Polymer-Graphene Nanocomposites*. Cambridge: Royal Society of Chemistry, 2012. doi: 10.1039/9781849736794.

[5] K. H. Liao, S. Kobayashi, H. Kim, A. A. Abdala, and C. W. Macosko, "Influence of functionalized graphene sheets on modulus and glass transition of PMMA," *Macromolecules*, vol. 47, no. 21, pp. 7674–7676, 2014, doi: 10.1021/ma501709g.

[6] S. Stankovich *et al.*, "Graphene-based composite materials," *Nature*, vol. 442, no. 7100, pp. 282–286, 2006, doi: 10.1038/nature04969.

[7] T. Ramanathan *et al.*, "Functionalized graphene sheets for polymer nanocomposites," *Nature Nanotechnology*, vol. 3, no. 6, pp. 327–331, 2008, doi: 10.1038/nnano.2008.96.

[8] S. Wang, M. Tambraparni, J. Qiu, J. Tipton, and D. Dean, "Thermal Expansion of Graphene Composites," *Macromolecules*, vol. 42, no. 14, pp. 5251–5255, Jul. 2009, doi: 10.1021/ma900631c.

[9] P. K. Mallick, *Processing of Polymer Matrix Composites*. CRC Press, 2018.

[10] U. Szeluga, S. Pusz, B. Kumanek, K. Olszowska, A. Kobyliukh, and B. Trzebicka, "Effect of graphene filler structure on electrical, thermal, mechanical, and fire retardant properties of epoxy-graphene nanocomposites

- a review," *Critical Reviews in Solid State and Materials Sciences*, vol. 46, no. 2, pp. 152–187, 2021, doi: 10.1080/10408436.2019.1708702.

[11] T. J. A. Brydson, *Brydson's Plastics Materials*. Elsevier, 2017. doi: 10.1016/C2014-0-02399-4.

[12] N. P. Singh, V. K. Gupta, and A. P. Singh, "Graphene and carbon nanotube reinforced epoxy nanocomposites: A review," *Polymer*, vol. 180, no. August, p. 121724, 2019, doi: 10.1016/j.polymer.2019.121724.

[13] B. Kim, J. Choi, S. Yang, S. Yu, and M. Cho, "Influence of crosslink density on the interfacial characteristics of epoxy nanocomposites," *Polymer*, vol. 60, pp. 186–197, Mar. 2015, doi: 10.1016/j.polymer.2015.01.043.

[14] G. Possart *et al.*, "Micro–macro characterisation of DGEBA-based epoxies as a preliminary to polymer interphase modelling," *International Journal of Adhesion and Adhesives*, vol. 29, no. 5, pp. 478–487, Jul. 2009, doi: 10.1016/j.ijadhadh.2008.10.001.

[15] J. H. Warner, F. Schaffel, M. Rummeli, and A. Bachmatiuk, *Graphene: Fundamentals and emergent applications*. Elsevier, 2013.

[16] S. C. Ray, *Applications of Graphene and Graphene Oxide Based Nanomaterials*. 2015.

[17] W. Gao, Ed., *Graphene Oxide: Reduction Recipes, Spectroscopy, and Applications*. Springer, 2015. doi: 10.1007/978-3-319-15500-5_1.

[18] A. Lerf, H. He, M. Forster, and J. Klinowski, "Structure of graphite oxide revisited," *Journal of Physical Chemistry B*, vol. 102, no. 23, pp. 4477–4482, 1998, doi: 10.1021/jp9731821.

[19] W. Gao, L. B. Alemany, L. Ci, and P. M. Ajayan, "New insights into the structure and reduction of graphite oxide," *Nature Chemistry*, vol. 1, no. 5, pp. 403–408, 2009, doi: 10.1038/nchem.281.

[20] K. Erickson, R. Erni, Z. Lee, N. Alem, W. Gannett, and A. Zettl, "Determination of the local chemical structure of graphene oxide and reduced

graphene oxide," *Advanced Materials*, vol. 22, no. 40, pp. 4467–4472, 2010, doi: 10.1002/adma.201000732.

[21] K. Zhou and B. Liu, *Molecular Dynamics Simulation: Fundamentals and Applications*. Elsevier, 2022.

[22] Q. H. Zeng, A. B. Yu, and G. Q. Lu, "Multiscale modeling and simulation of polymer nanocomposites," *Progress in Polymer Science*, vol. 33, no. 2, pp. 191–269, Feb. 2008, doi: 10.1016/j.progpolymsci.2007.09.002.

[23] W. E, *Principles of Multiscale Modeling*. Cambridge University Press, 2011.

[24] L. Deng *et al.*, "Multiscale modeling and simulation of polymer blends in injection molding: A review," *Polymers*, vol. 13, no. 21, pp. 1–26, 2021, doi: 10.3390/polym13213783.

[25] R. A. Latour, "Molecular Simulation Methods to Investigate Protein Adsorption Behavior at the Atomic Level," in *Comprehensive Biomaterials II*, vol. 3, no. July 2016, Elsevier, 2017, pp. 268–294. doi: 10.1016/B978-0-12-803581-8.09794-0.

[26] A. J. Cohen, P. Mori-Sánchez, and W. Yang, "Challenges for Density Functional Theory," *Chemical Reviews*, vol. 112, no. 1, pp. 289–320, Jan. 2012, doi: 10.1021/cr200107z.

[27] M. Born and R. Oppenheimer, "Zur Quantentheorie der Molekeln," *Annalen der Physik*, vol. 389, no. 20, pp. 457–484, 1927, doi: 10.1002/andp.19273892002.

[28] W. Koch and M. C. Holthausen, *A Chemist's Guide to Density Functional Theory*, 2nd ed. Wiley, 2001. doi: 10.1002/3527600043.

[29] E. G. Lewars, *Computational Chemistry*. Dordrecht: Springer Netherlands, 2011. doi: 10.1007/978-90-481-3862-3.

[30] P. Hohenberg and W. Kohn, "Inhomogeneous Electron Gas," *Physical Review*, vol. 136, no. 3B, pp. B864–B871, Nov. 1964, doi: 10.1103/PhysRev.136.B864.

[31] W. Kohn and L. J. Sham, “Self-Consistent Equations Including Exchange and Correlation Effects,” *Physical Review*, vol. 140, no. 4A, pp. A1133–A1138, Nov. 1965, doi: 10.1103/PhysRev.140.A1133.

[32] M. Orio, D. A. Pantazis, and F. Neese, “Density functional theory,” *Photosynthesis Research*, vol. 102, no. 2–3, pp. 443–453, Dec. 2009, doi: 10.1007/s11120-009-9404-8.

[33] E. N. Skountzos and V. G. Mavrantzas, “Molecular dynamics simulations of graphene-based polymer nanocomposites,” in *Carbon-Based Smart Materials*, De Gruyter, 2020, pp. 115–152. doi: 10.1515/9783110479133-005.

[34] H. Sun, P. Ren, and J. R. Fried, “The COMPASS force field: parameterization and validation for phosphazenes,” *Computational and Theoretical Polymer Science*, vol. 8, no. 1–2, pp. 229–246, Jan. 1998, doi: 10.1016/S1089-3156(98)00042-7.

[35] D. Frenkel and B. Smit, *Understanding Molecular Simulation: From Algorithms to Applications*. Academic Press, 1996. doi: https://doi.org/10.1063/1.881812.

[36] S. Sharma, Ed., *Molecular Dynamics Simulation of Nanocomposites Using BIOVIA Materials Studio, LAMMPS and Gromacs*. Elsevier, 2019. [Online]. Available: https://linkinghub.elsevier.com/retrieve/pii/B9780128169544099903

[37] P. O. J. Scherer, *Computational Physics*, vol. 5, no. 5. Berlin, Heidelberg: Springer Berlin Heidelberg, 2010. doi: 10.1007/978-3-642-13990-1.

[38] S. Yu, S. Yang, and M. Cho, “Multi-scale modeling of cross-linked epoxy nanocomposites,” *Polymer*, vol. 50, no. 3, pp. 945–952, Jan. 2009, doi: 10.1016/j.polymer.2008.11.054.

[39] J. Choi, S. Yu, S. Yang, and M. Cho, “The glass transition and thermoelastic behavior of epoxy-based nanocomposites: A molecular dynamics study,”

Polymer, vol. 52, no. 22, pp. 5197–5203, Oct. 2011, doi: 10.1016/j.polymer.2011.09.019.

[40] H. Shin, S. Yang, S. Chang, S. Yu, and M. Cho, "Multiscale homogenization modeling for thermal transport properties of polymer nanocomposites with Kapitza thermal resistance," *Polymer*, vol. 54, no. 5, pp. 1543–1554, 2013, doi: 10.1016/j.polymer.2013.01.020.

[41] B. Arab and A. Shokuhfar, "Molecular dynamics simulation of cross-linked epoxy polymers: The effect of force field on the estimation of properties," *Journal of Nano- and Electronic Physics*, vol. 5, no. 1, pp. 1–5, 2013.

[42] R. D. Guha, O. Idolor, and L. Grace, "An atomistic simulation study investigating the effect of varying network structure and polarity in a moisture contaminated epoxy network," *Computational Materials Science*, vol. 179, p. 109683, Jun. 2020, doi: 10.1016/j.commatsci.2020.109683.

[43] E. N. Brown, S. R. White, and N. R. Sottos, "Microcapsule induced toughening in a self-healing polymer composite," *Journal of Materials Science*, vol. 39, no. 5, pp. 1703–1710, Mar. 2004, doi: 10.1023/B:JMSC.0000016173.73733.dc.

[44] F. Aghadavoudi, H. Golestanian, and Y. Tadi Beni, "Investigating the effects of resin crosslinking ratio on mechanical properties of epoxy-based nanocomposites using molecular dynamics," *Polymer Composites*, vol. 38, no. 2, pp. E433–E442, Sep. 2017, doi: 10.1002/pc.24014.

[45] A. Shokuhfar and B. Arab, "The effect of cross linking density on the mechanical properties and structure of the epoxy polymers: Molecular dynamics simulation," *Journal of Molecular Modeling*, vol. 19, no. 9, pp. 3719–3731, 2013, doi: 10.1007/s00894-013-1906-9.

[46] K. W. Putz, M. J. Palmeri, R. B. Cohn, R. Andrews, and L. C. Brinson, "Effect of cross-link density on interphase creation in polymer nanocomposites," *Macromolecules*, vol. 41, no. 18, pp. 6752–6756, 2008, doi: 10.1021/ma800830p.

[47] C. M. Hadden, B. D. Jensen, A. Bandyopadhyay, G. M. Odegard, A. Koo, and R. Liang, "Molecular modeling of EPON-862/graphite composites: Interfacial characteristics for multiple crosslink densities," *Composites Science and Technology*, vol. 76, pp. 92–99, 2013, doi: 10.1016/j.compscitech.2013.01.002.

[48] L. C. Tang *et al.*, "The effect of graphene dispersion on the mechanical properties of graphene/epoxy composites," *Carbon*, vol. 60, pp. 16–27, 2013, doi: 10.1016/j.carbon.2013.03.050.

[49] S. Zhao, H. Chang, S. Chen, J. Cui, and Y. Yan, "High-performance and multifunctional epoxy composites filled with epoxide-functionalized graphene," *European Polymer Journal*, vol. 84, pp. 300–312, 2016, doi: 10.1016/j.eurpolymj.2016.09.036.

[50] R. Aradhana, S. Mohanty, and S. K. Nayak, "Comparison of mechanical, electrical and thermal properties in graphene oxide and reduced graphene oxide filled epoxy nanocomposite adhesives," *Polymer*, vol. 141, pp. 109–123, 2018, doi: 10.1016/j.polymer.2018.03.005.

[51] S. C. Shiu and J. L. Tsai, "Characterizing thermal and mechanical properties of graphene/epoxy nanocomposites," *Composites Part B: Engineering*, vol. 56, pp. 691–697, 2014, doi: 10.1016/j.compositesb.2013.09.007.

[52] A. Yarahmadi, M. Hashemian, D. Toghraie, R. Abedinzadeh, and S. Ali Eftekhari, "Investigation of mechanical properties of epoxy-containing Detda and Degba and graphene oxide nanosheet using molecular dynamics simulation," *Journal of Molecular Liquids*, vol. 347, p. 118392, Feb. 2022, doi: 10.1016/j.molliq.2021.118392.

[53] R. Rahman and A. Haque, "Molecular modeling of crosslinked graphene–epoxy nanocomposites for characterization of elastic constants and interfacial properties," *Composites Part B: Engineering*, vol. 54, no. 1, pp. 353–364, Nov. 2013, doi: 10.1016/j.compositesb.2013.05.034.

[54] A. P. Thompson *et al.*, "LAMMPS - a flexible simulation tool for particle-

based materials modeling at the atomic, meso, and continuum scales," *Computer Physics Communications*, vol. 271, p. 108171, 2022, doi: 10.1016/j.cpc.2021.108171.

[55] M. J. Frisch *et al.*, *Gaussian, Inc*. Wallingford CT, USA, 2009.

[56] Y. Zhao and D. G. Truhlar, "The M06 suite of density functionals for main group thermochemistry, thermochemical kinetics, noncovalent interactions, excited states, and transition elements: Two new functionals and systematic testing of four M06-class functionals and 12 other function," *Theoretical Chemistry Accounts*, vol. 120, no. 1–3, pp. 215–241, 2008, doi: 10.1007/s00214-007-0310-x.

[57] S. Grimme, J. Antony, S. Ehrlich, and H. Krieg, "A consistent and accurate ab initio parametrization of density functional dispersion correction (DFT-D) for the 94 elements H-Pu," *Journal of Chemical Physics*, vol. 132, no. 15, 2010, doi: 10.1063/1.3382344.

[58] J. Da Chai and M. Head-Gordon, "Long-range corrected hybrid density functionals with damped atom-atom dispersion corrections," *Physical Chemistry Chemical Physics*, vol. 10, no. 44, pp. 6615–6620, 2008, doi: 10.1039/b810189b.

[59] R. Ditchfield, W. J. Hehre, and J. A. Pople, "Self-consistent molecular-orbital methods. IX. An extended gaussian-type basis for molecular-orbital studies of organic molecules," *The Journal of Chemical Physics*, vol. 54, no. 2, pp. 720–723, 1971, doi: 10.1063/1.1674902.

[60] M. Bursch, J. M. Mewes, A. Hansen, and S. Grimme, "Best-Practice DFT Protocols for Basic Molecular Computational Chemistry**," *Angewandte Chemie - International Edition*, vol. 61, no. 42, 2022, doi: 10.1002/anie.202205735.

[61] Paul J. Flory, *Principles Of Polymer Chemistry*. Cornell University Press, 1953.

[62] C. F. Fan, B. D. Olafson, M. Blanco, and S. L. Hsu, “Application of molecular simulation to derive phase diagrams of binary mixtures,” *Macromolecules*, vol. 25, no. 14, pp. 3667–3676, Jul. 1992, doi: 10.1021/ma00040a010.

[63] B. H. Besler, K. M. Merz, and P. A. Kollman, “Atomic charges derived from semiempirical methods,” *Journal of Computational Chemistry*, vol. 11, no. 4, pp. 431–439, 1990, doi: 10.1002/jcc.540110404.

[64] A. Tkatchenko and M. Scheffler, “Accurate molecular van der Waals interactions from ground-state electron density and free-atom reference data,” *Physical Review Letters*, vol. 102, no. 7, pp. 6–9, 2009, doi: 10.1103/PhysRevLett.102.073005.

[65] D. N. Theodorou and U. W. Suter, “Atomistic modeling of mechanical properties of polymeric glasses,” *Macromolecules*, vol. 19, no. 1, pp. 139–154, Jan. 1986, doi: 10.1021/ma00155a022.

[66] H. Sun, S. J. Mumby, J. R. Maple, and A. T. Hagler, “An ab Initio CFF93 All-Atom Force Field for Polycarbonates,” *Journal of the American Chemical Society*, vol. 116, no. 7, pp. 2978–2987, Apr. 1994, doi: 10.1021/ja00086a030.

[67] A. K. Kaw, *Mechanics of Composite Materials*, 2nd ed. CRC Press, 2005. doi: 10.1201/9781420058291.